University of Alberta

Removal of Heavy Metal Ions and Diethylenetriamine Species from Solutions by Magnetic Activated Carbon

by

Kaiwen Liu

A thesis submitted to the Faculty of Graduate Studies and Research
in partial fulfillment of the requirements for the degree of

Master of Science
in
Materials Engineering

Department of Chemical and Materials Engineering

Spring 2013
Edmonton, Alberta

ABSTRACT

Even though activated carbon is widely used in the removal of contaminants from effluents, it is difficult to be completely recovered by screening or classification. In this project, we prepared a magnetic form of activated carbon (M-AC) by co-precipitation of iron oxides onto activated carbon surface. M-AC can be separated from solutions by applying an external magnetic field and regenerated for reuse.

The synthesized M-AC was characterized by X-ray diffraction, specific surface area measurement, and scanning electron microscope. Characterization results show that the major phase of coated iron oxides is magnetite (Fe_3O_4). Batch adsorption experiments were carried out for single-component and multi-component solutions. M-AC shows a better adsorption capacity for single-component of Cu (II), Ni (II), or diethylenetriamine (DETA) and for multiple-components of Cu-DETA and Ni-DETA complexes in deionized water than activated carbon. M-AC also shows the potential application in carbon-in-pulp process for gold recovery.

ACKNOWLEDGEMENT

I would like to express my deepest and sincerest gratitude appreciation to my supervisor, Dr. Qingxia (Chad) Liu, the scientific director for the Canadian Centre for Clean Coal/Carbon and Mineral Processing Technologies (C^5MPT). He patiently provided the vision, encouragement and invaluable guidance for me to proceed through this research and complete my thesis.

I would also like to thank Dr. Zhenghe Xu for his enthusiasm, constant support during the program. The suggestions and comments from Dr. Manqiu Xu and Dr. Jie Dong are greatly appreciated.

I would like to thank Dr. Peiling Sun for her helpful discussions and suggestions during the project. Her critical reviewing of the manuscripts and knowledgeable advice in surface chemistry are also appreciated. Appreciation also goes to Dr. Weiping Shi, Dr. Junxia Peng and Mr. Jui-Tse Chen for the help in the experiment set up. Thanks to Ms. Gayle Hatchard, Dr. Brent Rudyk, Dr. Xinsong Lin, Dr. Anqiang He for their help in characterization techniques.

I would like to thank all the members of the C^5MPT center for those valuable discussions and their friendship. The financial support from Vale Base Metal Technology Development and NSERC - CRD program are acknowledged.

Last but not the least, I would like to thank my parents, Beizhao Liu and Zhaoqun Liu for their support during my master program.

TABLE OF CONTENTS

LIST OF TABLES

LIST OF FIGURES

CHAPTER 1 INTRODUCTION

1.1 Overview

Diethylenetriamine (DETA) in combination with sodium sulfite is an effective pyrrhotite [Fe_xS_{1-x}] depressant in pentlandite [$(NiFe)_9S_8$] and chalcopyrite [$CuFeS_2$] flotation at Sudbury area in Canada [1-6]. Pyrrhotite which is an associated gangue with pentlandite and chalcopyrite is the major source of sulfur dioxide emission in smelting ores. Thus, it is critically important to reduce pyrrhotite injection to reduce sulfur dioxide emission [3, 6, 7]. A series of researches have been carried out to determine the effective DETA depressing conditions and mechanism during flotation for decades [2-4, 8].

DETA is a colorless hydroscopic liquid and soluble in water as well as in hydrocarbons [9]. As a strong chelating reagent with three pairs of non-bonding electrons, DETA can form stable complexes with specific metal ions [10], increasing the heavy metal concentrations in effluents of mineral industries. For example, Cu-DETA complexes are very stable in the wastewater after flotation and could not be precipitated by raising the pH above 11 with lime [10, 11]. Enhancing copper concentration in effluents is a major potential environmental concern at Vale since it might exceed the government regulations. Thus, it is important to develop an effective and economic method to reduce the concentrations of DETA and heavy metal in the wastewater after mineral flotation.

In this study, magnetic activated carbon (M-AC) was developed to remove DETA and heavy metal species from effluents. M-AC combines the magnetic properties

of magnetite with the loading features of activated carbon as well as magnetite. M-AC can be easily attracted by applying a magnetic field, and then be separated from solutions. Even though the surface area of M-AC was reduced after the deposition of magnetite compared with that of activated carbon, M-AC showed better loading property and removal efficiency for heavy metal ions and DETA species than pure activated carbon. In addition, the reuse of M-AC is feasible after adsorbed species were stripped from M-AC surface in the presence of acid followed by regeneration with alkaline solutions. Other than the application in wastewater treatment in mineral industry, M-AC showed good affinity with gold cyanide species and the potential application in the carbon-in-pulp process for gold recovery after the cyanidation of gold minerals.

1.2 Objectives

The objectives of this project include:

- To develop an effective and innovative technology to prepare magnetic activated carbon (M-AC) particles for the removal of metal ions and DETA species.
- To characterize the major properties of synthesized M-AC, including magnetization curve, crystal structure, specific surface area, average pore size, particles size distributions, and micro-morphologies.
- To study the adsorption of potential contamination species (copper ions, nickel ions, and DETA) onto M-AC after chalcopyrite-pentlandite flotation.

- To compare the adsorption properties of M-AC with those of pure activated carbon and pure magnetite.
- To model the adsorption curves to understand the fundamentals of adsorption system.
- To investigate the recycle and reuse of the M-AC particles and to optimize stripping and regenerating conditions.

CHAPTER 2 LITERATURE REVIEW

2.1 DETA Distributions in Pentlandite/Pyrrhotite Separation

Pyrrhotite [Fe_xS_{1-x}] is a major gangue commonly associated with pentlandite [$(NiFe)_9S_8$] and chalcopyrite [$CuFeS_2$] which are two valuable minerals for nickel and copper extraction at Sudbury area in Canada. Since pyrrhotite is the major source of sulfur dioxide emission in smelting ores, it is critically important to maximize pyrrhotite rejection in milling to reduce sulfur dioxide emission during metallurgy process. Among the pyrrhotite at Sudbury, about 70 wt.% of ferromagnetic pyrrhotite with monoclinic structure is rejected by magnetic separation. On the other hand, the hexagonal pyrrhotite which is weakly (para-) magnetic is normally separated from pentlandite and chalcopyrite through froth flotation [1-7].

A series of amino type of chelating chemicals have been investigated as pyrrhotite depressants for decades. Diethylenetriamine (DETA) in combination with sodium sulfite (Na_2SO_3) was found to be effective pyrrhotite depressant at Clarabelle Mill. The use of DETA and Na_2SO_3 greatly improved the nickel recovery and concentrate grade in flotation [1-6]. The researches were conducted to determine the effective DETA depressing conditions for pyrrhotite and to understand DETA depressing pyrrhotite mechanism during flotation [2-4, 8]. The proposed working mechanisms of pyrrhotite depression by DETA and sodium sulfite include: (1) DETA removes the Cu (II) and Ni (II) ions from the surface of pyrrhotite by forming metal-DETA complexes. (2) Hydrophilic precipitates formed from

combination of DETA, metal, and $S_2O_4^{2-}$ or $S_3O_6^{2-}$ may play an important role in pyrrhotite depression [3, 4, 12-16].

DETA is a colorless hydroscopic liquid and soluble in water as well as in hydrocarbons [9]. As shown in Figure 2.1, DETA molecule has three nitrogen atoms and each nitrogen atom has a pair of non-bonding electrons. DETA can either accept H^+ to form protonated species $[H_n(DETA)]^{n+}$ (n=1~3), or donate non-bonding electron pairs to specific metal ions to form metal-DETA complexes. For example, DETA can form $[Ni(DETA)]^{2+}$ and $[Ni(DETA)_2]^{2+}$ complexes with Ni^{2+} ions or react with Cu^{2+} ions to form $[Cu(DETA)]^{2+}$ and $[Cu(DETA)_2]^{2+}$ complexes, depending on the molar ratio of metal ions to DETA and solution pH in the system. DETA has been known as an excellent chelating agent for specific metals: Cu (II), Ni (II) and Zn (II) [10].

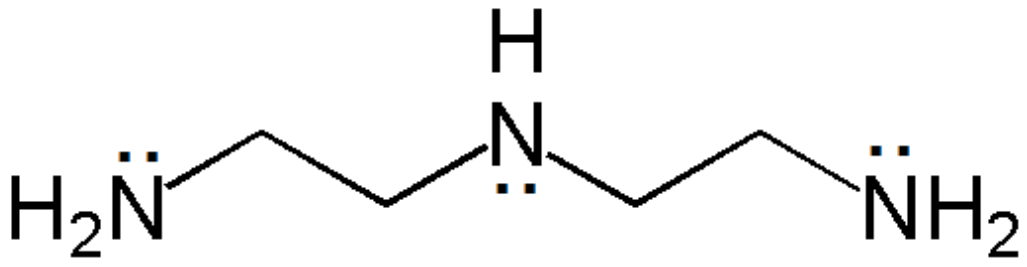

Figure 2.1 DETA molecule

However, a potential environmental issue regarding metal ion concentrations in effluents has drawn attention at the wastewater stream of Vale operation at Sudbury [11]. The increment of heavy metal species in effluents has become a major environmental concern at Vale since the concentration of heavy metal species in

Vale's treated wastewater might exceed the limit of government regulations. Since Cu-DETA complexes are very stable at the wastewater stream and could not be precipitated by raising the pH above 11 with lime addition [10], it is essential to develop an effective method to control DETA level as well as to reduce the concentration of copper species in waste effluents. The following strategies have been developed at Vale to control DETA level with the target to control the heavy metal concentrations [11]: (1) To develop DETA replacements as pyrrhotite depressants. (2) To reduce DETA concentration in liquid phase in wastewater stream based on the understanding of DETA adsorption mechanism on minerals and DETA species distributions, such as maximizing DETA adsorption onto pyrrhotite and rock tailings while minimizing DETA desorption from mineral surface into effluents during mineral processing and the disposal of tailings. (3) To add adsorbents to capture additional free or complexed DETA in the tailings water. Dong and Xu [11] investigated how to reduce DETA residual in tailing water with the mixture of zeolite and flotation tailings. They compared the DETA adsorption and desorption properties on pyrrhotite, rock tailings, natural zeolite and the mixtures. It was demonstrated that natural zeolite was a potential adsorbent for DETA and DETA-metal complexes. In addition, the tailings could adsorb extra DETA or metal-DETA complexes by the addition of small amount of zeolite [11].

2.2 Current Technologies for Heavy Metal Removal

Many technologies for removing heavy metal ions were considered to meet the mandatory discharge regulations of waste effluents. The most common technologies include chemical precipitations, ion exchange, reverse osmosis, ion flotation and adsorption, etc. A brief review of these existing technologies for heavy metal removal is introduced below [17, 18].

2.2.1 Ion exchange

The ion exchange process relies on the exchange of certain specific undesirable cations or anions in wastewater with sodium, hydrogen, chloride, etc. in porous polymer resins of either a styrene or an acrylic matrix. The ion exchange process could be stopped if the treated solution exhausts the resin exchange capacity. The exhausted resin can be regenerated by stripping off the captured ions in the ion exchange operation using other chemicals then converting the resin back to its initial composition for the next cycle use.

2.2.2 Reverse osmosis

Reverse osmosis (RO) is a membrane-technology filtration method that removes many types of large molecules and ions from solutions by applying pressure to the solution when it is on one side of a selective membrane. The result is that the solute is retained on the pressurized side of the membrane and the pure solvent/water is allowed to pass to the other side. To be "selective", this membrane should not allow large molecules or ions through the pores but should

allow smaller components of the solution (such as the solvent or water) to pass freely.

2.2.3 Ion flotation

The ion flotation involves the removal of surface-inactivate ions from aqueous solutions by the addition of surfactants to form ion-surfactant pairs. The subsequent passage of gas bubbles through the solutions is for flotation.

2.2.4 Precipitation

Precipitation is a well-known process capable of removing heavy metals from solutions [19, 20]. Hydroxide precipitation, for example, is an effective and easy method to remove large quantities of heavy metals from wastewater. The solution pH is enhanced by the addition of sodium hydroxide or lime. The metal hydroxides precipitate when the pH increased to exceed the solubility of metal hydroxides, reducing the metal concentrations in solutions. The precipitation method has been extended to industry application due to its simplification. However, problems associated with metal precipitations include the solid-liquid separation, the disposal of the voluminous sludge with a high water content, and inappropriate disposal of unstable precipitates which may potentially lead to secondary contamination of water because metal ions can be leached out from the precipitated sludge.

Moreover, as previously stated, copper ions and nickel ions at Vale wastewater stream could form stable complexes in the presence of DETA. The stable metal-

DETA species could not precipitate by adjusting pH to 11 using lime [11]. Thus, precipitation is not a satisfied method to reduce heavy metal concentrations in the presence of strong chelating agents.

2.2.5 Adsorption

The adsorption process is based on the adsorption of soluble contaminants onto solid adsorbents. Various materials, including sandstone, fly ash, natural minerals and other surface reactivate adsorbents have been widely used in wastewater treatment. Significant progresses have been developed in the past two decades. The adsorption process is capable for removing most contaminant species like heavy metal and organic compound from solution [21].

2.3 Use of Activated Carbon in Wastewater Treatment

Activated carbon has been used as an effective adsorbent due to its porous structure with a large surface area ranging among 500 ~ 2000 m^2/g [22, 23]. Activated carbon is able to adsorb different types of pollutants such as phenols [24], dyes [25], organic compounds, and specific metal ions [26-28]. Koshima and Onishi [29] studied the adsorption behavior of a series of metal ions, including Cu (II), Ni (II), Cd (II), Ce (III) etc. onto activated carbon in a pH range from pH 1 to pH 13. Marzal, Seco, and Gabaldon [30] investigated the effect of activated carbon on the adsorption of heavy metal ions in single component solutions with Cu (II)/Ni (II) and in binary component solutions with Cu (II)-Ni (II), Cu (II)-Cd (II), and Cu (II)-Zn (II) as a function of temperature, pH and metal ions vs. carbon ratio. A study about the removal of Cu (II) and Pb (II) ions from effluents by using activated carbon generated from hazelnut husks was reported by Imamoglu and Tekir [31].

Activated carbon used for water treatment is available in two main types: powdered activated carbon (PAC) and granular activated carbon (GAC). Most research work regarding the removal of pollutants from wastewater has been conducted by using GAC due to the fact that the GAC is easier to be isolated from the bulk fluid by screening or classification. PAC is less practical in the wastewater treatment since it is not efficient to be separated from the waste stream. However, PAC requires lower capital cost and less contact time than GAC [32].

Moreover, activated carbon is a not low-cost material hence its usage can sometimes be restricted due to economic considerations in spite of the efficiency and applicability for adsorbing various contaminants [33]. The activation and regeneration are great concerns of the activated carbon application in industry.

Therefore, the use of activated carbon in industry for wastewater treatment is limited since it is difficult to be separated from solutions and comparably expensive. In addition, the regeneration of the adsorbent and the cost for the loss of activated carbon need to be addressed.

2.4 Magnetic Carrier Technology

Magnetic carrier technology (MCT) refers to the tailoring of physical, chemical and surface properties of magnetic particles to enable selective or non-selective attachment of metal ions, small molecules, macromolecules, biological cells, and colloidal particles onto magnetic particles [34]. MCT was originated in the early 1940s from the study on wastewater treatment where the objective was to adsorb organic matter onto small magnetite (Fe_3O_4) particles and to subsequently separate the loaded magnetite from the process liquor by magnetic separation [35]. MCT technology extended its application to the adsorption of organic dyes by polymer coated magnetic particles, to the acceleration of sewages coagulation [36, 37], and to the uptake of heavy toxic metals and the purification of the hazardous wastewater by magnetic filtration/adsorption technology [18, 38, 39].

2.4.1 Magnetite

The magnetite (Fe_3O_4) has been investigated as adsorbent for some hazardous species. Most studies reported so far focus on laboratory scale without attempts to be applied at larger pilot or industrial scales [40].

The magnetite crystal structure is inverse spinel with a unit cell consisting of 32 oxygen atoms in a face centered cubic structure and a unit cell edge length of 0.839 nm [41]. The magnetic property of magnetite is due to the inter-valence charge transfer between Fe (II) in tetra sites and Fe (III) in octahedral sites [40]. The natural magnetite often results from the biological processes and lithogenic origin [42].

Magnetite (Fe_3O_4) exhibits some properties similar to metal, which is different with other forms of the iron oxides (e.g. goethite, hematite, and maghemite) [42]. Magnetite can be found commonly in igneous and metamorphic rocks.

A series of methods to synthesize magnetite with specific characteristics have been developed. Olowe and Genin [43] reported the difference in morphology and composition of synthetic magnetite from various routes which included reduction of hematite at 400 ℃ in hydrogen/air mixture as reducing atmosphere and oxidation of ferrous sulphate at alkaline condition by potassium nitrate. Ragazzoni et al. [44] investigated the method to synthesize magnetite from alkaline hydrolysis of ferrous sulphate followed by calcination at 500 ℃. Co-precipitation of magnetite from solution results from the alkaline hydrolysis of Fe (II) and Fe (III) salts in strong alkaline conditions. Several factors such as the alkali emulsifier, reaction temperature, and reaction time affect the formation of final product [45-48].

Erdemoğlu and Sarıkaya [49] investigated the hydration of iron oxide particles and the adsorption mechanism of heavy metal ions onto magnetite from the view of the zeta-potential of magnetite before and after heavy metal ions addition. In aqueous systems, iron oxide particles are hydrated and FeOH groups cover the surface of iron oxide particles completely. A charge of magnetite surface could be developed due to amphoteric dissociation of the surface hydroxide groups like $M^{x+}(OH)_x$ (aq) [50, 51]. The amphoteric dissociation reactions of hydrated iron oxide particles can be expressed in either path as follows, depending on aqueous environment.

$$Fe \cdot OH + H^+ \leftrightarrow Fe \cdot OH_2^+$$

$$Fe \cdot OH \leftrightarrow Fe \cdot O^- + H^+$$

$$Fe \cdot OH + OH^- \leftrightarrow Fe \cdot O^- + H_2O$$

The hydroxylated groups on the surface are available to react with H^+ or OH^- ions in solutions to form positively charged $FeOH_2^+$ or negative FeO^- depending on the pH of the electrolyte solution.

The surface charge of metal oxides dispersed in water is a highly pH-dependent phenomenon [52]. The isoelectronic point (IEP) of magnetite is around 4 - 7 at room temperature depending on the source of magnetite particles (synthetic or natural) and the way of synthesizing magnetite [49, 53]. Sun et al. [54] summarized that the hydroxyl groups on magnetite surface was protonated ($Fe \cdot OH_2^+$) at pH < IEP of magnetite and was negatively deprotonated ($Fe \cdot O^-$) at pH > IEP of magnetite.

The affinity between heavy metal ions and metal oxides of adsorbent surface can be usually stated as one of the following processes [55],

1) The exchange of metal ions in solution (M^{m+}) with the hydroxyl groups on adsorbent surface ($-M'OH$, surface chelation or surface complexation):

$$M^{m+} + n - M'OH\ (surface) \leftrightarrow -(M'O)_n mM^{m-n} + nH^+$$

2) The heavy metal ions in solution (M^{m+}) hydrolyze first, then the hydrolysis species adsorb onto oxides surface:

$$M^{m+} + nH_2O \leftrightarrow M(OH)_n^{(m-n)+} + nH^+$$

$$M(OH)_n^{(m-n)+} + surface \leftrightarrow M(OH)_n^{(m-n)+} \cdot surface$$

3) The electrostatic interaction between metal ions and metal oxides surface.

A large library of data pertaining to the adsorption of metal ions onto various iron oxides is available. However, it is important to further understand the adsorption process of various heavy metal ions onto magnetite particles.

2.4.2 Magnetic carrier technology

Magnetic carriers after loading target species such as metal ions and waste organic matter can be captured by applying a magnetic field, leading to an efficient separation from effluents. The application of MCT in the removal of contaminants from effluents is shown in Figure 2.2 [17, 56]. Magnetic component could be dispersed in effluent to adsorb contaminants. After complete adsorption, magnetic carriers could be easily separated from solutions by applying an external magnetic field.

Gédinas et al. [57] tried to couple DETA to functionalized magnetic carriers to reduce the copper ions from dilute streams utilizing the strong chelating effect between copper ions and DETA. Cu (II) from dilute streams was selectively adsorbed by the DETA-functionalized magnetic carriers prepared by γ-Fe_2O_3. The

results were confirmed by the complexmetric titration using a copper selective electrode [58, 59].

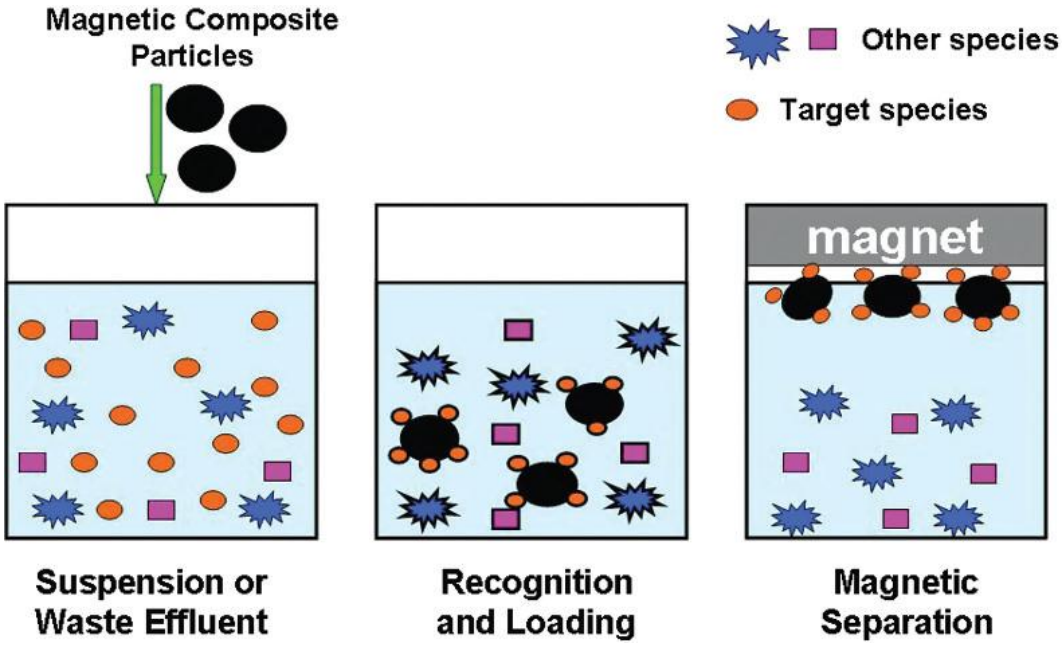

Figure 2.2 Magnetic carrier technology

2.4.3 Magnetic activated carbon

As aforementioned, activated carbon is widely used in the removal of organic or inorganic contaminants from wastewater due to its high surface area, porous structure, and specific surface reactivity. However, it is difficult to completely recover the activated carbon by screening or classification after adsorption. Thus, the applications of activated carbon are limited due to the difficulty in separation and high cost of materials. Our idea is to coat magnetic particles on the surface of activated carbon. The features of activated carbon such as porous structure and

high surface area are utilized with the magnetic properties of magnetite by depositing the magnetic particles on activated carbon.

Oiliveira et al. [60] investigated the preparation of iron oxide modified activated carbon by co-precipitation method and its application in organic compound adsorption. The characterization results by powder X-way diffraction (XRD), thermo-gravimetric analysis (TGA), magnetization measurements, chemical analyses, and Mössbauer spectroscopy suggested the magnetic phase of iron oxide modified activated carbon was the mixture of maghemite (γ-Fe_2O_3) and magnetite (Fe_3O_4). Then they reduced maghemite to magnetite by treating iron oxide modified activated carbon with H_2 at 600 ℃ from temperature programmed reduction (TPR) profiles. The adsorption of volatile organic compounds, e.g. phenol, chloroform and chlorobenzene from solutions onto synthetic iron oxide modified activated carbon were studied. Yang et al. [61] tried to impregnate Fe_3O_4 particles into pores of modified activated carbon with the assistance of an ultrasonic bath in the study of the removal of dye, methylene blue (MB) from effluents. To validate the structure of iron oxides inside porous carbon, X-ray diffraction (powder XRD) and transmission electron microscopy (TEM) were employed.

Cu (II), Co (II), Cd (II) adsorption onto carbon-encapsulated magnetic nanoparticles (CEMNPs) were studied and compared with those adsorption onto pure activated carbon by Pyrzyńska and Bystrzejewski [62]. They investigated the adsorption of heavy metal ions onto activated carbon, carbon nanotubes, and

CEMNPs as a function of pH and initial metal concentrations. They confirmed that activated carbon had a lower affinity of metal ions than CEMNPs does, even though the MB-relative surface area of activated carbon was obviously higher than that of CEMNPs. They suggested that the adsorption mechanism of cations may vary at various pH values since the pH affects the structure of the adsorbent surface and the structure of adsorbate existing in the aqueous solution. It is commonly believed that the adsorption mechanism is attributed to the interaction between the metal ions and the surface functional groups (e.g. -COOH) on the surfaces of carbon adsorbents [63]. Pyrzyńska and Bystrzejewski [62] introduced the concept of surface charge density (SCD) to compare the adsorption efficiencies among different carbon materials. They drew the conclusion that the low SCD resulted in weak probability of appearance of the sites with the divalent negative charge (i.e. two carboxylic groups located in a confined area). The adsorptions of metal ions on the surfaces of carbon-based materials were strongly affected by surface characteristics of adsorbents.

2.5 Carbon-in-Pulp in Gold Recovery

Cyanidation is an important process of extracting gold from its ores in the past 100 years [64]. The carbon-in-pulp (CIP) process has been an alternative form rather than zinc cementation for gold recovery from cyanide solutions in gold extraction industries since CIP was introduced in 1880 [65, 66]. The principle of the gold extraction method with activated carbon is to attack the minerals with aqueous potassium cyanide solution in presence of air and to transform gold metal to gold cyanide which is preferentially adsorbed onto activated carbon [67, 68]. The adsorption of gold onto activated carbon and the regeneration of the activated carbon for reuse are two very important processes in the cyanidation process of gold leaching and recovery [69].

Several investigations regarding the mechanism of the adsorption of gold cyanide on activated carbon have been carried out. Even though the exact mechanism of gold cyanide adsorption onto activated carbon is not quite clear, it is generally accepted that: (1) The extraction of $Au(CN)_2^-$ is strongly enhanced with the presence of electrolytes such as KCl or $CaCl_2$ in the adsorption medium. (2) The adsorption is strongly pH dependent: adsorption could be increased by enhancing the acidity of the adsorption effluents. The possible mechanisms of aurocyanide adsorption on activated carbon were hypothesized by researchers. Those different mechanisms for the gold cyanide adsorption onto activated carbon could be summarized as follows [69]:

1) Gold is present as aurocyanide ions.

2) Gold is present as a compound other than the aurocyanide ion (e.g., precipitated AuCN).
3) Aurocyanide is reduced to metallic gold.

McDougall et al. [69] studied the gold cyanide adsorption on activated carbon with or without electrolytes and acids with X-ray photoelectron spectroscopy (XPS). They found that gold had an oxidation state of Au (I) after loaded on the surface of activated carbon. Thus, they postulated that the aurocyanide adsorption onto activated carbon involved the adsorption of less soluble $M^{n+}[Au(CN)_2]_n$ complex ($M = Na^+$, K^+, Ca^{2+}, H^+) at the initial adsorption stage, and followed by a reduction step in which either a sub-stoichiometric $Au(CN)_x$ surface species or a cluster-type compound of gold was formed.

Even though the mechanism of gold cyanide adsorption onto activated carbon is not clear at present, the CIP process has already been used successfully in commercial gold mine. Chapman [70] patented the process of using activated carbon for the gold recovery in 1943. Fine activated carbon was added to a cyanide pulp to adsorb gold. The loaded carbon was recovered by floating in the presence of a frother. The flotation froth was collected and then smelted for gold extraction.

The most challenge in CIP is to establish a suitable means of stripping adsorbed gold from loaded carbon [71]. In the early process to recovery gold from slime at the Gechell Mine in Nevada, the loaded granular carbon was smelted to recover gold, followed by electro winning which was a costly procedure [72]. The carbon process in gold recovery did not get great improvement until the Zadra process was

developed [73]. In Zadra process, thermal reactivation and regeneration of chemically eluted carbon were employed before carbon recycle at about 650 ℃ in the absence of air in an indirectly fired rotary kiln.

In addition, the particle size of activated carbon has a significant effect on the rate of gold adsorption according to Davidson's preliminary study about the activated carbon in gold-plant solutions [71]. Cho et al. [74, 75] found that the size of carbon granules affected the initial rate of gold adsorption and observed faster rates for the smaller size fractions. Here comes the problem that the smaller particles of activated carbon are harder to be separated from liquids with traditional methods.

Based on the previous review, objectives of this research are to develop an effective and uncomplicated method to prepare M-AC, to characterize synthesized M-AC, to study the adsorptive behavior of M-AC for potential contamination species (copper, nickel and DETA) and compare with that of activated carbon or iron oxides, to model the adsorption data to get a satisfactory adsorption isotherm, to investigate the recycle and reuse of M-AC and to study the potential use of M-AC in gold recovery.

CHAPTER 3 EXPERIMENTS

3.1 Materials

Ferric chloride hexahydrate ($FeCl_3\ 6H_2O$), ferrous chloride tetrahydrate ($FeCl_2\ 4H_2O$), sodium hydroxide (NaOH), copper sulfate pentahydrate ($CuSO_4\ 5H_2O$), nickel sulfate hexahydrate ($NiSO_4\ 6H_2O$) and hydrochloric acid (HCl, 1 M) were purchased from Fisher Scientific (Canada) with reagent grade and used as received. Potassium dicyanoaurate (I) ($KAu(CN)_2$, trace metal basis) was purchased from Sigma-Aldrich Inc. (USA) and used as received. Activated carbon (-100 mesh) was purchased from Sigma-Aldrich Inc. (USA), followed by screening the particle size in the range of 45 ~ 106 μm prior to use. Unless otherwise stated, all the experiments were carried out with deionized water prepared by Elix-5 system followed by purification with a Millipore-UV unit with final resistance of 18.2 MΩ.

3.2 Methodology

3.2.1 X-ray diffraction (XRD)

X-ray technique is based on observing the scattered intensity of an X-ray beam hitting a sample as a function of incident and scattered angle, polarization and wavelength or energy of the incident X-ray beam. X-ray diffraction pattern is direct evidence for the periodic atomic structure of crystals postulated according to the Bragg's law:

$$n * \lambda = 2d * sin\theta$$

where n is an integer, the variable λ is the wavelength of the incident X-ray beam, the variable d is the distance between atomic layers in a crystal, and θ reflects the X-ray beams at certain angles of incidence.

In this study, the crystal structure of sample was determined using a powder x-ray diffraction system, RIGAKU rotating anode XRD system (Rigaku Corp., Japan) equipped with Rigaku RU-200B as generator which used copper as anode target. The power was set at 40 Kv, 110 mamp s. Refelctive mode (scan both the theta and 2 theta axis) was employed.

3.2.2 Magnetization measurement

The magnetization curve measurement was carried using Torque Magnetometer in physical property measurement system (Quantum Design 9T-PPMS magnetometer, Quantum Design Inc., USA). A magnetic field in the range of ± 30

kOe at 300 K with 100 Oe scanning per second was used for magnetization measurement. The samples were sealed in plastic wrap and then mounted on a sample holder.

The Torque Magnetometer option performs angular-dependent measurements of the magnetic torque $\tau = m \times B$ experienced by a sample of magnetic moment m in an applied magnetic field B. When the torque of the samples is known, the moment of the sample can be determined.

3.2.3 Surface area/pore size analyzer

The surface areas of materials were determined through gas adsorption analysis based on BET theory, an extension of Langmuir theory. BET theory is a theory of multilayer gas adsorption with the following hypotheses: (a) physical adsorption of gas molecules on a surface; (b) no interaction between each adsorbed gas layer; and (c) Langmuir theory is applicable to each adsorption layer [9].

Surface area and pore size distribution measurements were conducted by Autosorb-1-MP (Quantachrome Instruments, USA) with nitrogen as probing gas. All the samples were degased at room temperature for 12 hours prior to adsorption/desorption process. Seven points of adsorption, five points of BET followed by seven points of desorption were chosen for measurements.

3.2.4 Total carbon analyzer

The carbon content in M-AC particles were measured through CM5300 Furnace module (UIC Inc., USA) followed by CM5015 CO_2 coulometer (UIC Inc., USA). The combustion temperature was selected at 1100 ℃ to completely oxidize all forms of carbon. The sample combustion gases are swept through the barium chromate catalyst/scrubber to ensure complete oxidation of carbon to CO_2. Non-carbon combustion products, such as SO_2, SO_3, H_X and NO_x, are removed from the gas stream by a series of chemical scrubbers. The CO_2 is then measured with the CO_2 coulometer.

The coulometer is used as the detector with different carbon front-end units to detect carbon. The coulometer cell is filled with a proprietary solution containing monoethanolamine and a colorimetric pH indicator. The cell assembly is then placed in the coulometer cell compartment between a light source and a photodetector in the coulometer. As a CO_2-containing gas stream passes into the cell, the CO_2 is quantitatively absorbed, reacting with the monoethanolamine to form a titratable acid. This acid causes the color indicator to fade. Photodetection monitors the change in the color of the solution as a percent transmittance (% T). As the % T increases, the titration current is automatically activated to electrochemically generate base at a rate proportional to the % T. The current stops when the solution returns to its original color (original % T). The titration current is measured continually and integrated to operator selected units.

3.2.5 Laser particle sizer

The particle size distributions were measured by laser particle sizer (Malvern Mastersizer 2000, UK). The Mastersizer 2000 is a laser diffraction-based analyzer capable of testing the size distribution ranging from 0.02 to 2000 micrometer.

A Mastersizer 2000 system is made up of three main parts: optical bench, sample dispersion unit and instrument software. A dispersed sample passes through the measurement area of the optical bench, where a laser beam illuminates the particles. A series of detectors then accurately measure the intensity of light scattered by the particles within the sample over a wide range of angles. Sample dispersion is controlled by a range of wet and dry dispersion units. These ensure the particles are delivered to the measurement area of the optical bench at the correct concentration and in a suitable, stable state of dispersion. The Mastersizer 2000 software controls the system during the measurement process and analyzes the scattering data to calculate a particle size distribution. Deionized water was used as dispersant.

3.2.6 Scanning electron microscope (SEM)

A scanning electron microscope (SEM) is a type of electron microscope that images a sample by scanning it with a beam of electrons in a raster scan pattern. The electrons interact with the atoms that make up the sample producing signals containing information about the sample's surface topography, composition, and other properties such as electrical conductivity.

The types of signals produced by a SEM include secondary electrons (SE), back-scattered electrons (BSE), characteristic X-rays, light (cathodoluminescence), specimen current and transmitted electrons depending on various models. Secondary electron detectors are common in all SEMs. The signals result from interactions of the electron beam with atoms at or near the surface of the sample. In the most common or standard detection mode, secondary electron imaging (SEI) can produce very high-resolution images of a sample surface, revealing details less than 1 nm in size. Due to the very narrow electron beam, SEI micrographs have a large depth of field yielding a characteristic three-dimensional appearance useful for understanding the surface structure of a sample.

Backscattered electrons (BSE) consist of high-energy electrons originated from the electron beam which are reflected or back-scattered out of the specimen interaction volume by elastic scattering interactions with specimen atoms [77]. Heavy elements which with higher atomic numbers enable to backscatter electrons strongly than light elements with lower atomic numbers appear brighter in the image compared with lighter elements. Backscattered electrons combined with energy-dispersive x-ray spectroscopy (EDS) which relies on the interaction of some source of X-ray excitation and sample are used to detect the contrast between areas with different chemical compositions.

Two different models of scanning electron microscope were employed to study the particle morphology in this project:

a) Hitachi S-2700 Scanning Electron Microscope

Hitachi S-2700 scanning electron microscope (Hitachi High Technologies America, Inc., USA) equipped with a PGT (Princeton Gamma-Tech, USA) IMIX digital imaging system and a PGT PRISM IG (Intrinsic Germanium, USA) detector for energy dispersive X-ray spectroscopy (EDS) was used in this study.

The backscattered electron detector (electronics system 47 four quadrant solid state backscattered electron detector) was used. Backscattered electrons (BSE) are beam electrons that are reflected from the sample by elastic scattering. BSE are often used in analytical SEM along with the spectra made from the characteristic X-rays, because the intensity of the BSE signal is strongly related to the atomic number (Z) of the specimen. BSE images can provide information about the distribution of different elements in the sample. Characteristic X-rays are emitted when the electron beam removes an inner shell electron from the sample, causing a higher-energy electron to fill the shell and release energy. These characteristic X-rays were used to identify the composition and measure the abundance of elements in the sample.

b) SEM-Vega 3

Scanning electron microscope Vega-3 (Tescan, Czech Republic) was equipped with EDXS detector (Oxford Instruments, UK). The Vega 3 was set at high vacuum mode (pressure $< 3 \times 10^{-3}$ Pa). EDXS was set at 133 eV resolutions.

3.2.7 Zeta-potential measurement

Zeta-potential measurements were carried out by Brookhave ZetaPALS (Brookhave Instruments Corp., USA). Surface charges of fine particles were measured in aqueous solution using phase analysis light scattering to determine the electrophoretic mobility of charged suspension.

3.2.8 Trace nitrogen analysis

Nitrogen analysis was conducted on an Antek 9000 Series Nitrogen/Sulfur Analyzer with 735 syringe model (Antek/PAC, Houston, USA). Antek 9000NS Analyzer has two detector channels: channel A (detector A) was designed to detect nitrogen, and channel B (detector B) was designed for sulfur. In this study, only the nitrogen signal in channel A was recorded and analyzed.

For nitrogen analysis, the oxidant furnace temperature was set at 1050 ℃. The mass flow of gases was set at: inlet argon, 130 ml/min; inlet O_2: 25 ml/min; Pyro O_2: 450 ml/min and nitrogen ozone: 35 ml/min. A certain amount of liquid sample (10 μL) was injected into the furnace via the 735 syringe for analysis. Standard solutions of DETA ranging in concentration from 0 to 25 mg/L were used to acquire calibration curve. The amount of DETA in sample was calculated according to the calibration curve of channel A.

3.2.9 Atomic absorption spectroscopy (AAS)

Atomic absorption spectroscopy was conducted in a SpectrAA 220FS (Varian Inc., USA) to determine the total concentration of Cu, Ni, Fe and Au in solution. SpectrAA 220FS is a double beam system using flames to atomize samples. The absorbance can be used to quantitatively determine the Cu/Ni/Fe/Au concentration in the solution according to the Beer-Lambert law.

Standard solutions for atomic absorption spectrometry with 1000 mg/L Cu/Ni/Fe/Au were purchased (Fisher Scientific, USA) and diluted to a series of desired concentrations for calibration prior to measurement.

3.2.10 Time-of-flight secondary ion mass spectroscopy (TOF-SIMS)

TOF-SIMS refers to a powerful surface analytical technique which is a combination of secondary ion mass spectroscopy (SIMS) and time-of-flight mass spectrometer. When fast ions (primary ions) hit the surface of a material, all or partial of their energy is transferred to the target atoms and may cause some of the target atoms ejected as ions (secondary ions). The secondary ions could be separated by a TOF mass spectrometer and detected by a SIMS. Since the secondary ions originate predominantly from surface within 5 nm depth, TOF-SIMS is the most sensitive method among all surface techniques to detect the trace chemicals on the surface.

In this study, TOF-SIMS analysis was completed in an ION-TOF-SIMS IV instrument (ION-TOF GmbH). A Bi^+ ion gun was used as an analysis source,

operating at 15 keV and 0.5 pA. A flood gun was applied to compensate the charging effect of samples during spectra acquisition and ion imaging. TOF-SIMS IV instrument was operated in a burst-alignment mode. The mass spectra for samples were collected from an area of ~ 200 * 200 μm^2.

3.3 Preparation of Magnetic Particles

Procedures for the synthesis of magnetic activated carbon (M-AC) were as follows:

i. Dissolved $FeCl_3$ $6H_2O$ (945 mg, 3.5 mmol), $FeCl_2$ $4H_2O$ (348 mg, 1.75 mmol) in 50 ml deionized water, dispersed 247 mg of commercial activated carbon (45 ~ 106 μm) in solution in a three-necked flask, and prepared 15 ml NaOH solution (5 M).

ii. Stirred mixtures and purged nitrogen into the mixtures for 30 minutes.

iii. Preheated the mixtures at 70 ℃ in an oil bath for 10 minutes.

iv. Added prepared NaOH solution dropwisely to precipitate iron oxides on activated carbon surface slowly. Kept the reaction for 90 minutes.

v. Kept the mixtures overnight.

vi. Washed sample ten times with deionized water to remove uncoated activated carbon. Separated magnetic particles using a hand magnet.

vii. Filtered the sample with 1 μm pore filter paper, rinsed the solid three times with deionized water, and then collected the solids.

viii. Dried samples in a freeze dryer for overnight.

3.4 Batch Adsorption Experiments

The removal of heavy metal ions and DETA species from solution were carried out in solutions with various adsorbate by adding different amount of adsorbents into the solutions. The detailed procedures of sample preparation were as follows:

i. Prepared fresh stock solution for 1000 mg/L DETA, 1000 mg/L $CuSO_4$, 1000 mg/L $NiSO_4$, 1000 mg/L $KAu(CN)_2$ with deionized water.
ii. Diluted the stock solutions to a series of solutions with desired concentrations.
iii. Added solid adsorbents into the desired volume of solutions with pre-set weight.
iv. Mixed sample in a 4 oz bottle for with desired time in a shaker at 300 rpm.
v. Separated adsorbents from solutions by magnetic separation for magnetic adsorbents and filter it with 0.45 μm filter paper for activated carbon; collected clear filtrate for further analysis.
vi. Analyzed metal ion concentrations in filtrate by AAS and DETA amount by trace nitrogen analysis.

Process water simulating the flotation environment at Vale was prepared with 2.0 g $CaSO_4.2H_2O$, 0.38 g $MgSO_4.7H_2O$, 0.6 g $MgCl_2.6H_2O$, 50 mg Na_2SO_3 and 50 mg potassium xanthate (PAX) in 1 L water.

3.5 Stripping Off Species and Regeneration of Magnetic Particles

After Cu (II), Ni (II) or DETA adsorption onto magnetic particles (M-AC or Fe_3O_4), magnetic particles were collected through magnetic separation. The collected magnetic particles were mixed with HCl solutions (dosage: 0.1 wt.% for metal ions and 0.5 wt.% for DETA) with a series of concentrations. The mixture was shaken at 300 rpm for 30 minutes, and then centrifuged at 3500 rpm for 10 minutes. The supernatant was collected and further analyzed using AAS for metal concentration and trace nitrogen analyzer for DETA concentration.

The separated magnetic particles after HCl washing were regenerated through mixing with NaOH solution (dosage: 0.1 wt.% for metal ions and 0.5 wt.% for DETA) of different concentrations or deionized water using a shaker at 300 rpm for 30 minutes, followed by 10 minutes centrifuging at 3500 rpm. Again, the supernatant was collected and further analyzed. Separated magnetic particles were collected for the next cycle of adsorption experiments.

CHAPTER 4 RESULTS AND DISCUSSION

4.1 Characterizations of Magnetic Activated Carbon (M-AC)

4.1.1 Magnetic properties

The obtained M-AC particles were immediately and completely attracted to a magnet when applying a hand magnet as shown in Figure 4.1, suggesting a good magnetic property of synthesized M-AC particles.

Figure 4.1 M-AC particles attracted by a hand magnet

Figure 4.2 shows the hysteresis loop measured at 300 K with the inset presenting the hysteresis in low magnetic field region. The ferromagnetic behavior of prepared M-AC was shown with a saturation magnetization of 38.3 emu/g and a coercivity of 50 Oe. Remanence magnetization of 1.2 emu/g was measured. This indicates the excellent magnetization property of M-AC particles. In addition, the

ferromagnetization behavior of M-AC is similar to that of magnetite, suggesting the magnetic iron oxides phase on M-AC surface could be magnetite.

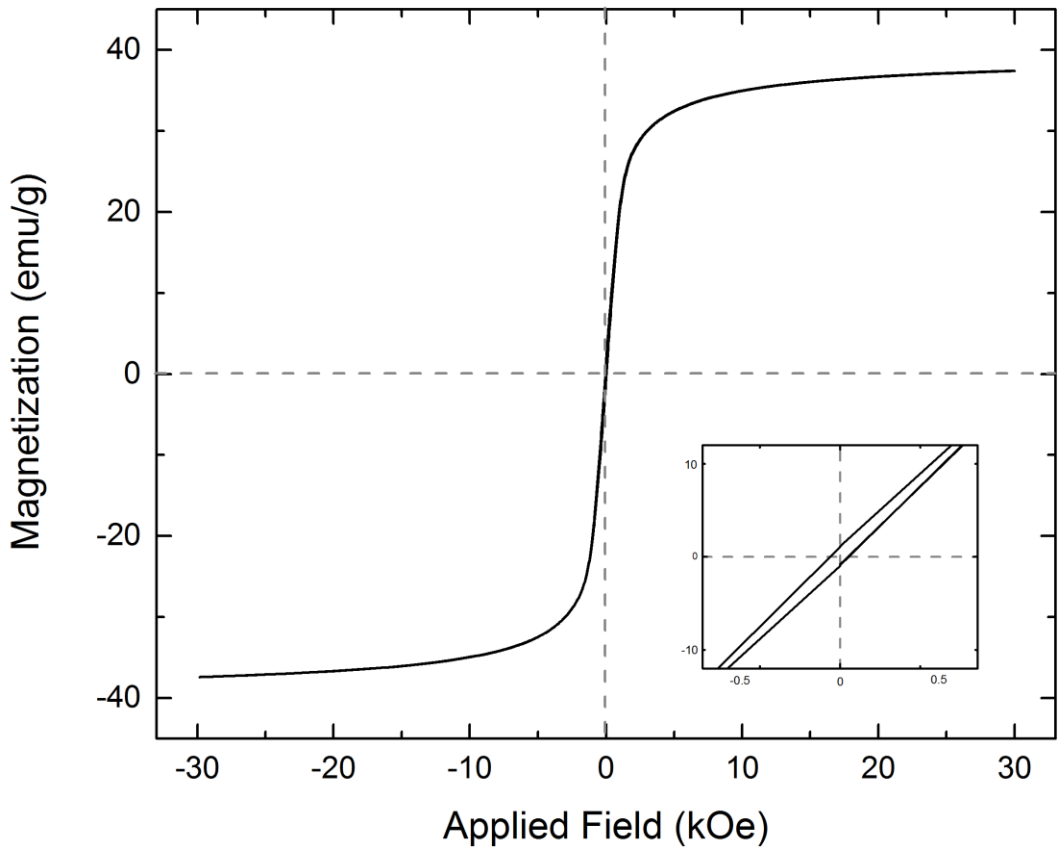

Figure 4.2 Hysteresis loop of M-AC (Inset shows hysteresis in low field region.)

4.1.2 Crystal structure of the iron oxide deposited on M-AC

Figure 4.3 (a) – (c) showed the XRD spectra of M-AC, magnetic iron oxides, and pure commercial activated carbon. The XRD spectrum of M-AC shown in Figure 4.3 (b) suggests the synthesized iron oxide was magnetite (Fe_3O_4), indicating the predominant phase of iron oxides deposited on synthetic M-AC surface was magnetite since the XRD spectra of M-AC and magnetite are consistent. That is consistent with the ferromagnetic behavior of M-AC in Figure 4.2 as magnetite is a typical ferromagnetic material.

The crystal structure and phase of the iron oxide on M-AC could be controlled by different ratios of ferrous vs. ferric ions, pH of solutions, reaction temperature and reaction time [48, 78]. The related chemical reaction is shown as follows:

$$Fe^{2+} + 2Fe^{3+} + 8OH^- \Leftrightarrow Fe_3O_4 \downarrow + 4H_2O$$

Ferrous and ferric ions co-precipitated as the form of Fe_3O_4 on the surface of activated carbon in strong alkaline condition under experiment conditions.

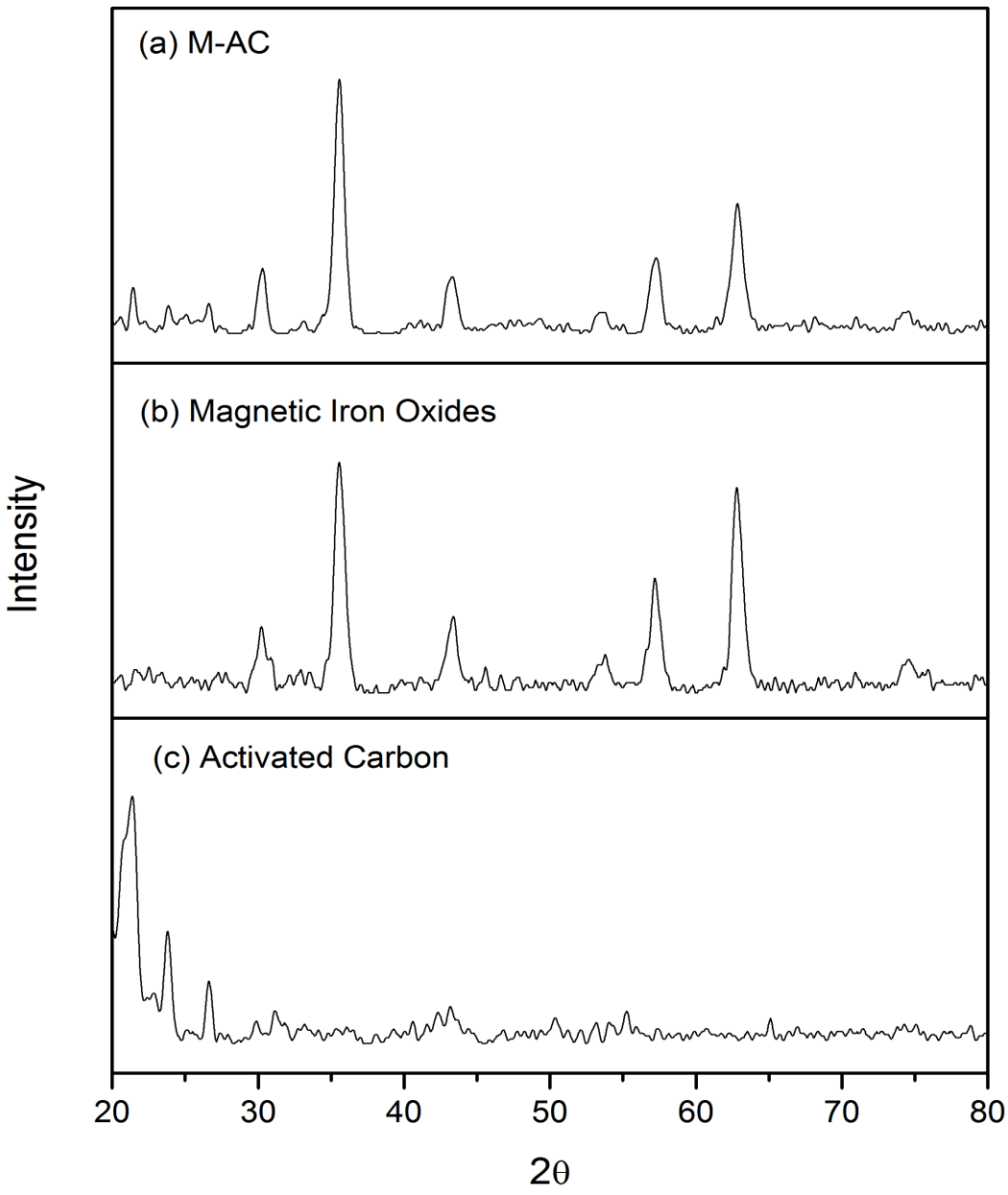

Figure 4.3 XRD spectra of (a) M-AC, (b) synthesis magnetic iron oxides, and (c) pure activated carbon

4.1.3 Particle size, specific surface area and average pore size

Particle size distributions of activated carbon and M-AC are shown in Figure 4.4. After screening to 45 ~ 106 μm, the activated carbon particle size was predominant in the range of 30 ~ 110 μm in diameter, while some fine particles (1 ~ 10 μm in diameter) were still retained due to the difficult separation in sieving. Coated with iron oxides, the size of M-AC particles is in the range of 30 to 110 μm in diameter, similar to the major particle size of activated carbon before Fe_3O_4 deposition. This phenomenon approved that the coated Fe_3O_4 was formed as a thin layer on the surface. In addition, the third peak shown on the particle size distribution graph of M-AC indicated that small amount of Fe_3O_4 formed very fine particles which was very difficult to be separated from M-AC due to the weak magnetic attraction.

Table 4.1 presents the specific surface area and pore size results from N_2 auto sorb measurements. The surface area of pure activated carbon was 1195.8 m^2/g while it was reduced to 543.5 m^2/g of M-AC after coating magnetic iron oxides on its surface. The surface area of Fe_3O_4 was only 56.6 m^2/g, much lower than M-AC. The average pore diameter for M-AC after depositing iron oxides was 38.2 Å which was similar with average pore diameter of pure activated before depositing. According to the total carbon analyzer results, the carbon content in M-AC particle was 27.7 % by weight.

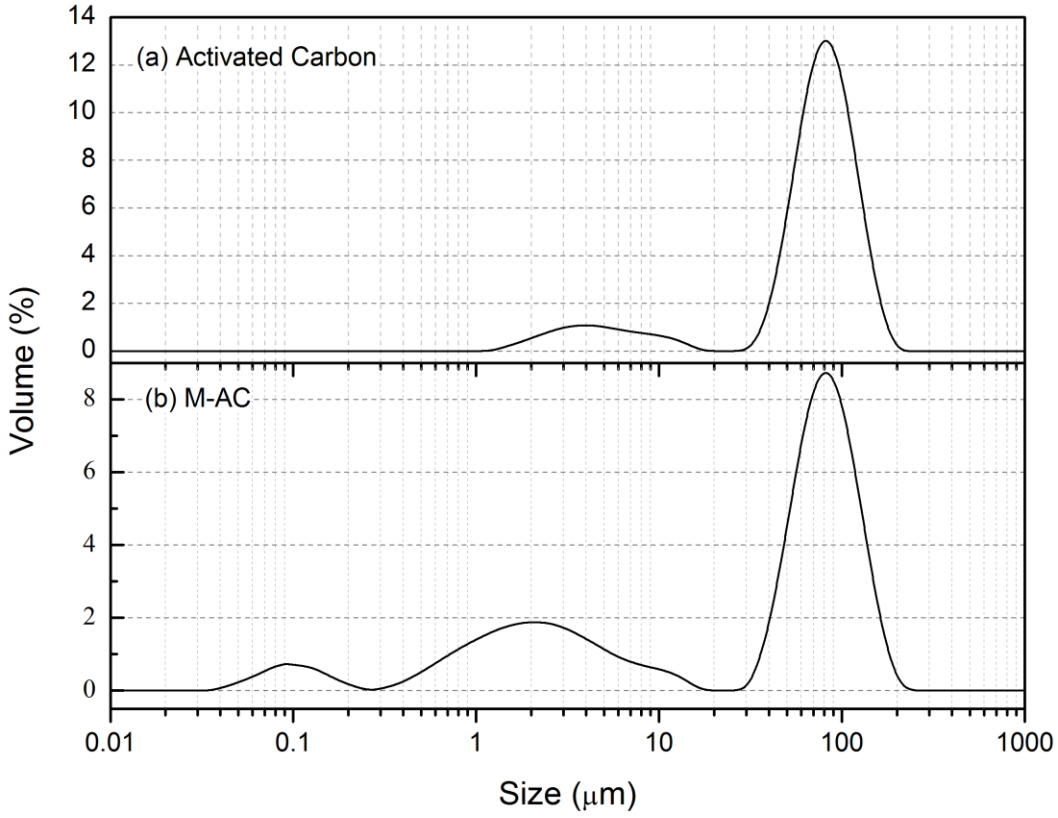

Figure 4.4 Particle size distributions of (a) activated carbon and (b) M-AC

Table 4.1 Surface area and pore size measurements

Sample	Surface area (m^2/g)	Average pore diameter (Å)
Activated carbon	1195.8	36.6
Fe_3O_4	56.6	-
M-AC	543.5	38.2

4.1.4 Micro-morphologies

a) SEM images

The morphologies of activated carbon, synthetic magnetite and M-AC were studied by SEM under BSE mode, respectively shown from Figure 4.5 (a) to (f) with different resolutions. Figure 4.5 (a) and (b) show the images of pure activated carbon after screening. Figure 4.5 (c) and (d) indicate the morphologies of synthetic magnetite. In Figure 4.5 (f), magnetite precipitations with relatively brighter surface pointed out by white arrow could be observed on the relatively darker surface of activated carbon.

b) EDX mapping images

To further study the element distribution on the surface of M-AC, EDX mapping images of C, Fe and O (Figure 4.6) were required. The EDX mapping of C and Fe are complementary to each other. This indicates the coating layer of Fe_3O_4 on the activated carbon in M-AC.

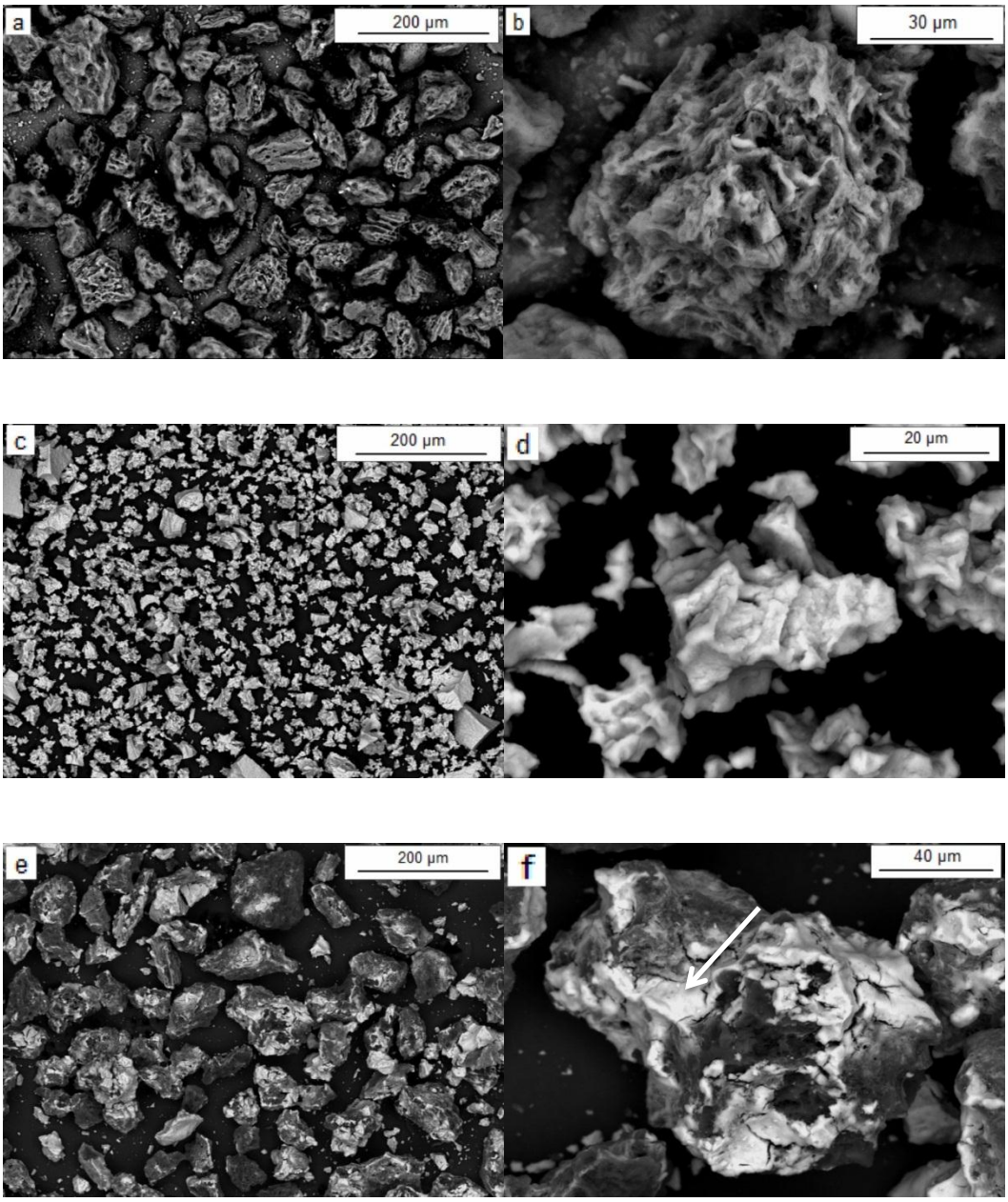

Figure 4.5 SEM images of (a) pure activated carbon, (b) higher resolution of (a), (c) pure Fe_3O_4 particles, (d) higher resolution of (c), (e) M-AC, and (f) higher resolution of (e)

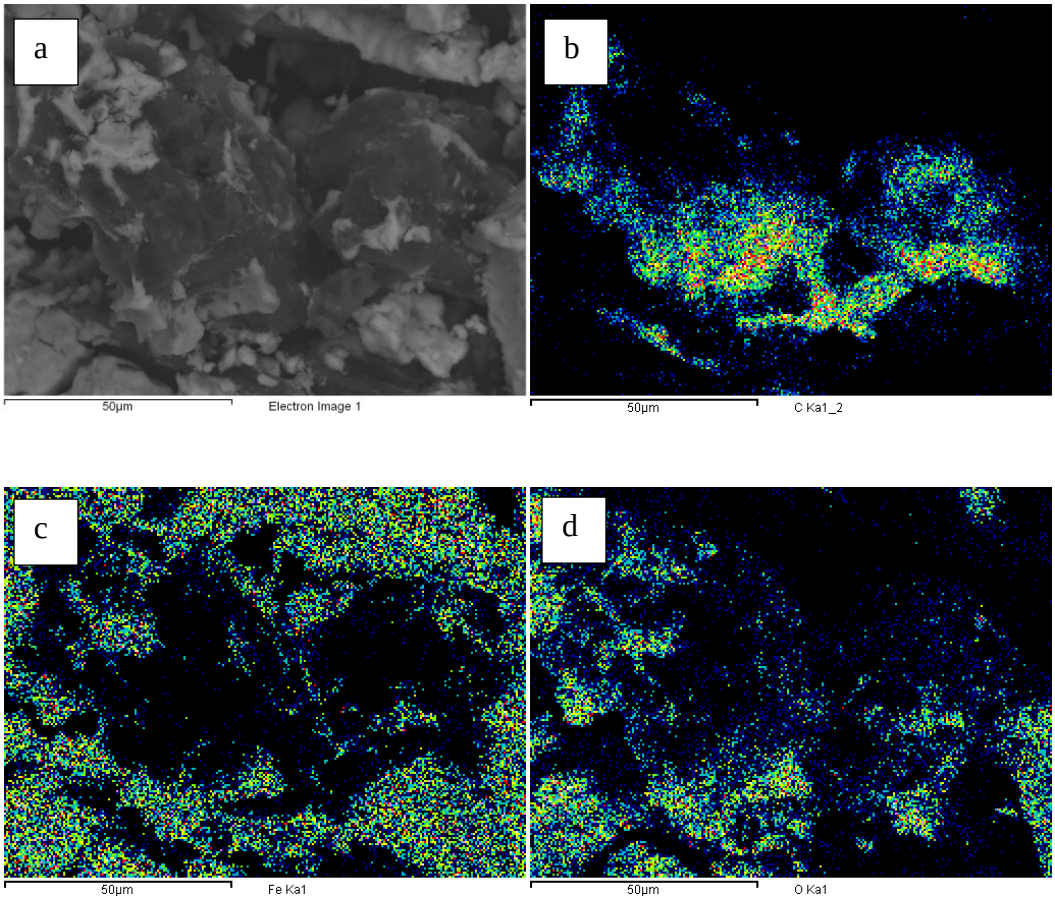

Figure 4.6 (a) SEM image of M-AC, and EDX mapping images of (b) C, (c) Fe, and (d) O for the same area of the SEM image

4.2 M-AC Applications in Single-component Solution

4.2.1 Heavy metal ions adsorption

The effects of adsorbent dosage, contact time, solution pH, and initial metal ion concentrations on the adsorption of Cu (II)/Ni (II) onto M-AC, activated carbon, and Fe_3O_4 were investigated at room temperature. The contact time for batch adsorption experiment was set for 120 minutes since it is far enough to reach equilibrium according to previous kinetic studies for contamination species adsorption [79, 80].

Removal efficiency expressed as removal percentage was used as a significant parameter to investigate the affinity of waste species with various adsorbents. The removal efficiency ($Removal\ \%$) of contaminants was calculated as follows:

$$Removal\ (\%) = \frac{C_i - C_f}{C_i} * 100\% \qquad [4 - 1]$$

where C_i indicates the initial concentration of the specific contaminant in mg/L and C_f, the final concentration of the specific contaminant in mg/L after adsorption.

Firstly, we studied the effect of M-AC dosages (0.5 wt.% and 0.1 wt.%) on the adsorption of Cu (II) with initial Cu (II) concentrations in the range of 5 ~ 25 mg/L. The initial Cu (II) concentration range was used to simulate the copper ion concentration in practical Vale's operation [5]. Figure 4.7 shows that both dosages of M-AC (0.5 wt.% and 0.1 wt.%) could remove more than 99 % copper ions from effluents. To achieve a higher efficiency for practical applications, the

adsorbent dosage 0.1 wt.% was chosen for further studies in copper ions adsorption experiments. As nickel ion is similar to copper ion in size, ion charge and some chemistry properties, the 0.1 wt.% M-AC dosage was also used in the study of nickel ions adsorption onto M-AC particles.

Secondly, the effect of adsorbent contact time on copper ions removal was investigated. As shown in Figure 4.8, the Cu (II) removal efficiency onto M-AC increased sharply with enhancing contact time. The 100 % removal of copper ions was achieved at 60 minutes and kept consistent with more contact time up to 150 minutes, indicating that equilibrium status for copper ions loading was achieved at 60 minutes. The pre-set condition of 120 minutes contact time should be enough to get adsorption equilibrium. As previously stated, the contact time for nickel ions adsorption was also set at 120 minutes due to the similarities between nickel ion and copper ion.

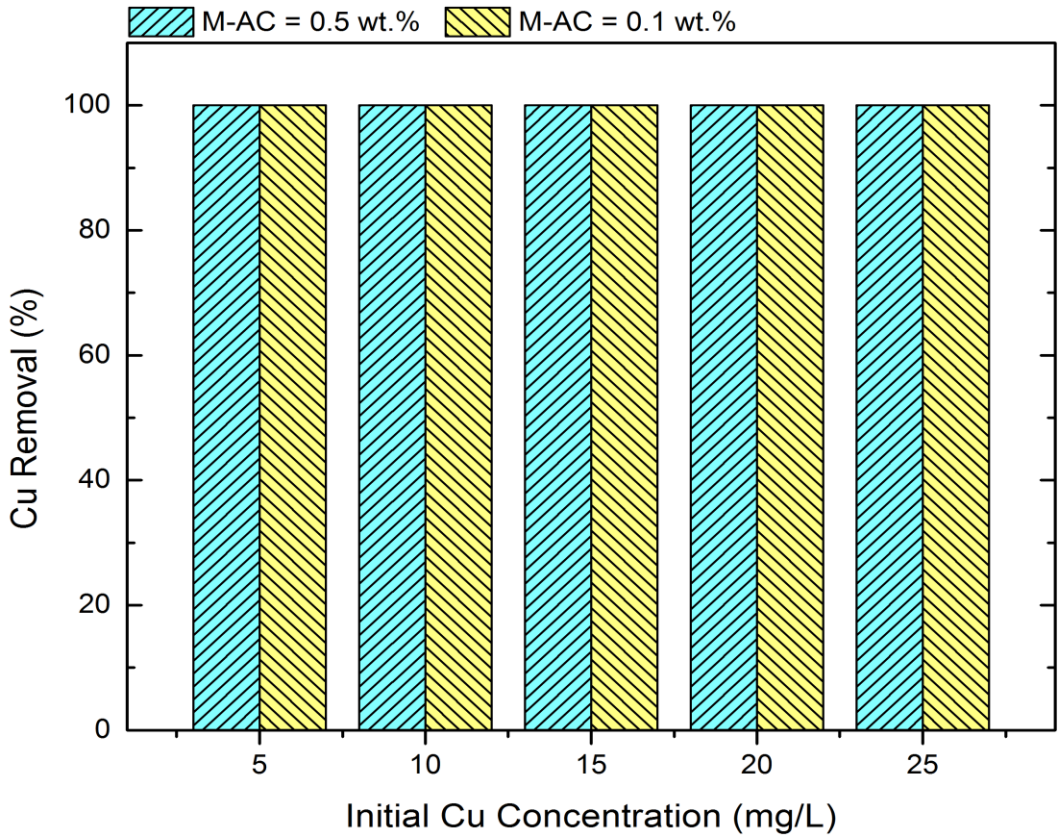

Figure 4.7 Cu (II) removal efficiency by M-AC with different dosages (0.5 wt.% and 0.1 wt.%) as a function of initial Cu (II) concentrations (initial solution pH = 4, contact time = 120 minutes)

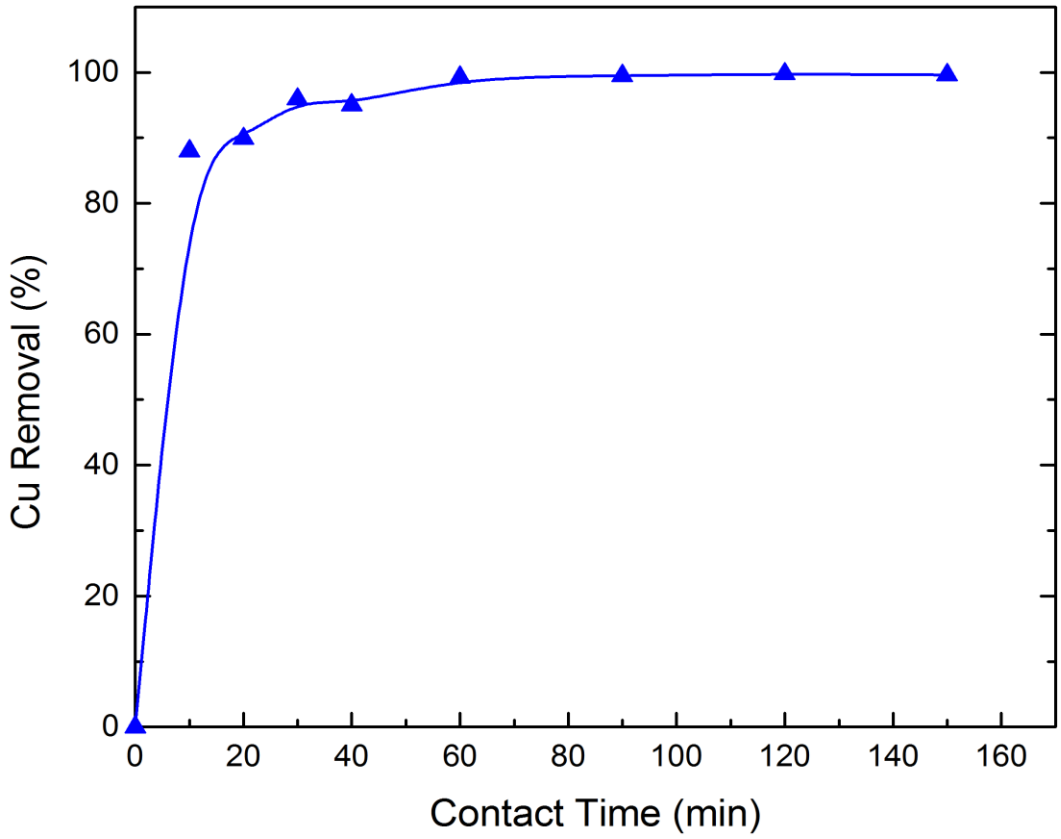

Figure 4.8 Cu (II) removal efficiency by M-AC as a function of contact time (C_i = 10 mg/L, adsorbent dosage = 0.1 wt.%,)

Thirdly, we studied the effects of solution pH on the Cu (II) adsorption onto M-AC and activated carbon respectively (Figure 4.9). The initial Cu (II) concentration was 10 mg/L. For both activated carbon and M-AC, the Cu (II) removal efficiency increased with enhancing pH values. For activated carbon, about 4 % of copper ions were removed at pH 3, and more than 99 % of copper ions were removed at pH 7. For M-AC, the Cu (II) removal efficiency by M-AC was 15 % at pH 3 while it rapidly reached high removal efficiency (> 99 %) at pH 4 and kept the same at higher pH. The previous studies regarding metal adsorption onto various adsorbents suggested metal hydroxides precipitation in alkaline condition may account for heavy metal ion deduction [81]. As copper hydroxides start to precipitate at pH 5 and are predominant at higher pH values [82], high copper removal efficiency (99 %) above pH 5 might be partly attributed to the copper hydroxides precipitation not only as a result of activated carbon or M-AC uptake. At acidic conditions (pH = 3, 4, 5), the removal efficiency of copper ions increased as the pH of aqueous solutions enhanced and increased more significantly by M-AC compared with activated carbon. Pyrzyńska and Bystrzejewski [62] investigated the comparative heavy metal ion adsorption onto different carbon materials, suggesting that the low adsorption in the acidic region could be partially attributed to the competition adsorption between hydrogen ions and metal ions onto the same surface binding sites. In addition, the particle surface becomes more negatively charged with pH increasing (will be discussed later with zeta-potential measurements), leading to an increment of the electrostatic attraction between metal cations and adsorbent surfaces.

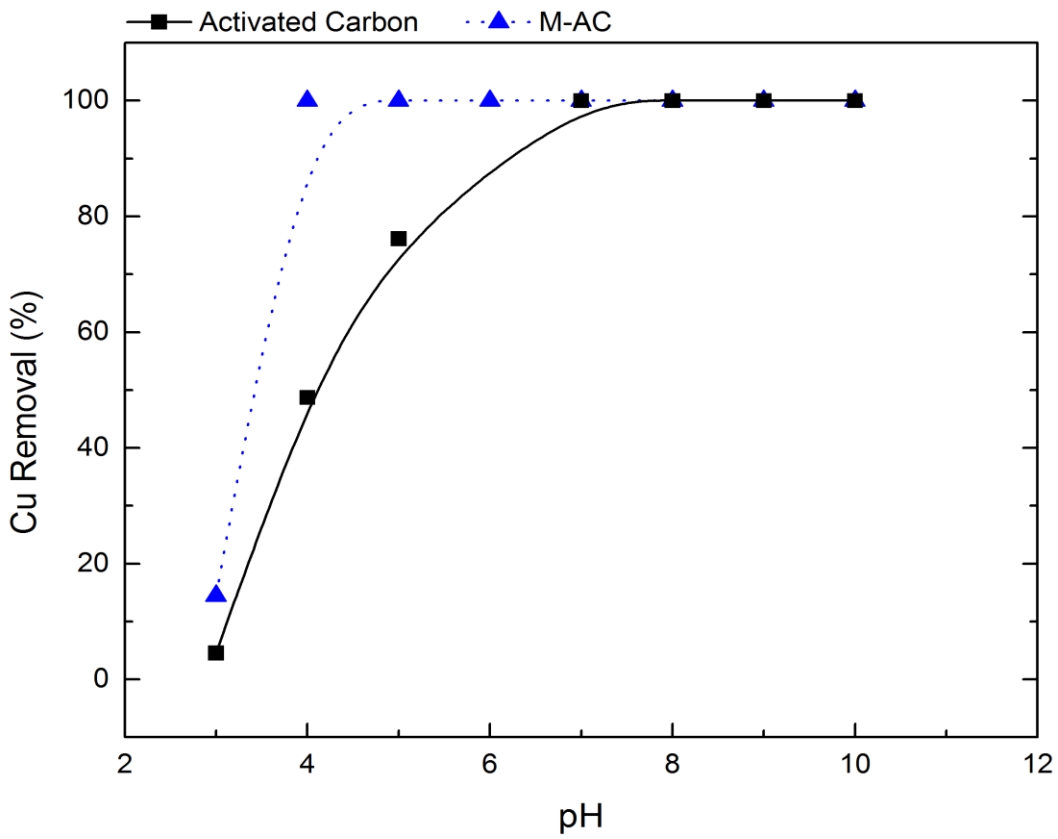

Figure 4.9 Cu (II) removal efficiency by activated carbon and M-AC as a function of pH (C_i = 10 mg/L, adsorbent dosage = 0.1 wt.%, contact time = 120 minutes)

After that, we investigated the maximum heavy metal ions adsorption onto various adsorbents. As aforementioned, M-AC with a lower surface area showed a higher removal efficiency for copper ions than that of pure activated carbon. Thus, Fe_3O_4 which was another major composition in M-AC was introduced for batch adsorption experiments to study its adsorption property. The adsorption behaviours of heavy metal ions onto activated carbon, M-AC and Fe_3O_4 were studied and compared. In this step, the initial solutions with copper concentrations in the range of 20 ~ 180 mg/L were used in batch adsorption experiments. Since the copper hydroxide precipitations start to be dominant above pH 5 [82], the adsorption experiments were carried out at pH 4 to ensure that the reduction of copper concentration was only related to the adsorption onto adsorbents rather than copper hydroxide precipitation. The adsorbent dosage was chosen at 0.1 wt. % based on preliminary results.

Figure 4.10 (a) shows that the Cu (II) removal efficiency of activated carbon, M-AC, and Fe_3O_4 decreased as initial Cu (II) concentrations increased. For activated carbon, it could remove 86.2 % of copper ions from the initial 20 mg/L Cu (II) solution and removed about 20 % of copper ions when initial copper concentration exceeded 90 mg/L. At low Cu (II) concentration (20 mg/L), both M-AC and Fe_3O_4 could remove more than 99 % copper ions from solutions. Cu (II) removal efficiency by M-AC was lower than that of Fe_3O_4 and still higher than that of activated carbon in the studied Cu (II) concentration range. At the highest initial copper ions concentration (180 mg/L), Fe_3O_4 could remove 32.8 %

of copper ions, M-AC could only remove 20.0 % of copper ions, and pure activated carbon removed 18.0 % of copper ions.

Besides the removal efficiency, the species adsorption capacity (Q_e) is another important parameter to study adsorption behaviour since it determines the amount of species adsorbed onto per mass of adsorbent in equilibrium. The adsorption capacity (Q_e) was obtained as:

$$Q_e = \left[\left(C_i - C_f\right) * V\right]/m \qquad [4 - 2]$$

where V indicates the volume of solution in L and m, the weight of adsorbent in g.

The maximum adsorption capacity (Q_{max}) indicates the maximum amount of adsorbate loaded onto per mass of adsorbent when the surface of adsorbent is saturated. The maximum adsorption capacity which is a unique property among various adsorbents with single adsorbed specie is a significant parameter to compare the adsorption efficiency among different adsorbents. Figure 4.10 (b) presents the Cu (II) adsorption onto per mass of various adsorbents as a function of initial Cu (II) concentrations. It shows that Cu (II) adsorption onto carbon materials and magnetic particles are highly concentration dependent. The Cu (II) adsorption onto activated carbon and magnetic particles enhanced with increasing initial Cu (II) concentrations, then reached a plateau at higher concentration. The copper adsorption curve onto Fe_3O_4 reached the plateau at which the maximum Cu (II) adsorption capacity was 61.1 mg/g with 160 mg/L copper ions initially,

while the maximum Cu (II) adsorption capacity onto M-AC was 36.3 mg/g in solutions with initial 120 mg/L Cu (II).

As three studied particles have different surface area, the species adsorption onto per unit area (m^2) of adsorbents was also investigated. The species adsorption onto per unit of surface area (per m^2) was calculated as following:

$$Q_s = \frac{(C_i - C_f) * V}{m * S} \qquad [4 - 3]$$

where S is the surface area of each specific adsorbent in m^2/g.

Figure 4.10 (c) shows the Cu (II) adsorption onto per unit area of adsorbents as a function of initial Cu (II) concentrations. For the each unit of specific surface area, the Cu (II) adsorption onto Fe_3O_4 was significantly higher than that onto either pure activated carbon or M-AC.

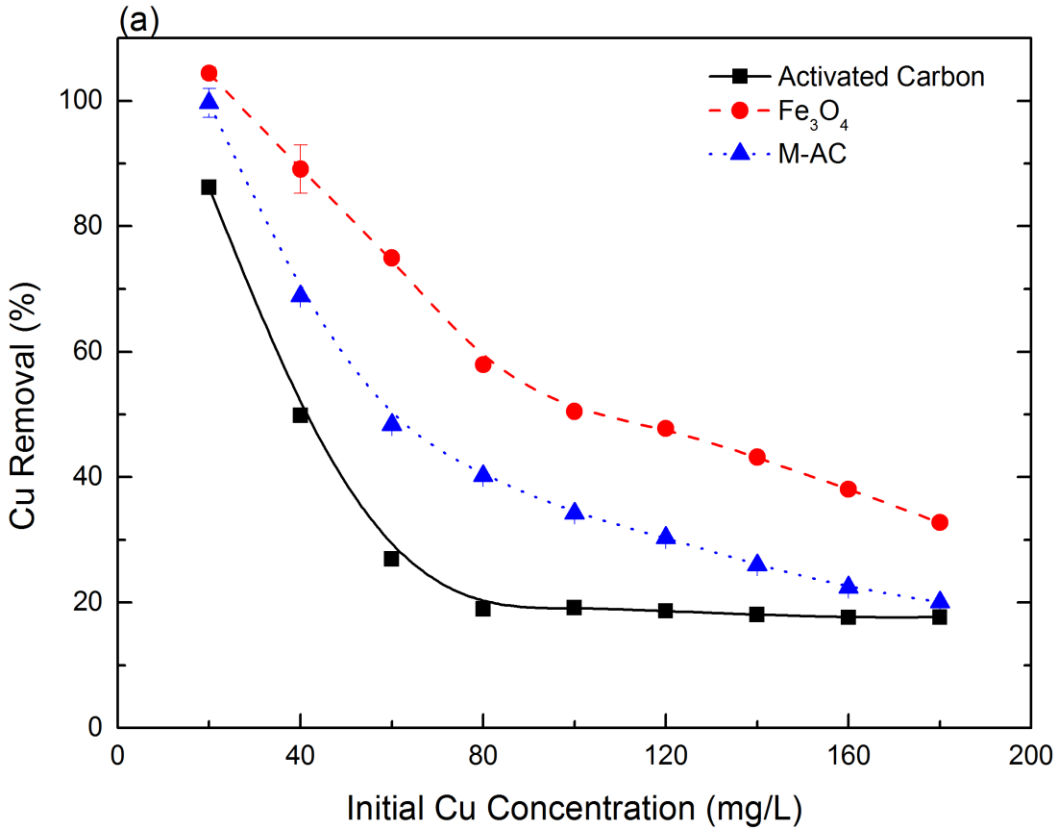
(a)
Activated Carbon
Fe3O4
M-AC
Cu Removal (%)
Initial Cu Concentration (mg/L)
0
20
40
60
80
100
0
40
80
120
160
200

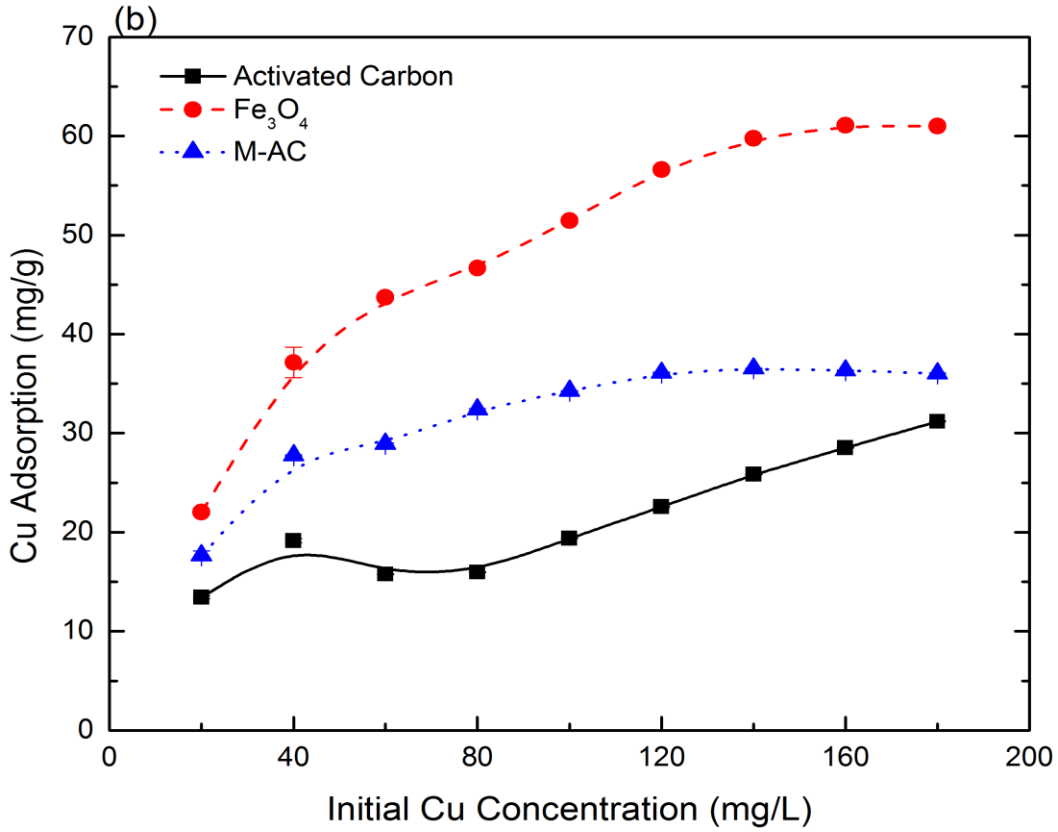
(b)
Activated Carbon
Fe3O4
M-AC
Cu Adsorption (mg/g)
Initial Cu Concentration (mg/L)
0
10
20
30
40
50
60
70
0
40
80
120
160
200

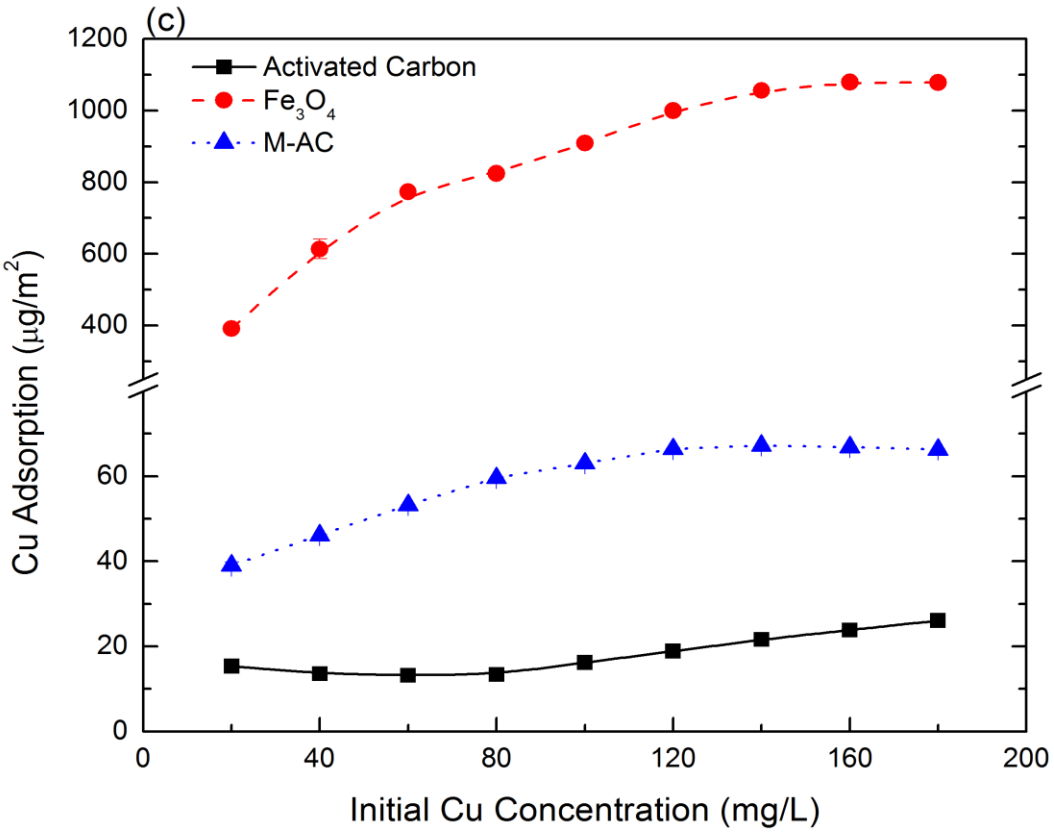

Figure 4.10 (a) Cu (II) removal efficiency from solutions with various adsorbents, (b) Cu (II) adsorption capacity onto per mass of various adsorbents, (c) Cu (II) adsorption onto per unit surface area of various adsorbents, as a function of initial Cu (II) concentrations (initial solution pH = 4, adsorbent dosage = 0.1 wt.%, contact time = 120 minutes)

Many research results regarding Cu (II) adsorption onto magnetite and activated carbon have been reported. It is unfair to directly compare the maximum adsorption capacity of copper ions onto various adsorbents among different investigations since the maximum adsorption capacity relies on a series of factors including adsorbent size, surface area of adsorbent, batch adsorption conditions like solution pH values and adsorption temperatures, etc. However, a lot of research results reported in literatures indicate that the metal adsorptions onto carbon materials are highly concentration dependent, consistent with the previously presented results.

A series of factors would be considered when discussing the mechanism of metal adsorption by carbon materials. Mohan and Chander [83] investigated the single-component and multi-component adsorption of metal ions onto activated carbon, suggesting metal adsorption is a complicated process and no single mechanism could explain the metal ions adsorption onto carbon materials from aqueous solution. Ion exchange, functional groups on activated carbon surface as well as the electrostatic interaction between cations and negatively charged surface of carbons might play a role in metal ions adsorption onto activated carbon. The well-accepted mechanism of carbon materials loading metal ions suggests that cations (and their complexes) are adsorbed due to their interactions with the anionic functional groups on carbon surfaces [63]. In this work, activated carbon does not show the best adsorption capacity for copper ions even though it has the highest surface area while Fe_3O_4 removed most copper ions from liquids with the lowest surface area. That reflects the surface functionalities of adsorbent surfaces

rather than the total surface area play a predominant role in metal loading. Similar conclusions could be found from Pyrzyńska and Bystrzejewski's conclusions [62] and Celis's work [84] regarding Cu (II) and Co (II) adsorption onto activated carbon or carbon base materials, as well as the study about Ni (II) adsorption onto carbon nanotubes by Boehm [85].

On the other hand, iron oxides also revealed high efficiency in copper ions removal from effluents. In published data [86-89], the isoelectric point (IEP) of magnetite was between pH 4 to pH 7, depending on the various source of Fe_3O_4. Figure 4.11 shows the zeta-potential of three different adsorbents as a function of pH. The zeta-potential of adsorbents decreased from positive to negative with increasing pH values. Figure 4.11 shows that the IEP of Fe_3O_4 is around pH 4 which is similar to the IEP of M-AC. Fe_3O_4 was nearly neutral charged under current experiment conditions (pH = 4) in copper ions adsorption. Based on the copper species distribution plot [82] and listed equilibrium constants in Appendix, the primary copper species are cations, Cu^{2+} or $Cu(OH)^{+}$ at pH 4. Thus, only electrostatic interaction between copper ions and particle is not sufficient to explain the high adsorption capacity of copper species onto Fe_3O_4. According to previous investigations [40, 55], the adsorption mechanism of metal ions by iron oxides could be due to the interaction between surface hydroxyl groups with the metal ions or the hydrolysed metal ions. It could occur through either ion-exchange with metal ions or directly adsorption followed by metal ions hydrolysis, as discussed in 2.4.1.

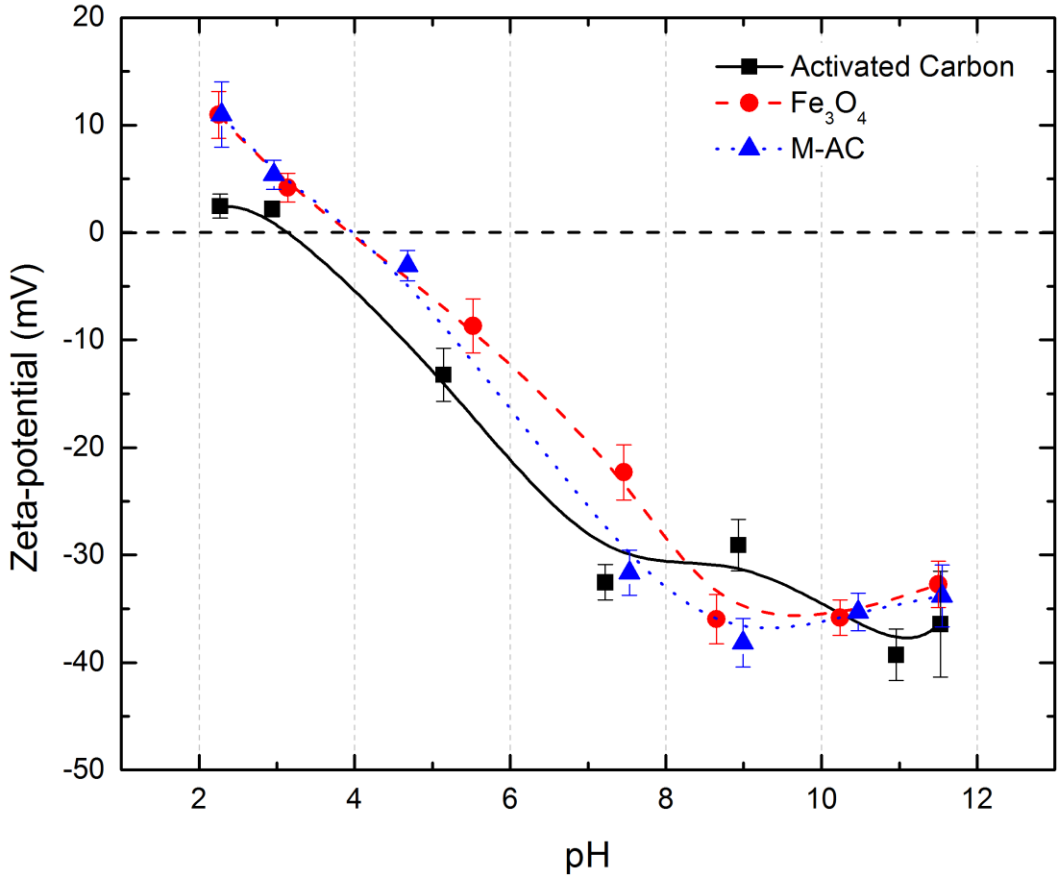

Figure 4.11 Zeta-potential of activated carbon, Fe_3O_4, and M-AC as a function of pH

M-AC poses the combination properties of activated carbon and Fe_3O_4. The loading ability of M-AC for copper ions is between activated carbon and Fe_3O_4. The removal efficiency of M-AC was improved over pure activated carbon by precipitating the magnetite on its surface. The affinity of M-AC with coppers is taking advantages of both the functional groups on activated carbon surface as well as on magnetite surface. As magnetite has very high affinity with copper ions, the M-AC showed a better loading property than activated carbon.

Moreover, the final solution pH values (Table 4.2) after Cu (II) adsorptions were measured for each adsorbent respectively with an initial pH at 4. For three adsorbents (activated carbon, Fe_3O_4 and M-AC), the final pH values was higher than initial pH of the solution while final pH decreased with increasing initial Cu (II) concentrations. The reduction of final pH when initial metal concentration increased may be due to a higher release of hydrogen ions and indicate the ion-exchange between copper ions and functional groups on activated carbon surface or iron oxide surface [80, 90]. However, it is possible that those hydrogen ions are from hydrolysis of metal ions in solutions. The increasing final pH after adsorption compared with initial pH is due to the release of hydroxyl ions by adsorbents (activated carbon, Fe_3O_4 and M-AC). That could be the hydrolysis of adsorbents when suspended in solutions. At the same time, for the adsorption at the same initial metal ion concentration, the final pH values for the three adsorbents always followed this range: Fe_3O_4 > M-AC > activated carbon, which was in the same order as the Cu (II) removal efficiency. This indicates that the higher hydrolysis on adsorbent surface leads to higher affinity between copper

ions and adsorbents in solutions. As discussed 2.4.1, here is another evidence to suggest the ion-exchange process during adsorption.

Table 4.2 Selected pH values after Cu (II) adsorption onto various adsorbents with initial pH 4 (adsorbent dosage = 0.1 wt.%, contact time = 120 minutes)

Initial Cu (II) concentration (mg/L)	Final pH after adsorption		
	Activated carbon	Fe_3O_4	M-AC
20	6.28	9.97	7.40
40	5.80	9.20	6.16
60	5.43	8.63	5.77
80	5.06	8.46	5.45
100	4.91	6.37	5.28

The Ni (II) removal efficiency and adsorption capacity curve onto different adsorbents as a function of initial concentration are shown in Figure 4.12 (a) – (c). For all three studied particles, Ni (II) removal efficiency reduced while the adsorption capacity increased with increasing Ni (II) concentrations. Similar to Cu (II) adsorption, the Fe_3O_4 showed the best removal efficiency for nickel ions from solutions. At lower nickel concentrations (20 mg/L), Fe_3O_4 was able to remove more than 99 % of Ni (II) from solutions while only 60 % of Ni (II) adsorbed on M-AC and 40 % of Ni (II) adsorbed on activated carbon. Compared with copper ions, nickel ions were less likely to adsorb on magnetic particles or carbon materials. That was consistent with the previous reports [49] and suggested the affinity between involved adsorbents and copper ions is stronger than nickel ions.

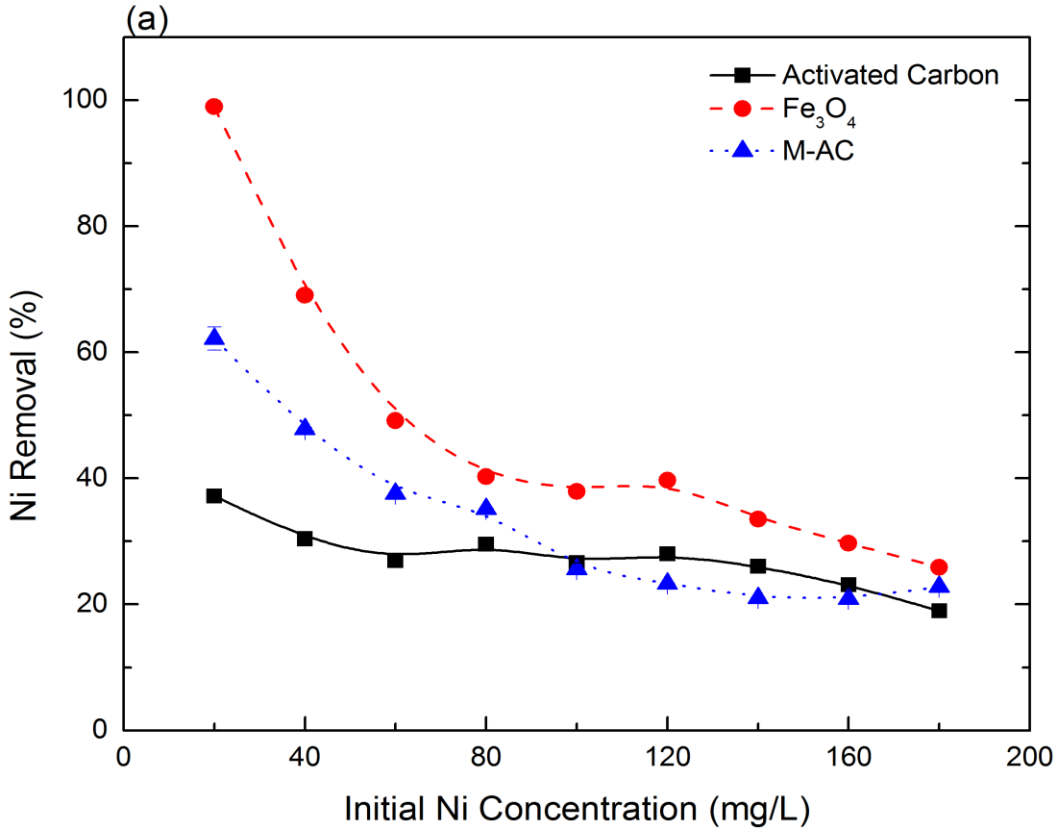
(a)
Activated Carbon
Fe3O4
M-AC
Ni Removal (%)
0
20
40
60
80
100
0
40
80
120
160
200
Initial Ni Concentration (mg/L)

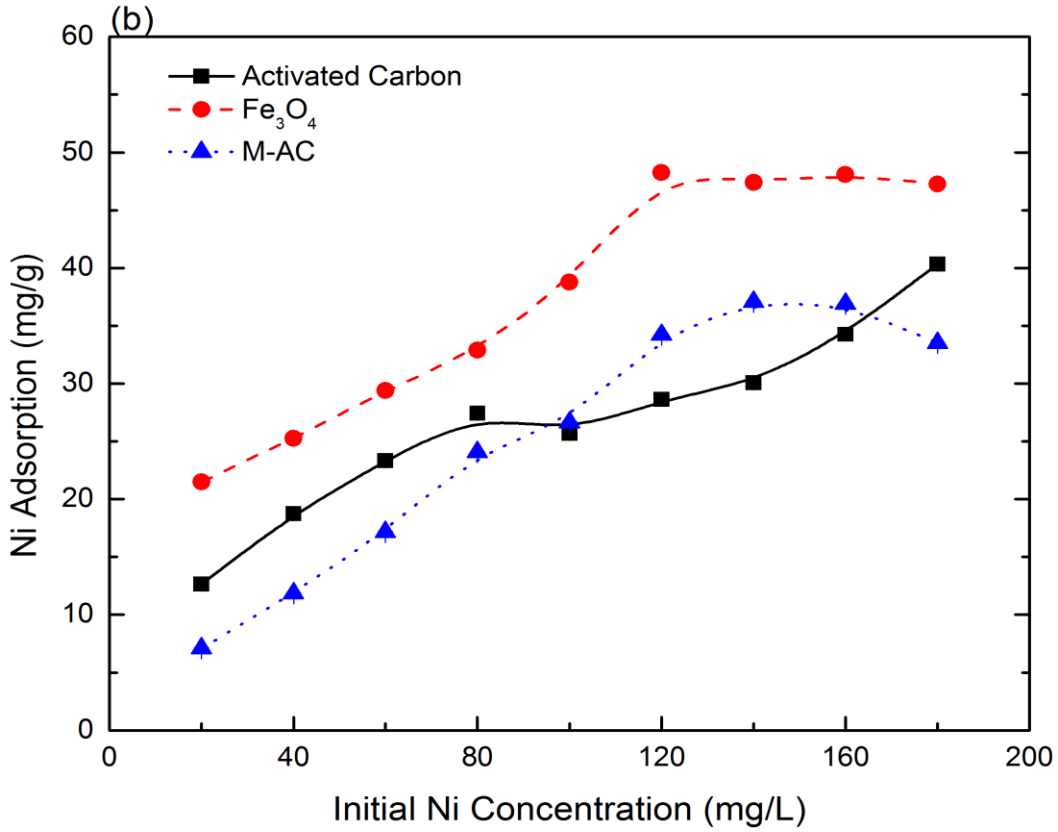
(b)
Activated Carbon
Fe3O4
M-AC
Ni Adsorption (mg/g)
0
10
20
30
40
50
60
0
40
80
120
160
200
Initial Ni Concentration (mg/L)

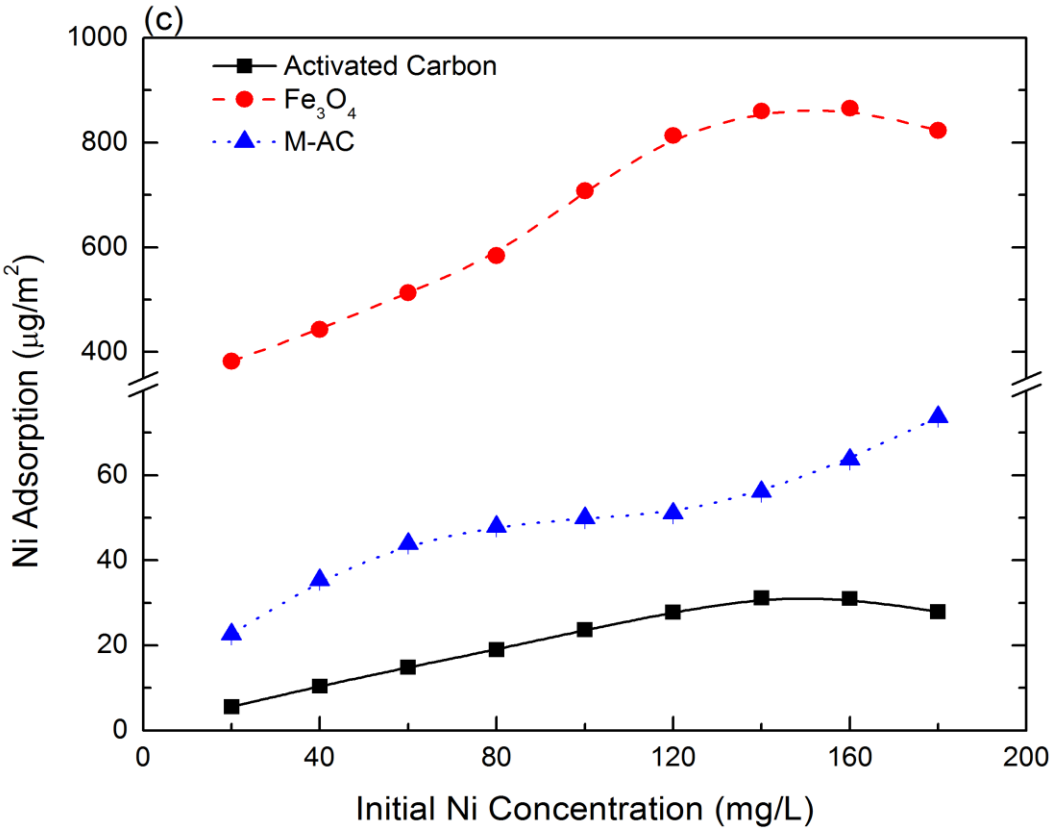

Figure 4.12 (a) Ni (II) removal efficiency from solutions with various adsorbents, (b) Ni (II) adsorption capacity onto per mass of various adsorbents, (c) Ni (II) adsorption onto per unit surface area of various adsorbents, as a function of initial Ni (II) concentrations (initial solution pH = 4, adsorbent dosage = 0.1 wt.%, contact time = 120 minutes)

4.2.2 DETA species adsorption

The DETA species adsorption onto M-AC is one of the most significant applications in this study. The effect of M-AC dosage on DETA adsorption was investigated under room temperature. The highest DETA concentration level at Vale operation will not exceed 25 mg/L so concentration range in this step was set between 5 ~ 25 mg/L for DETA adsorption. Figure 4.13 shows the DETA removal efficiency by M-AC with different dosages as a function of initial DETA concentrations. M-AC with different dosages removed about 40 % ~ 90 % of DETA from solutions. M-AC with 0.1 wt.% dosage has gradually decreased DETA removal efficiency as initial DETA concentrations increased. Unlike 0.1 wt.% of M-AC, DETA removal efficiency by 0.5 wt.% and 1 wt.% of M-AC increased as initial DETA concentrations increased. The 0.1 wt.% of M-AC removed about 64.6 % of DETA species from solution with 5 mg/L of DETA initially and removed only 42.5 % of DETA at 25 mg/L initially. The M-AC with 0.5 wt.% or 1 wt.% dosage removed more than 70 % of DETA from solutions, while M-AC with 0.1 wt.% dosage removed less than 65 % of DETA. In addition, compared with 0.5 wt.% dosage of M-AC, 1 wt.% dosage of M-AC did not show greater improvements in DETA removal. Thus, 0.5 wt.% of M-AC was chosen as the M-AC dosage for further DETA adsorption experiments. Furthermore, as shown in Figure 4.14, the DETA removal efficiency increased sharply at the beginning of shaking while becoming slowly as shaking a little bit longer. It reached equilibrium at 90 minutes with more than 99 % of DETA removal.

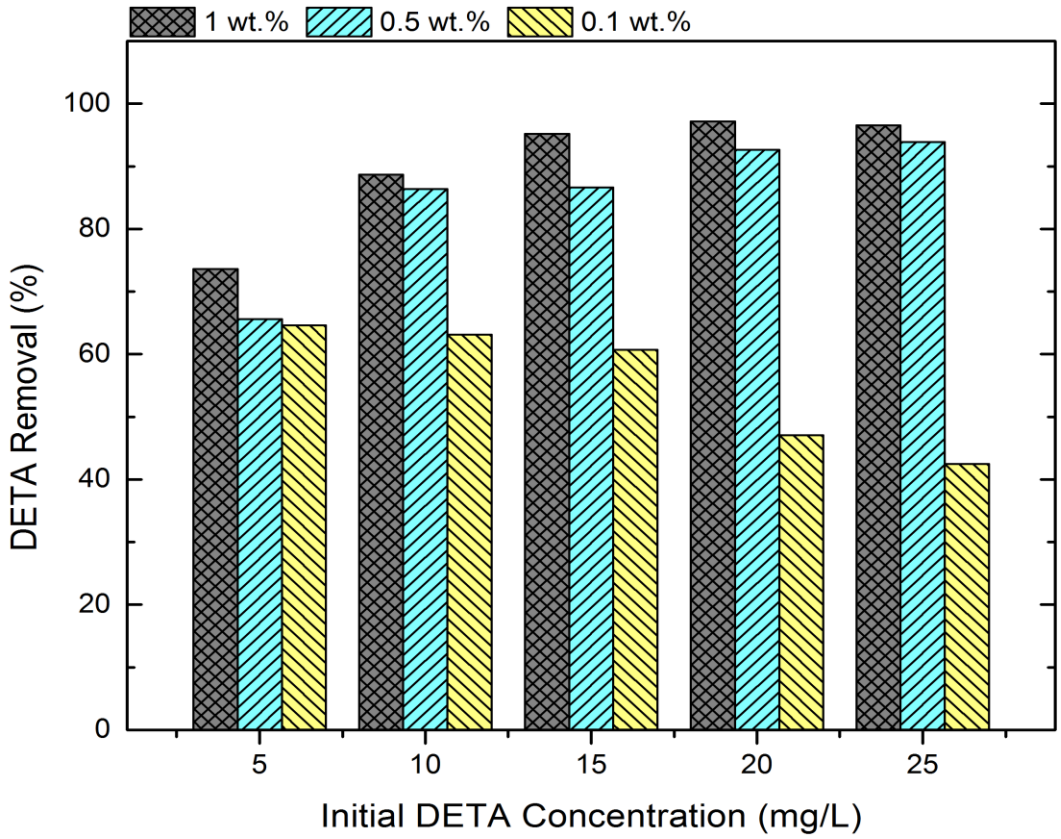

Figure 4.13 DETA removal efficiency by M-AC with different dosages (1 wt.%, 0.5 wt.% and 0.1 wt.%) as a function of initial DETA concentrations (initial solution pH = 9, contact time = 120 minutes)

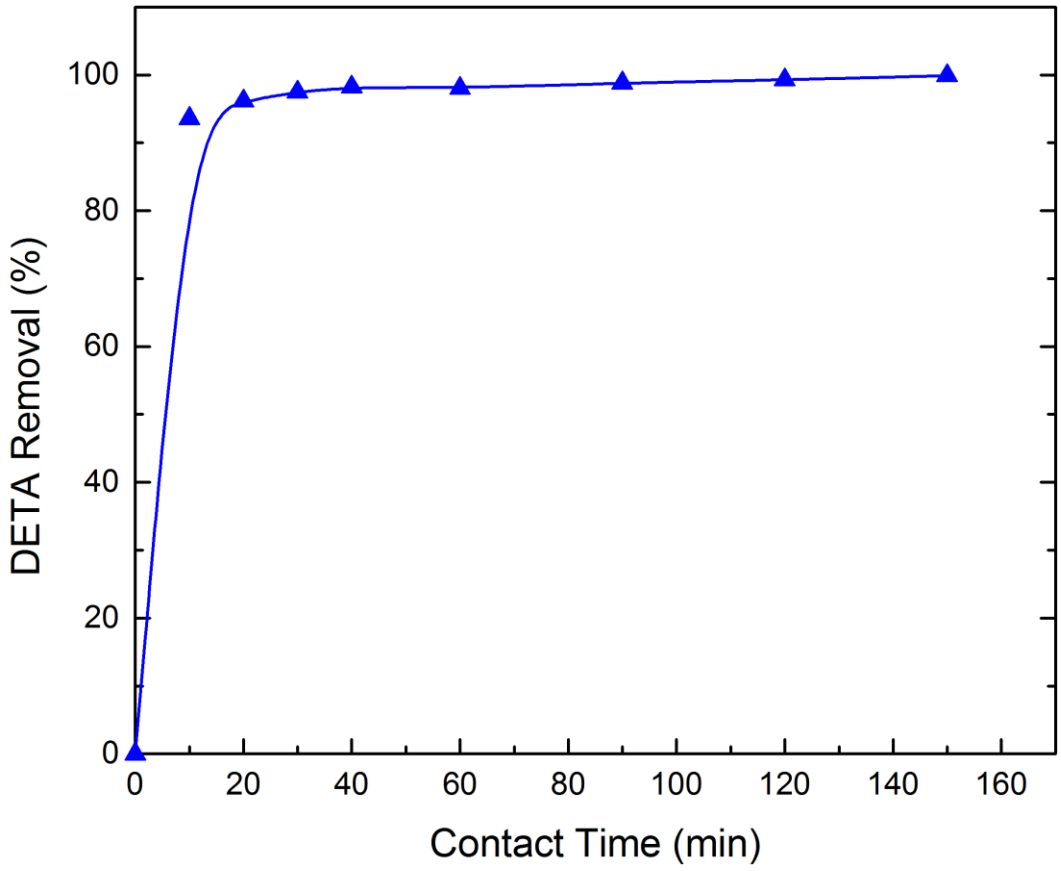

Figure 4.14 DETA removal efficiency by M-AC as a function of contact time (initial solution pH = 9, C_i = 25 mg/L, adsorbent dosage = 0.5 wt.%,)

The DETA species adsorption experiments were carried out at pH 9 which was similar to the flotation system condition (pH = 9.5) at Vale. The initial DETA concentration range was 20 ~ 220 mg/L to investigate the maximum adsorption capacity of DETA onto the prepared materials. Figure 4.15 (a) and (b) respectively present the DETA removal efficiency and DETA adsorption capacity onto per mass of adsorbents as a function of initial DETA concentrations. Figure 4.15 (a) shows that the removal efficiency of activated carbon gradually decreased with increasing initial DETA concentrations. At lower DETA concentrations (20 ~ 60 mg/L), M-AC could remove more than 85 % of DETA from solutions. DETA removal efficiency of M-AC decreased with increasing initial DETA concentrations. In contrast, pure activated carbon only removed 65.9 % of DETA from solution at low DETA concentration (20 mg/L). It is interesting to note that M-AC plays a better role in removing DETA than pure activated carbon even though the surface area of M-AC (543.5 m^2/g) is much lower than that of activated carbon (1195.8 m^2/g). In addition, the difference in DETA removal efficiency between M-AC and activated carbon becomes smaller at higher initial DETA concentrations. To compare the adsorption capacity of M-AC and activated carbon, Fe_3O_4 was introduced to batch adsorption experiments for DETA species. Fe_3O_4 showed a similar tendency in DETA removal efficiency as M-AC did, but DETA removal efficiency of Fe_3O_4 was always lower than that of M-AC. The DETA removal efficiency of Fe_3O_4 was higher than that of pure activated carbon when initial DETA concentrations were

less than 100 mg/L but lower than that of activated carbon when initial DETA concentration was more than 100 mg/L.

In Figure 4.15 (b), for all three studied adsorbents, the DETA adsorption onto per mass of adsorbents increased with increasing initial DETA concentrations and reached plateau at certain DETA concentrations. This indicated the saturation loading on the surface of adsorbent particles. M-AC obtained the maximum DETA adsorption capacity (21.9 mg/g) while the maximum DETA adsorption capacity onto activated carbon and pure Fe_3O_4 was 18.2 mg/g and 13.8 mg/g respectively.

According to Rashchi, Finch and Sui [91], the predominant DETA species at pH 9 are protonated species ($[H_2(DETA)]^{2+}$ and $[H(DETA)]^{+}$). Equilibrium constants are listed in Appendix. From Figure 4.11, at pH 9, the zeta-potential values of activated carbon, Fe_3O_4, and M-AC are - 30 mV, - 35 mV, and - 38 mV, respectively. Thus, physical adsorption through the electrostatic attraction might be one of the adsorption mechanisms in the DETA adsorption process. However, activated carbon with the highest specific surface area did not show the best DETA loading efficiency, similar to metal adsorptions onto activated carbon. This indicated that physical adsorption could not explain the DETA adsorption mechanism onto carbon materials or iron oxides. In addition, the zeta-potential of three involved particles at pH 9 did not show obvious difference, but the DETA adsorptions on them were so variable. Thus, chemical adsorption mechanism must be involved in DETA adsorption process other than physical adsorption through

electronic interaction. However, the DETA adsorption process onto involved adsorbents is not clear at present.

Figure 4.15 (c) shows that for given specific surface area, Fe_3O_4 has adsorption capacity of 10 ~ 8 times more than that of the adsorption capacity of M-AC, and M-AC has adsorption capacity of 3 ~ 2 times more than that of activated carbon. The strong DETA adsorption on Fe_3O_4 may be explained by attraction occurred between DETA species and the surface hydroxyl groups of Fe_3O_4. As previously discussed, Fe_3O_4 exposed on the surface of activated carbon during deposition process. Compared with certain mass of pure Fe_3O_4, the relatively higher surface area of M-AC explains the reason why M-AC has the best DETA adsorption capacity onto per mass of adsorbent (mg/g) among three adsorbents (Figure 4.15 (b)). However, pure Fe_3O_4 has the best Cu (II)/Ni (II) adsorption capacity (mg/g) among three adsorbents (Figure 4.10 (b) and Figure 4.12 (b)) rather than M-AC. This phenomenon could be explained by the size difference between DETA and Cu (II)/Ni (II) ions. As the size of DETA is much larger than the size of Cu (II) or Ni (II) ion, DETA adsorption on pure Fe_3O_4 (per m^2) reached plateau at relatively low concentration (80 mg/L) while Cu (II)/Ni (II) adsorption on pure Fe_3O_4 (per m^2) reached plateau at relatively high concentration (140 mg/L). M-AC shows a better adsorption capacity to adsorb larger species than Fe_3O_4 as pure Fe_3O_4 has limited surface area for large molecules.

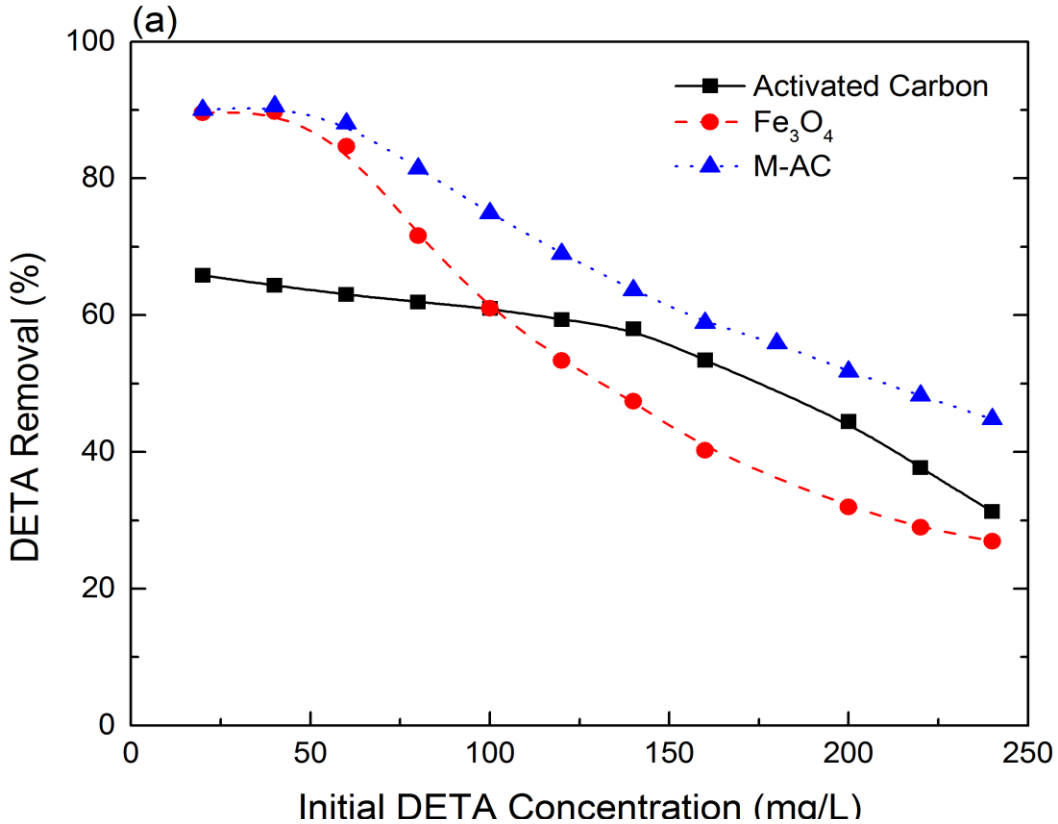
(a)
Activated Carbon
Fe3O4
M-AC
DETA Removal (%)
Initial DETA Concentration (mg/L)
0
20
40
60
80
100
0
50
100
150
200
250

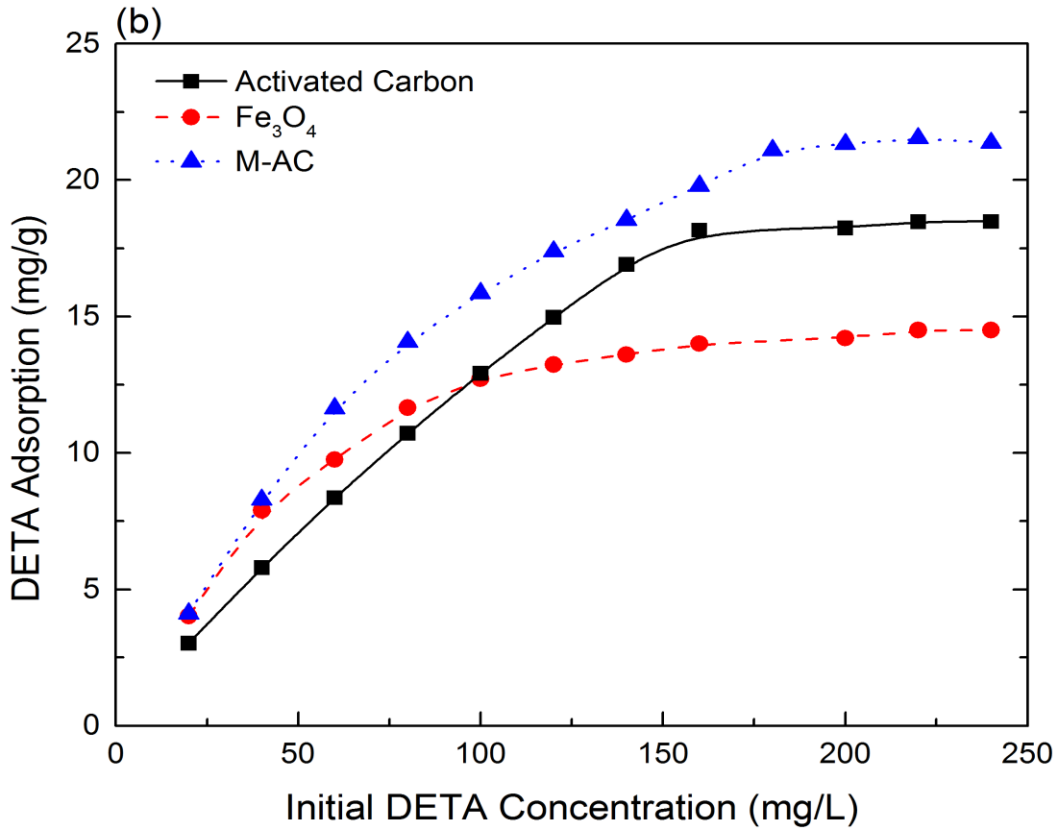
(b)
Activated Carbon
Fe3O4
M-AC
DETA Adsorption (mg/g)
Initial DETA Concentration (mg/L)
0
5
10
15
20
25
0
50
100
150
200
250

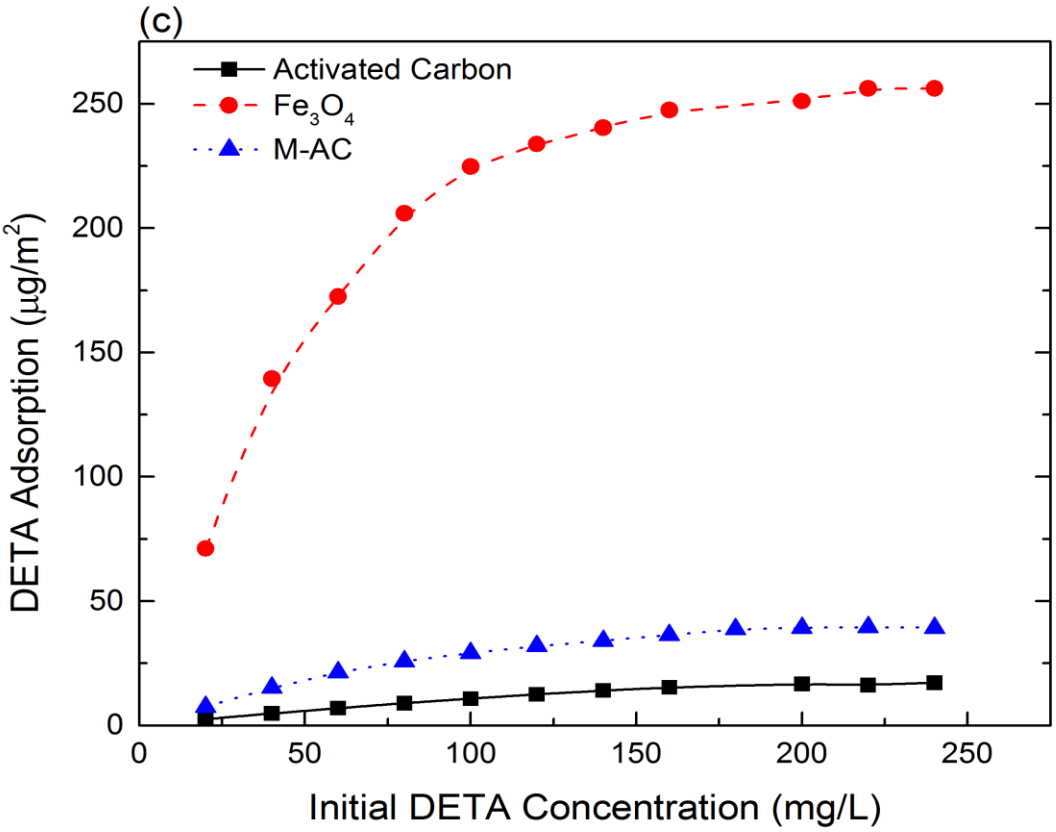

Figure 4.15 (a) DETA removal efficiency from solutions with various adsorbents, (b) DETA adsorption capacity onto per mass of various adsorbents, (c) DETA adsorption onto per unit surface area of various adsorbents, as a function of initial DETA concentrations (initial solution pH = 9, adsorbent dosage = 0.5 wt.%, contact time = 120 minutes)

4.3 M-AC Applications in Multi-component Solution

M-AC has shown a good adsorption of single component such as Cu (II), Ni (II) and DETA. In this study, two binary systems (Cu-DETA, Ni-DETA) and one ternary system (Cu-Ni-DETA) were selected to investigate the adsorption ability of M-AC in multi-components solutions. As previously stated, the highest DETA concentrations at Vale operation will not exceed 25 mg/L while the highest copper concentration would be less than 20 mg/L. Thus, in this study, the DETA concentration was stabilized at 25 mg/L with increasing heavy metal concentrations up to 25 mg/L. The pH of initial solutions was set at 9.5 to simulate the flotation environment at Vale operation.

Figure 4.16 and Figure 4.17 show the metal/DETA removal efficiency by pure activated carbon, Fe_3O_4, and M-AC in binary component solutions containing Cu-DETA or Ni-DETA respectively. For single component systems, M-AC with 0.1 wt.% dosage was chosen for heavy metal adsorption and M-AC with 0.5 wt.% dosage was used for DETA adsorption. Here, in multi-component solution, M-AC with 0.5 wt.% dosage was employed due to the presence of DETA in solutions.

According to the species distribution of Cu-DETA and Ni-DETA in the previous reports [16], the components in metal-DETA binary system are highly pH dependence (equilibrium constants are listed in Appendix). At pH 9.5, the major components in Cu-DETA solution are $[Cu(DETA)]^{2+}$, $[Cu(DETA)_2]^{2+}$ and $[Cu(OH)(DETA)]^{+}$ and the major components in Ni-DETA solution are $[Ni(DETA)]^{2+}$ and $[Ni(DETA)_2]^{2+}$. The results show that M-AC has higher

metal/DETA removal efficiency in binary component systems than either activated carbon or Fe_3O_4. Even though Fe_3O_4 presented the highest affinity with copper or nickel ions in single-component solutions, it did not perform as well as M-AC in solutions containing binary components (metal-DETA). Since major metal ions (Cu/Ni) existed in the form as DETA complexes, the iron oxides with a lower adsorption capacity for DETA due to its low surface area did not show high removal efficiency for metal-DETA complexes. M-AC could adsorb more than 99 % of heavy metal ions (copper/nickel) and 99 % of DETA species from metal-DETA solution in the studied concentration range. Similar to single-component system, activated carbon did not show the metal/DETA removal efficiency as high as the other two adsorbents.

The removal efficiencies of activated carbon, Fe_3O_4 and M-AC in a ternary system (Cu-Ni-DETA) were studied in deionized water and process water respectively. The M-AC dosage was chosen at 0.5 wt.%, while the concentration of DETA was stabilized at 25 mg/L, and the pH of solution was adjusted to 9.5. For the ternary system (Cu-Ni-DETA) in pure water (Figure 4.18), M-AC could remove nearly 100 % of Cu (II)/Ni (II) and more than 97% of DETA from solutions. Meanwhile, Fe_3O_4 could remove more than 80 % of Cu (II), more than 90 % of Ni (II) and 80 % of DETA from solutions. Activated carbon removed around 40 % of DETA from solutions, up to 65 % of Cu (II) and 96 % of Ni (II) from solutions. Moreover, it is noticeable that activated carbon removed more nickel than copper at various concentrations. Since copper ions are more favourable than nickel ions to form complexes with DETA (equilibrium constants

listed in Appendix) and DETA concentration after loading on activated carbon was still higher than 16 mg/L, copper ions were more likely to remain in solutions to form stable complexes with DETA rather than adsorbed onto activated carbon. This explains why the copper removal efficiency was lower than nickel in Cu-Ni-DETA system on activated carbon.

In process water system, M-AC (Figure 4.19) did not show absolute advantages in removing containments compared with pure activated carbon but better than pure iron oxides. Figure 4.19 shows that the removal efficiency of Fe_3O_4 for contaminants in process water decreased more significantly than other two carbon materials in process water. This indicated that iron oxides had poor selectivity in the presence of other competitive species during adsorption process. Iron oxides adsorb other contaminants in process water to occupy the binding sites, which leads to low removal efficiency for Cu/Ni/DETA species in process water. The decreasing species removal efficiency of M-AC in process water is partly due to the deposited iron oxides.

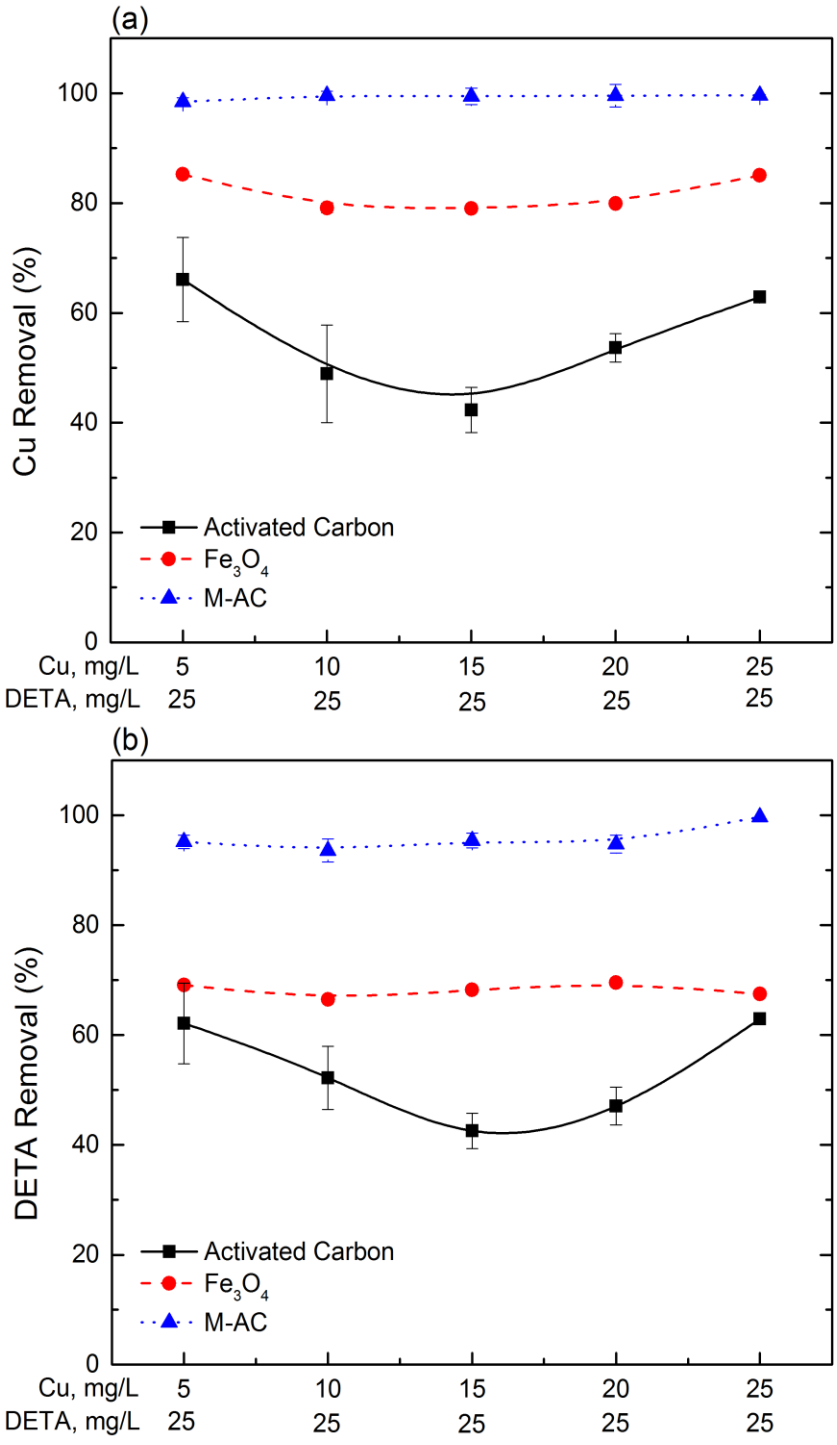

Figure 4.16 Removal efficiency by various adsorbents for (a) Cu (II) and (b) DETA in solution containing Cu-DETA species (initial solution pH = 9.5, adsorbent dosage = 0.5 wt.%, contact time = 120 minutes)

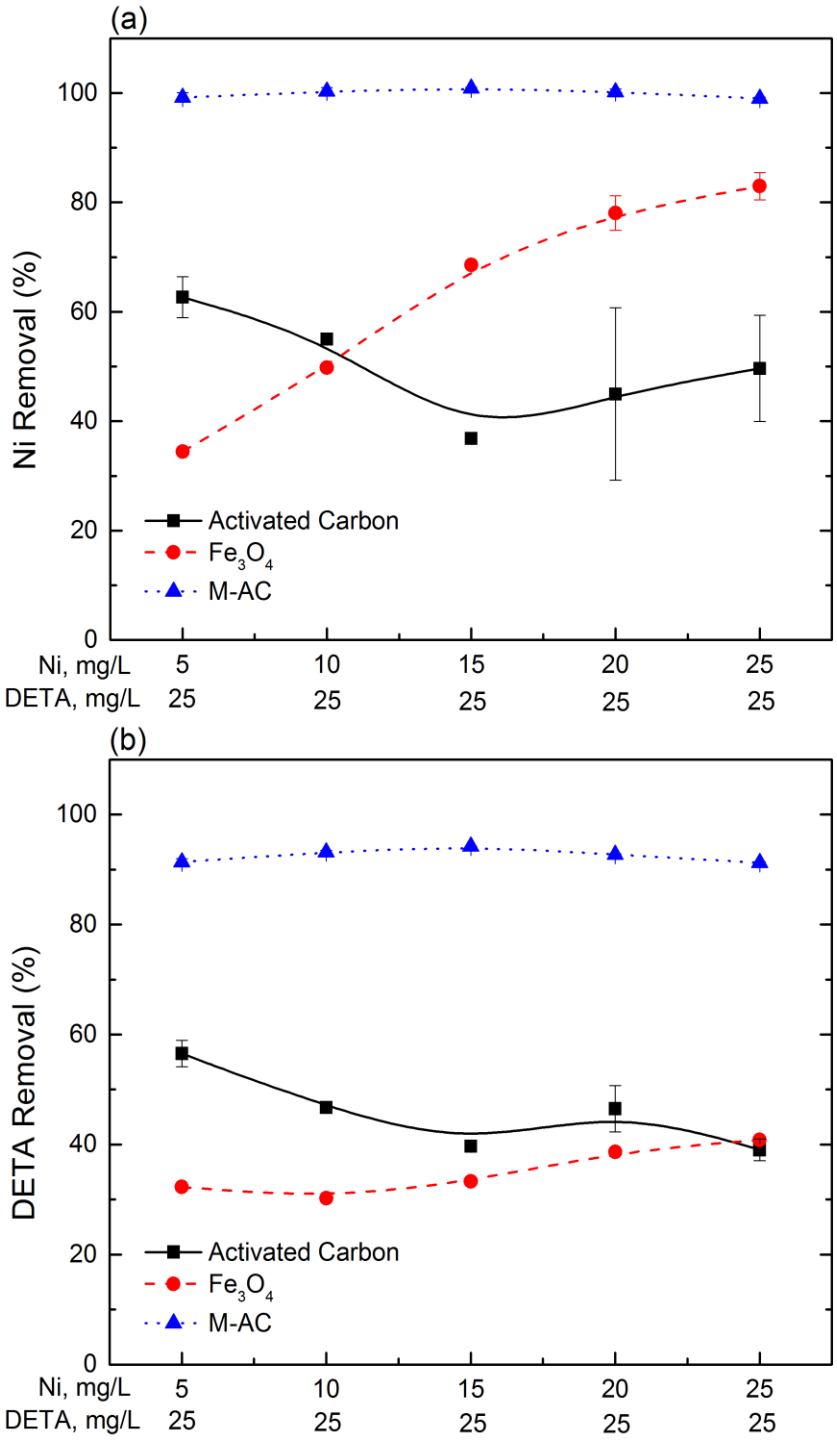

Figure 4.17 Removal efficiency by various adsorbents for (a) Ni (II) and (b) DETA in solution containing Ni-DETA species (initial solution pH = 9.5, adsorbent dosage = 0.5 wt.%, contact time = 120 minutes)

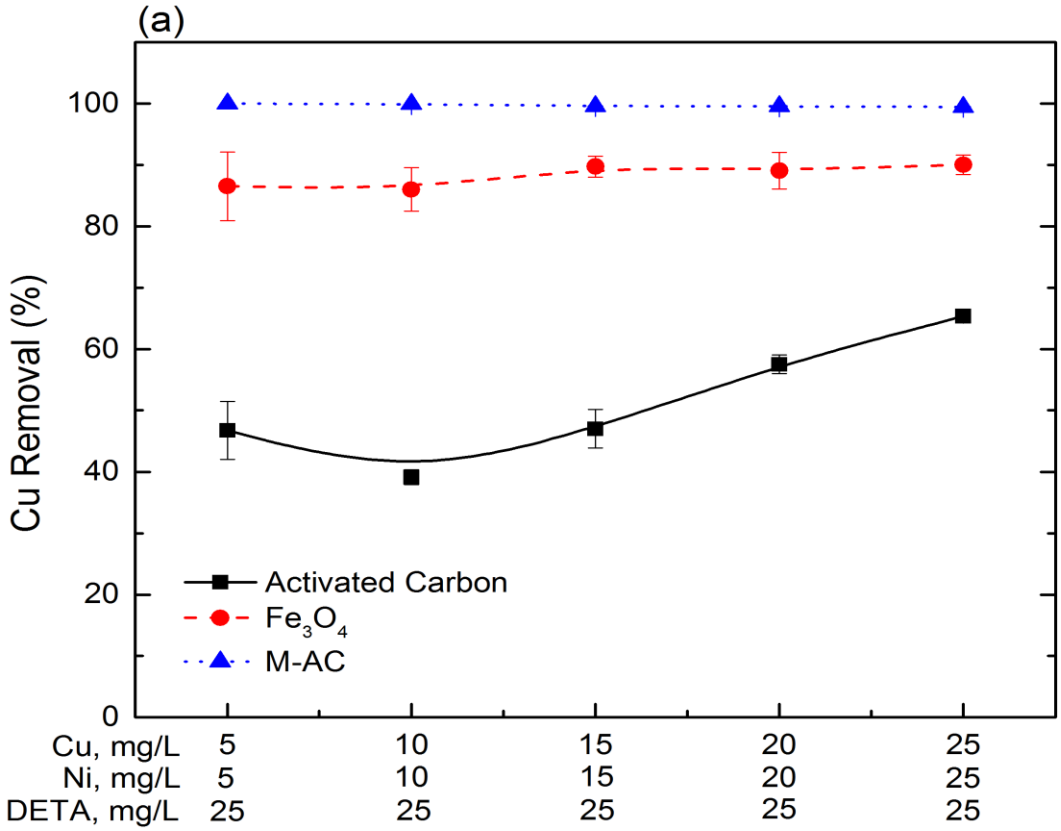
(a)
Cu Removal (%)
100
80
60
40
20
0
Activated Carbon
Fe3O4
M-AC
Cu, mg/L 5 10 15 20 25
Ni, mg/L 5 10 15 20 25
DETA, mg/L 25 25 25 25 25

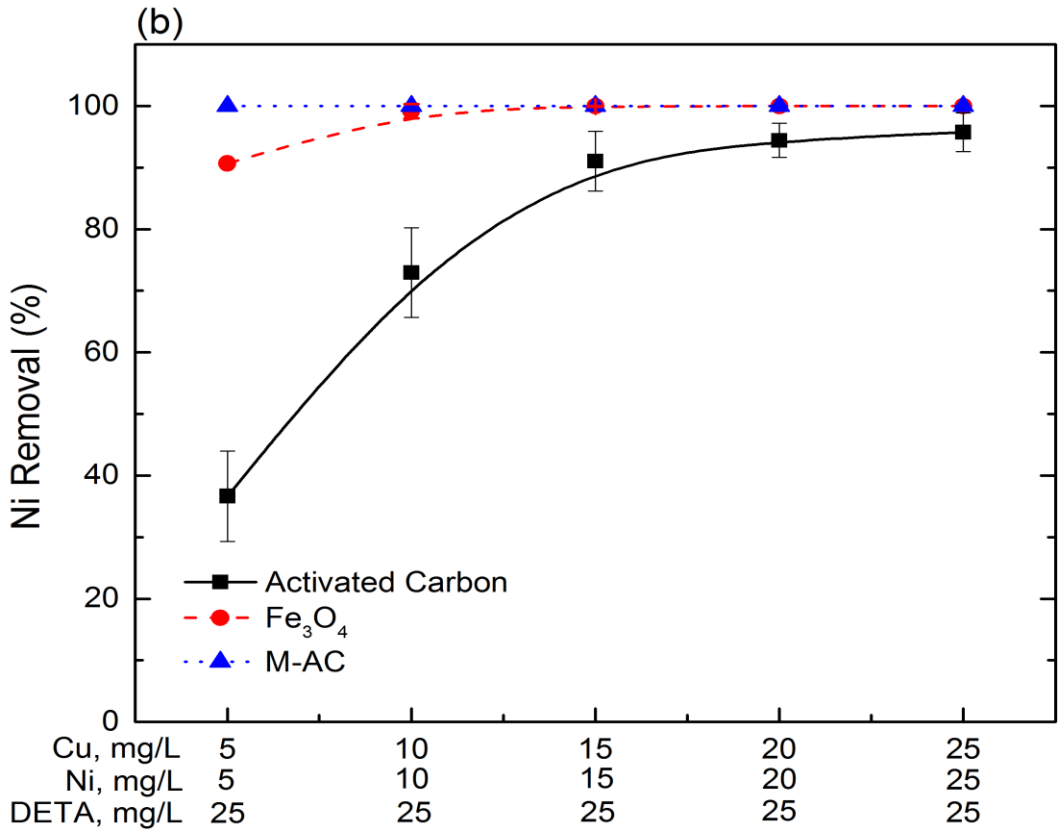
(b)
Ni Removal (%)
100
80
60
40
20
0
Activated Carbon
Fe3O4
M-AC
Cu, mg/L 5 10 15 20 25
Ni, mg/L 5 10 15 20 25
DETA, mg/L 25 25 25 25 25

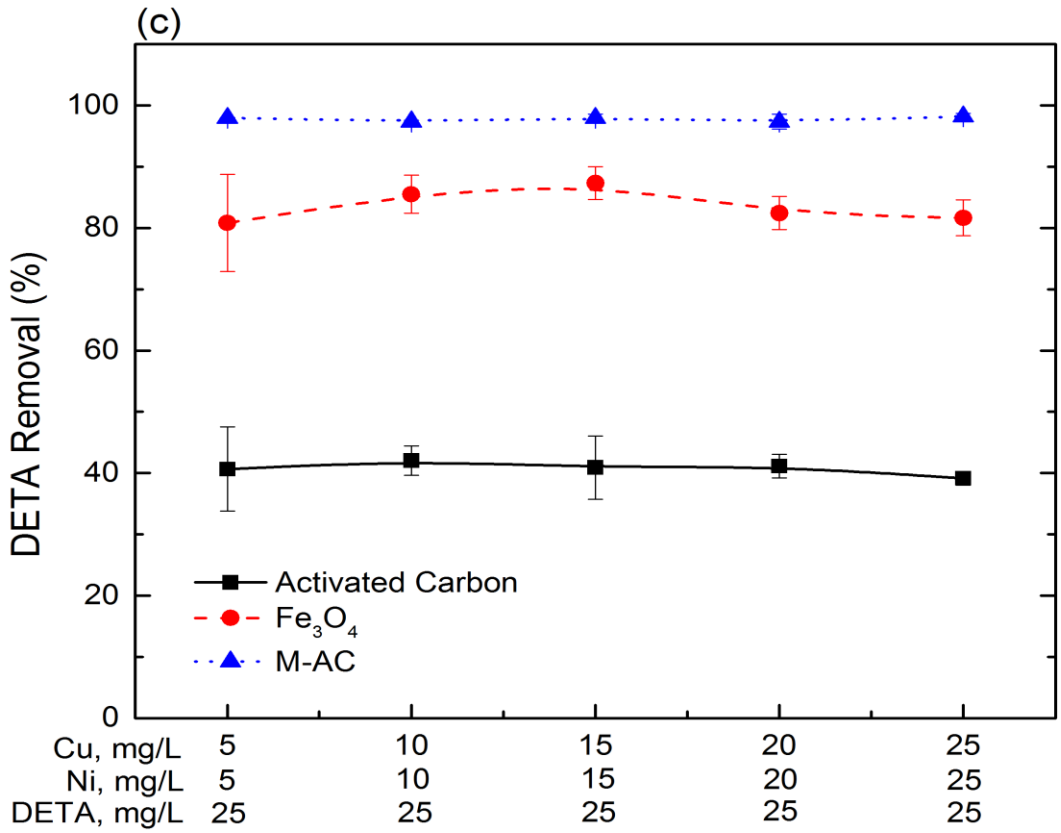

Figure 4.18 Competitive adsorption in pure water system: (a) Cu removal efficiency, (b) Ni removal efficiency, (c) DETA removal efficiency (initial solution pH = 9.5, adsorbent dosage = 0.5 wt.%, contact time = 120 minutes)

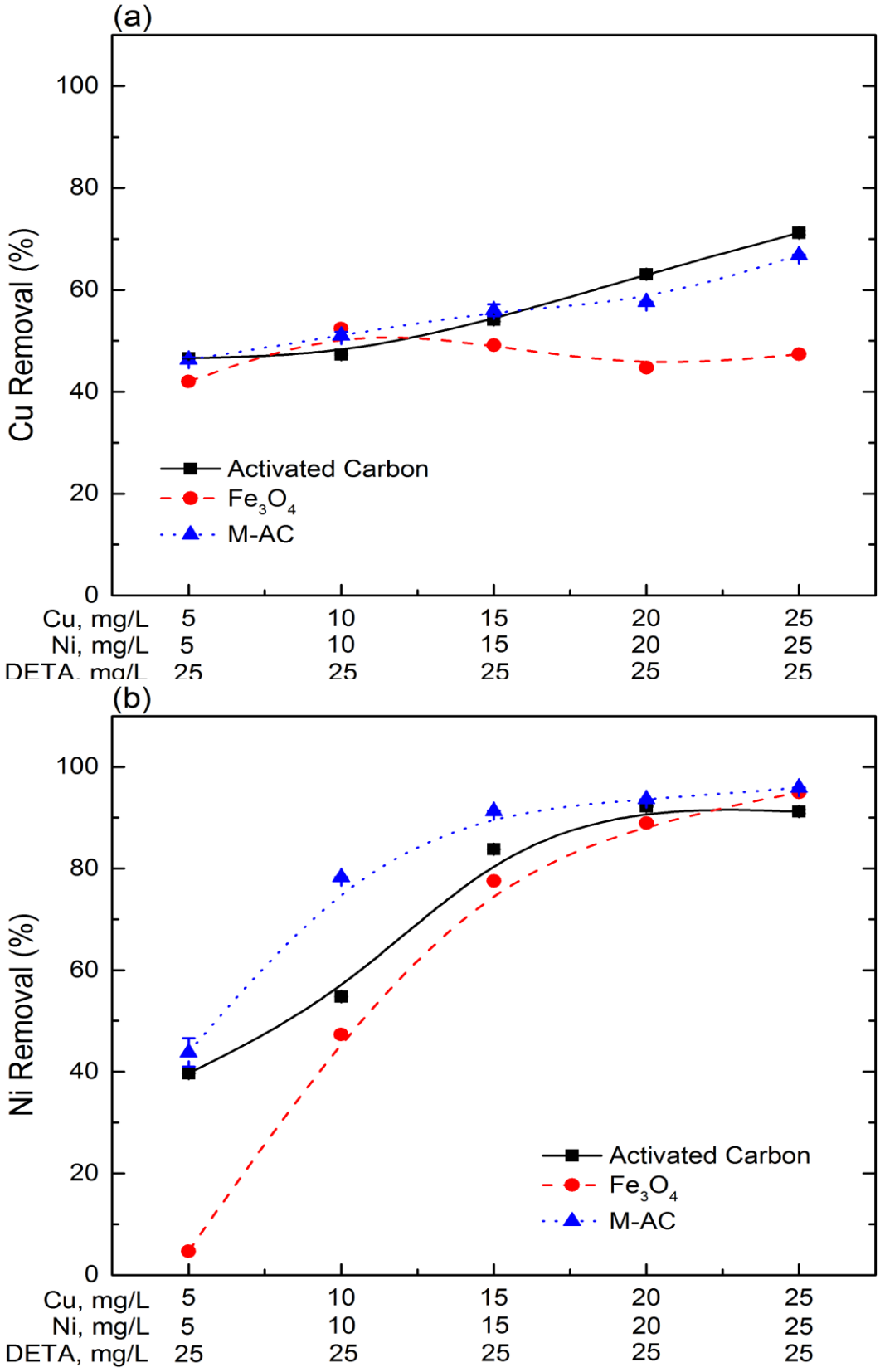
(a)
Cu Removal (%)
100
80
60
40
20
0
Activated Carbon
Fe3O4
M-AC
Cu, mg/L 5 10 15 20 25
Ni, mg/L 5 10 15 20 25
DETA, mg/L 25 25 25 25 25
(b)
Ni Removal (%)
100
80
60
40
20
0
Activated Carbon
Fe3O4
M-AC
Cu, mg/L 5 10 15 20 25
Ni, mg/L 5 10 15 20 25
DETA, mg/L 25 25 25 25 25

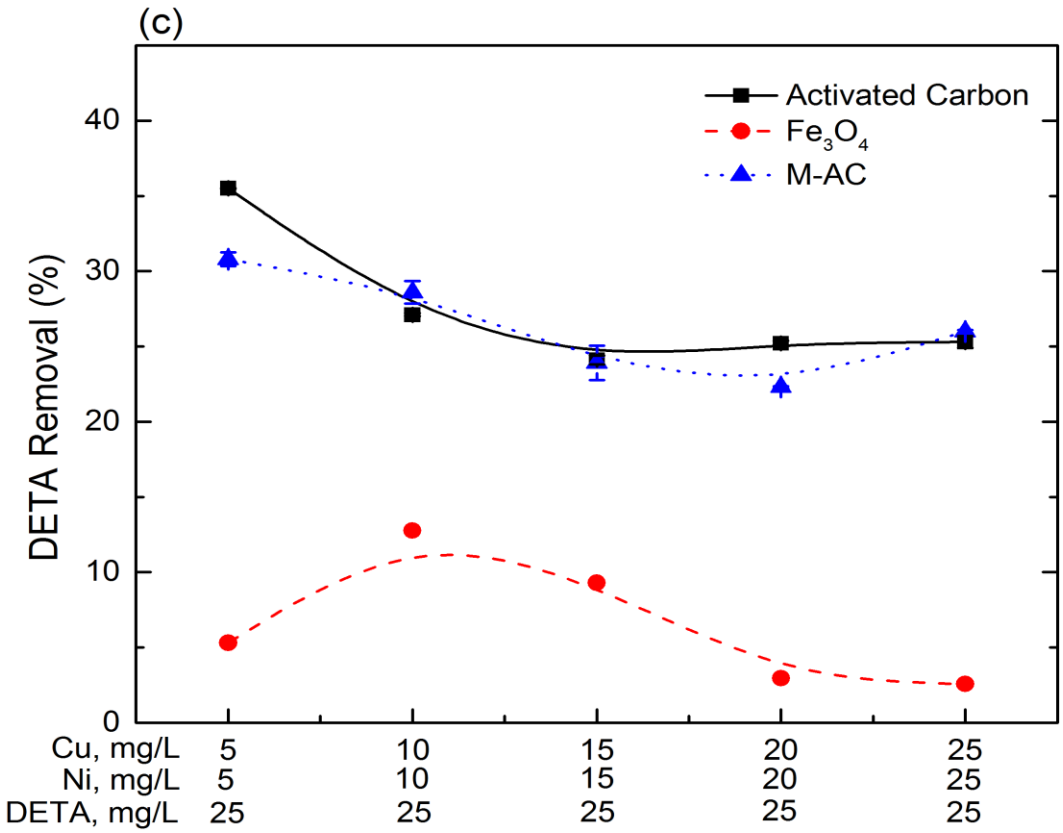

Figure 4.19 Competitive adsorption in process water system: (a) Cu removal efficiency, (b) Ni removal efficiency, (c) DETA removal efficiency (initial solution pH = 9.5, adsorbent dosage = 0.5 wt.%, contact time = 120 minutes)

To further understand the fundamental principle how metal-DETA species adsorb on M-AC, TOF-SIMS was employed to investigate the surface images of M-AC after metal-DETA species adsorption. To simplify the system, images were taken after loading in binary component system. Here solution containing 15 mg/L copper combined with 25 mg/L DETA was chosen. As shown, Figure 4.20 (a) – (c) are images of the basic materials. It shows the ion pieces of carbon, oxide, and iron oxides which are components of M-AC. Figure 4.20 (d) is the isotope copper ion which indicates the adsorption of copper ions on M-AC surface. Figure 4.20 (e) is the C_2H_4N ion piece which could come from the segments of the DETA molecule. Figure 4.20 (f) is the image of $CH_2N^{63}Cu$ captured from Cu-DETA complexes. This suggests that the copper adsorption on M-AC is in the form of copper-DETA complex. The affinity between M-AC surface and copper/DETA species are not strong enough to separate copper or DETA from Cu-DETA complexes. Instead, Cu-DETA complexes are present on the M-AC surface. In addition, copper ions, DETA and Cu-DETA complexes are found in the area with oxide and iron oxide signal only but without carbon signal, as indicated by white arrow. This suggests the interaction between iron oxides on carbon surface and the species in solutions, confirming that iron oxides deposited on activated carbon surface significantly affect the adsorptive behavior of M-AC compared with pure activated carbon.

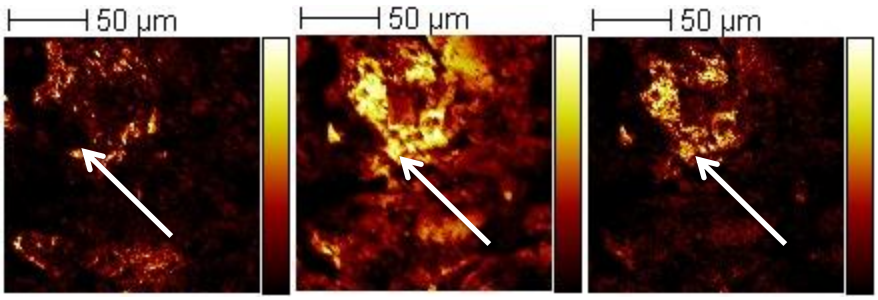

(a) C (b) O (c) FeO

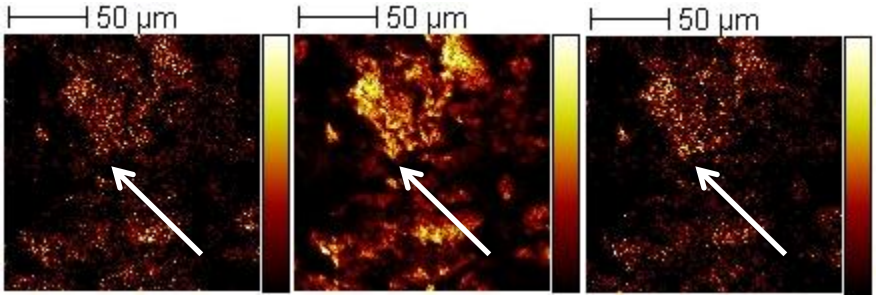

(d) ^{63}Cu (e) C_2H_4N (f) $CH_2N^{63}Cu$

Figure 4.20 TOF-SIMS images of M-AC after adsorption (15 mg/L Cu + 25 mg/L DETA, initial solution pH = 9.5, adsorbent dosage = 0.5 wt.%)

4.4 Adsorption Isotherm

In order to describe the equilibrium adsorptive behavior for Cu (II), Ni (II) and DETA on three kinds of adsorbents, various adsorption isotherm models were introduced to study the satisfactory adsorption isotherm equations for experimental data. An adsorption isotherm equation expresses the relation between the amount of solute loaded on adsorbents and the concentration of the solute in the fluid phase at a given constant temperature. In this study, all adsorption data were collected at room temperature.

4.4.1 Adsorption isotherm models

The Langmuir and Freundlich isotherm models [21, 79, 92] were employed for modeling the experimental adsorption data between the two phases as follows:

a) Langmuir equation

The Langmuir equation is generally corresponded to monolayer adsorption which is based on four important assumptions: (1) Adsorption only occurs at definite localized "sites" on the adsorbent surface. (2) Only one molecule of adsorbent species could be bonded onto each site. (3) Adsorption energy between adsorbent molecule and each site of adsorbent is the same for all sites. (4) There is no interaction around the adsorbed species molecules.

$$\frac{C_e}{Q_e} = \frac{1}{b*q_m} + \frac{C_e}{q_m} \qquad [4 - 4]$$

where C_e is the equilibrium concentration of solutes in solutions in mg/L, Q_e is the amount adsorbed onto adsorbent at equilibrium in mg/g. q_m and b are two parameters. The parameter q_m (mg/g) is the maximum value that Q_e tends towards as C_e becomes larger. Physically q_m represents the concentration of the adsorbed species on the adsorbent surface when complete monomolecular layer of coverage is achieved. b is a constant parameter reflecting the binding energy between adsorbent surface sites and the adsorbing species due to the assumed homogeneity of the adsorption surface sites.

b) Freundlich equation

$$Q_e = K{C_e}^{1/n} \qquad [4 - 5]$$

where the n indicates bond energies between adsorbed species and the adsorbent, and K is related to the bond strength in Freundlich equation. It is important to point out that, unlike Langmuir equation, Freundlich equation as shown allows Q_e increasing without limit as C_e increases, but it is physically impossible. Thus, Freundlich equation will not be a suitable model with very high C_e values since it might be failed in fitting experimental data.

Unlike Langmuir model, Freundlich model do not impose any requirement to the complete monolayer coverage. The Freundlich model implies that the energy distribution for the adsorption onto surface is essentially of an exponential type, more consistent with experimental evidence. It means that some surface “sites”

are more energetic to bind the adsorbed species more strongly while some other "sites" are less energetic to bind solute compared with high energetic sites.

4.4.2 Adsorption isotherm in single/multi component adsorption

Figure 4.21 to Figure 4.26 respectively present the linearized Langmuir and Freundlich isotherm plots for adsorption of Cu (II)/Ni (II)/DETA onto different adsorbents in three single systems, two binary systems and one ternary system. Table 4.3 to Table 4.7 list the various calculated isotherm constants and correlations coefficients (R^2) which indicate the goodness-of-fit of experimental data: The closer to 1 R^2 value is, the better relative model fits experimental data. For single component systems, the Langmuir isotherm fitting is more suitable for Cu (II), Ni (II) and DETA adsorption onto Fe_3O_4 and M-AC. Meanwhile, the Freundlich isotherm fitting is more suitable for Cu (II), Ni (II) and DETA adsorption onto activated carbon as shown in Figure 4.27.

As discussed in section 4.4.1, Langmuir is more suitable for a uniformly physical monolayer adsorption whereas Freundlich is more suitable for a rough and exponential adsorption process onto surfaces with uneven binding sites. The previous studies show that the functional groups and charging are not even on the surface of activated carbon. The Freundlich isotherm which implies that the energy distribution for the adsorption "sites" is an exponential type essentially is a better alternative to describe the metal ions and DETA adsorption onto activated carbon surface. On the other hand, the fitting results suggest that the metal ions and DETA adsorption onto magnetite fits Langmuir isotherm better, suggesting

adsorption onto magnetite is more uniform compared with activated carbon. The chemical adsorption is involved in the studied species adsorption onto M-AC and iron oxides since the experimental data fits better to the Langmuir isotherm which reflects the monolayer chemical adsorption. Moreover, the adsorption behaviour of M-AC is more similar to that of iron oxides than activated carbon since both M-AC and iron oxides adsorption data fits Langmuir isotherm better while activated carbon adsorption process fits Freundlich isotherm better. This phenomenon suggests that the magnetite deposited on activated carbon plays a significant role in heavy metal ions and DETA loading, consistent with the previous experimental results.

In addition, by comparing the Langmuir parameter q_m of various adsorptions, we found that q_m of the Cu (II)/Ni (II) adsorption onto Fe_3O_4 is higher than q_m of adsorption onto M-AC, indicating Fe_3O_4 has the larger maximum Cu (II)/Ni (II) adsorption ability than M-AC. In contrast, as shown in Table 4.5 for the DETA adsorption onto Fe_3O_4 and M-AC with Langmuir fitting, q_m of DETA adsorption on M-AC is higher than that of Fe_3O_4. This indicates Fe_3O_4 has lower maximum DETA adsorption capacity than M-AC.

The isotherm fittings in multi-component adsorption are presented from Figure 4.24 to Figure 4.26. For multi-component system, the Freundlich isotherm fitting (Figure 4.27) is more suitable than Langmuir isotherm fitting. The fitting methods were not employed for Ni (II) in binary systems after M-AC adsorption as the final concentrations of Ni (II) were too low to be detected by AAS.

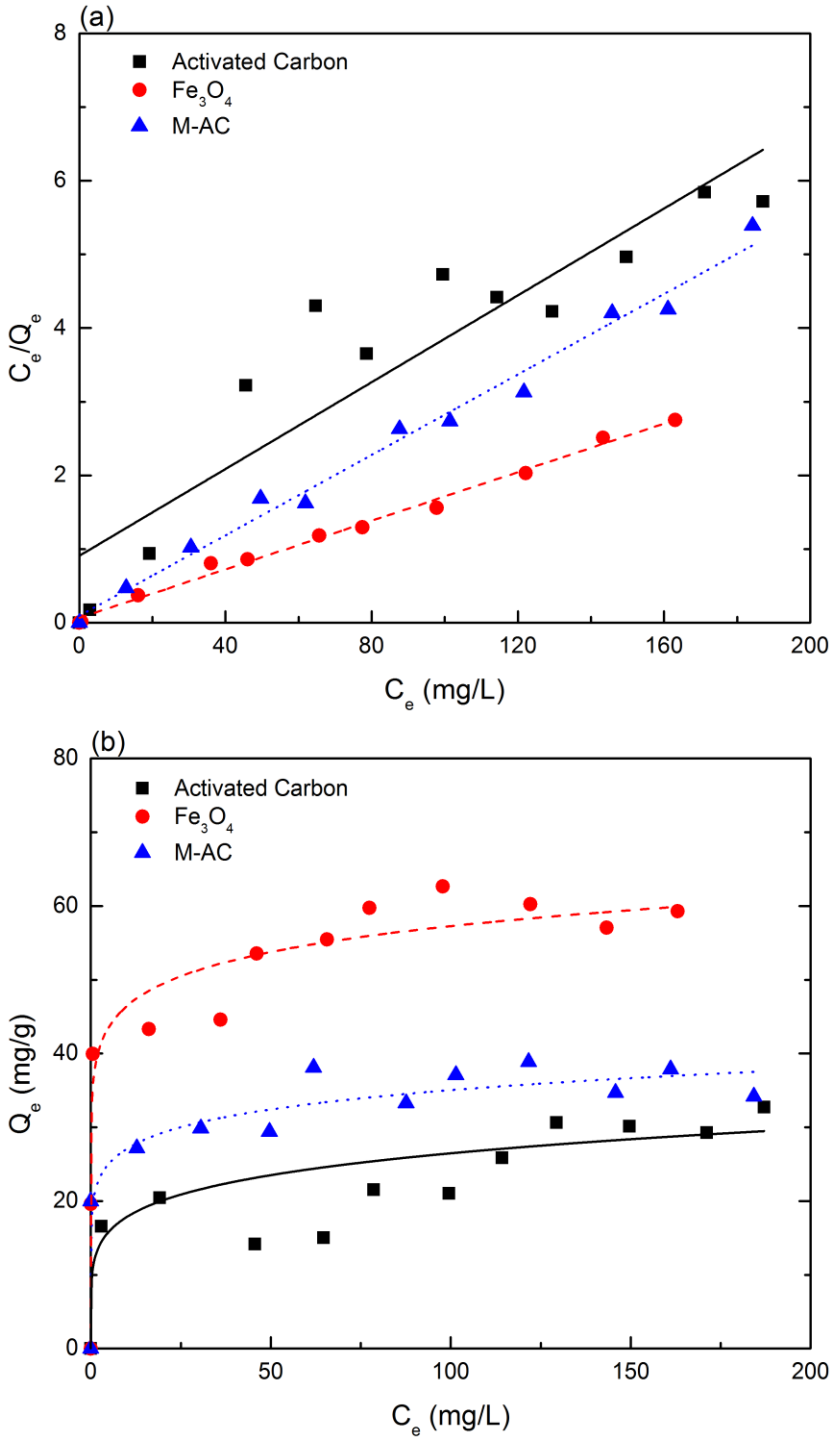

Figure 4.21 (a) Langmuir isotherm plot, and (b) Freundlich isotherm plot for adsorption of Cu (II) onto various types of adsorbents

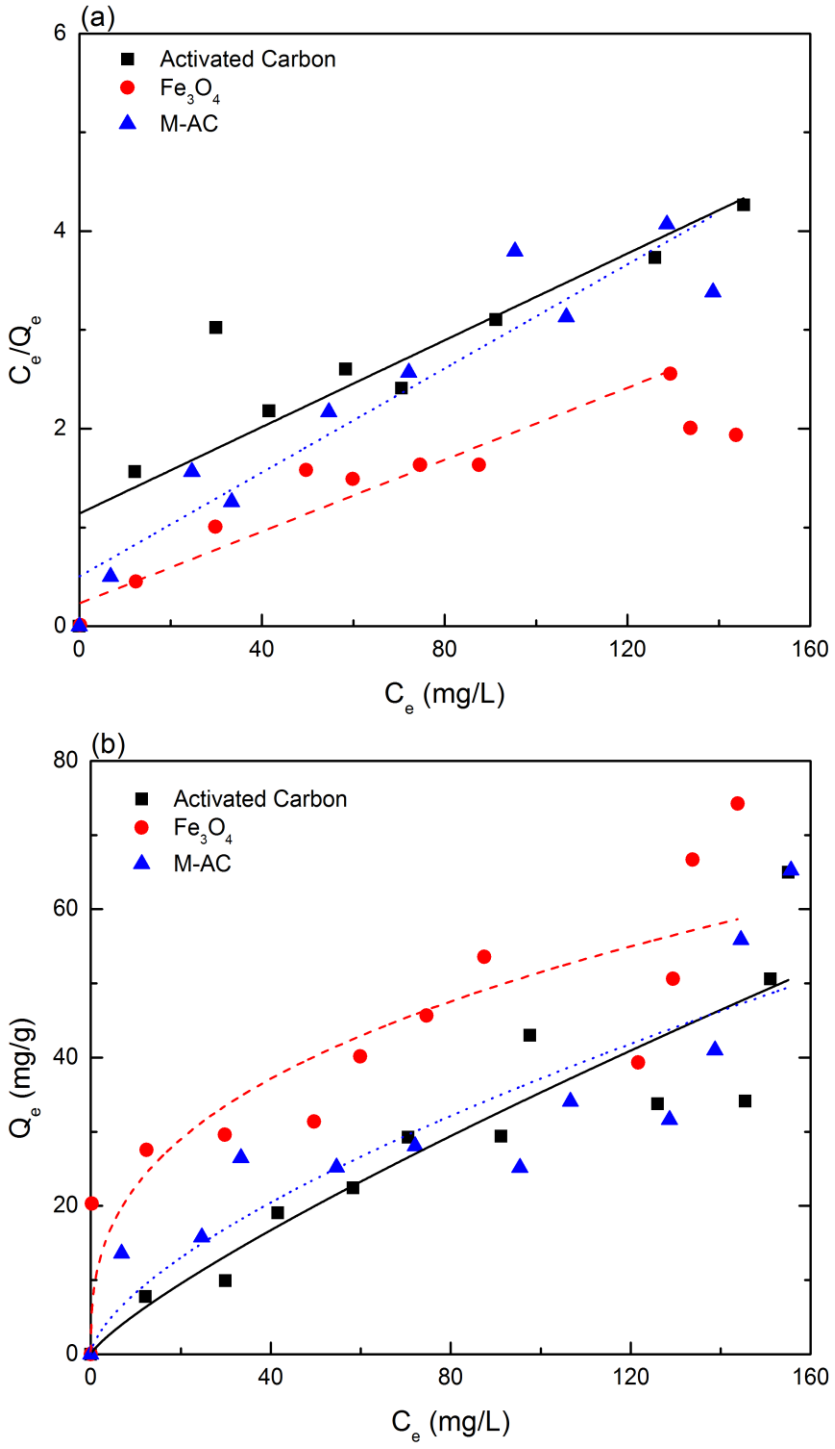

Figure 4.22 (a) Langmuir isotherm plot, and (b) Freundlich isotherm plot for adsorption of Ni (II) onto various types of adsorbents

Table 4.3 Estimated isotherm models and their constant values for Cu (II) adsorption onto various types of adsorbents

Adsorbent type	Langmuir equation $\frac{C_e}{Q_e} = \frac{1}{b * q_m} + \frac{C_e}{q_m}$			Freundlich equation $Q_e = KC_e^{1/n}$		
	R^2	b	q_m	R^2	K	n
Activated Carbon	0.8523	0.032	33.94	0.9126	12.02	5.83
Fe_3O_4	0.9932	60.60	60.65	0.8642	37.64	10.98
M-AC	0.9873	0.29	36.62	0.6469	20.93	8.94

Table 4.4 Estimated isotherm models and their constant values for Ni (II) adsorption onto various types of adsorbents

Adsorbent type	Langmuir equation $\frac{C_e}{Q_e} = \frac{1}{b * q_m} + \frac{C_e}{q_m}$			Freundlich equation $Q_e = KC_e^{1/n}$		
	R^2	b	q_m	R^2	K	n
Activated Carbon	0.7606	0.019	45.56	0.8458	0.83	1.23
Fe_3O_4	0.9596	0.079	54.95	0.7888	9.95	2.80
M-AC	0.8956	0.052	37.98	0.7825	1.84	1.53

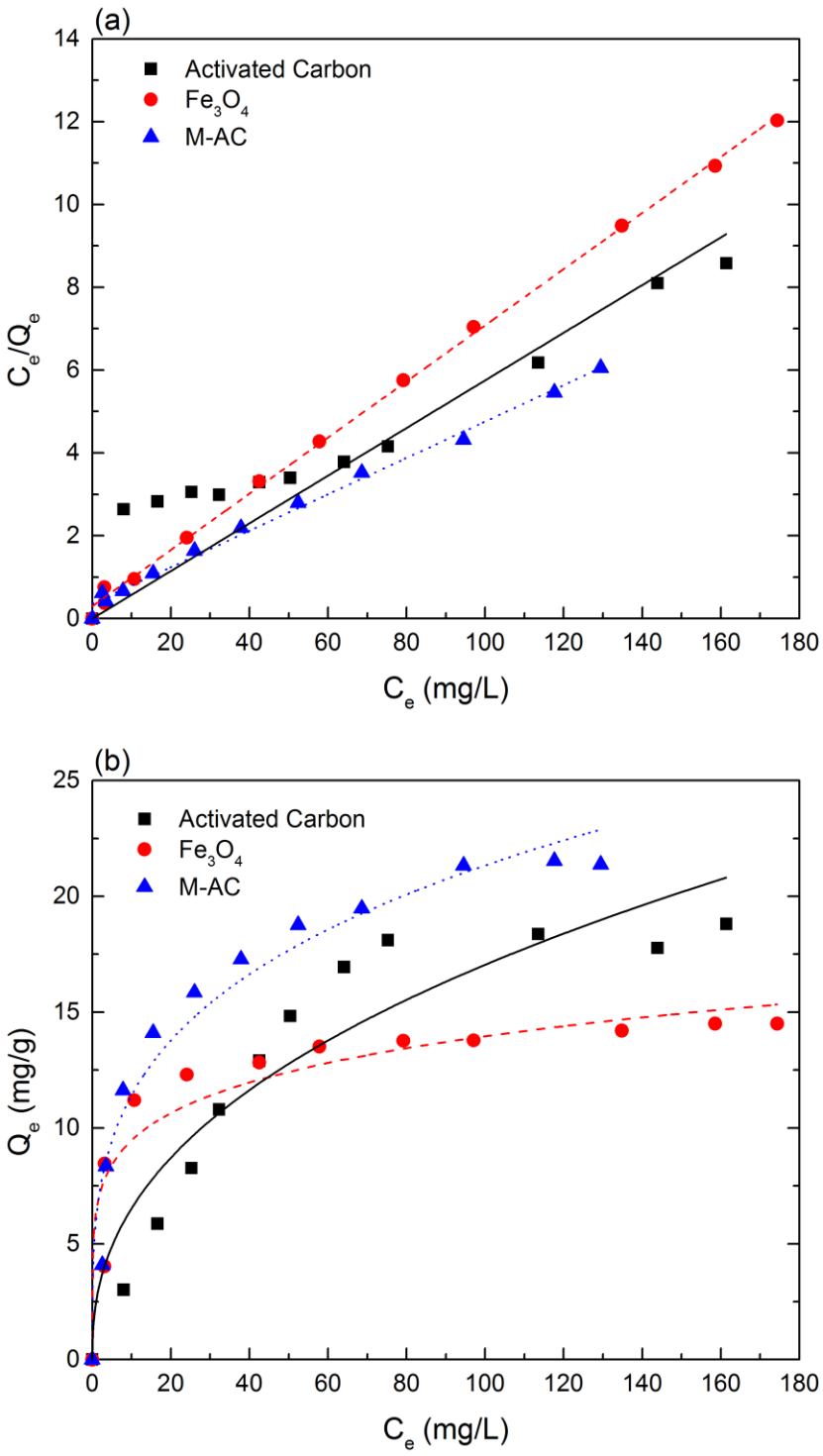

Figure 4.23 (a) Langmuir isotherm plot, and (b) Freundlich isotherm plot for adsorption of DETA species onto various types of adsorbents

Table 4.5 Estimated isotherm models and their constant values for DETA adsorption onto various types of adsorbents

Adsorbent type	Langmuir equation $\frac{C_e}{Q_e} = \frac{1}{b * q_m} + \frac{C_e}{q_m}$			Freundlich equation $Q_e = K{C_e}^{1/n}$		
	R^2	b	q_m	R^2	K	n
Activated Carbon	0.7863	$-4.15*10^{19}$	17.38	0.9036	2.50	2.40
Fe_3O_4	0.9987	0.22	14.75	0.9106	6.42	5.93
M-AC	0.9937	0.12	22.74	0.9601	6.11	3.68

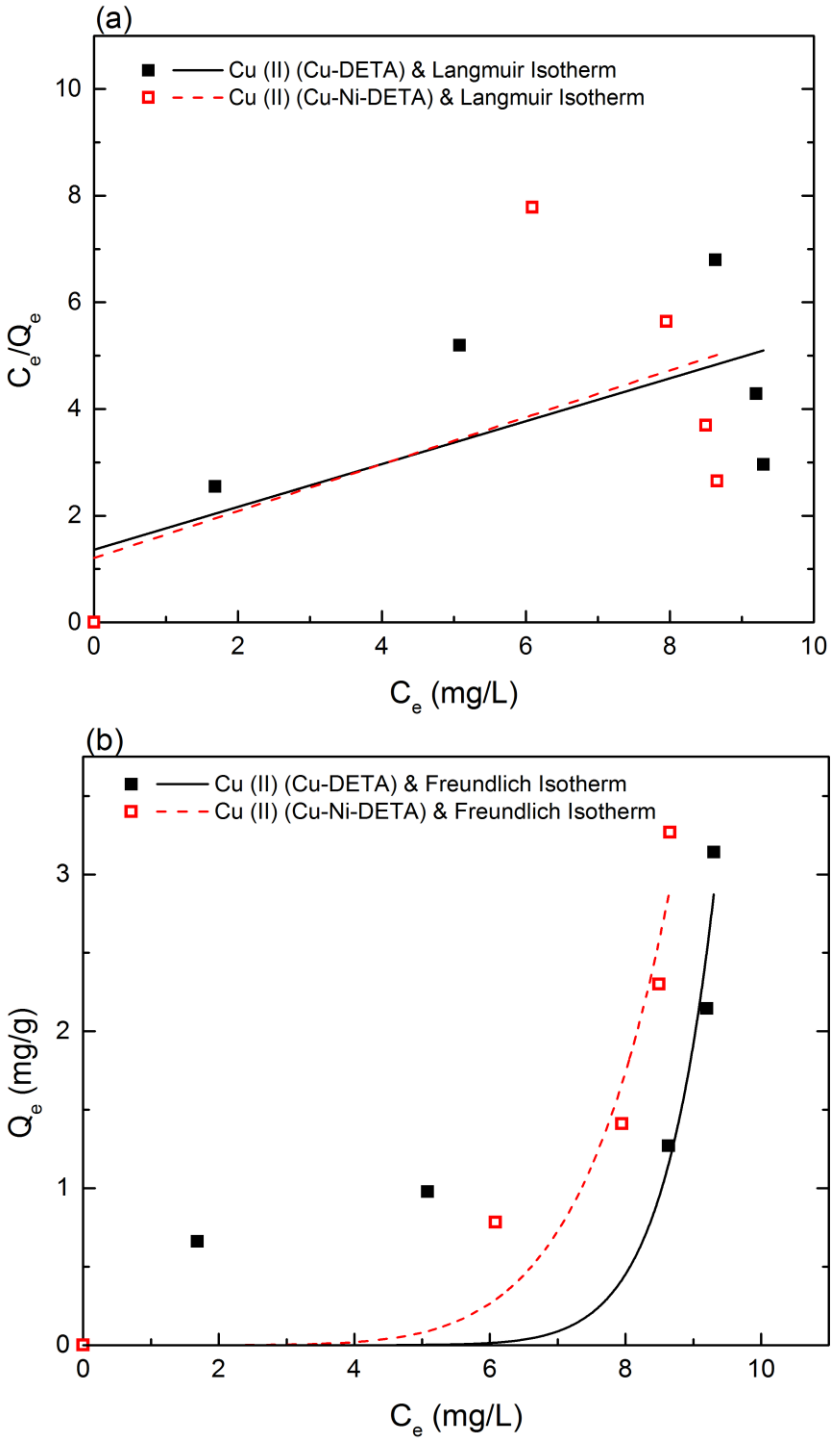
(a)
Cu (II) (Cu-DETA) & Langmuir Isotherm
Cu (II) (Cu-Ni-DETA) & Langmuir Isotherm
C_e/Q_e
C_e (mg/L)
(b)
Cu (II) (Cu-DETA) & Freundlich Isotherm
Cu (II) (Cu-Ni-DETA) & Freundlich Isotherm
Q_e (mg/g)
C_e (mg/L)

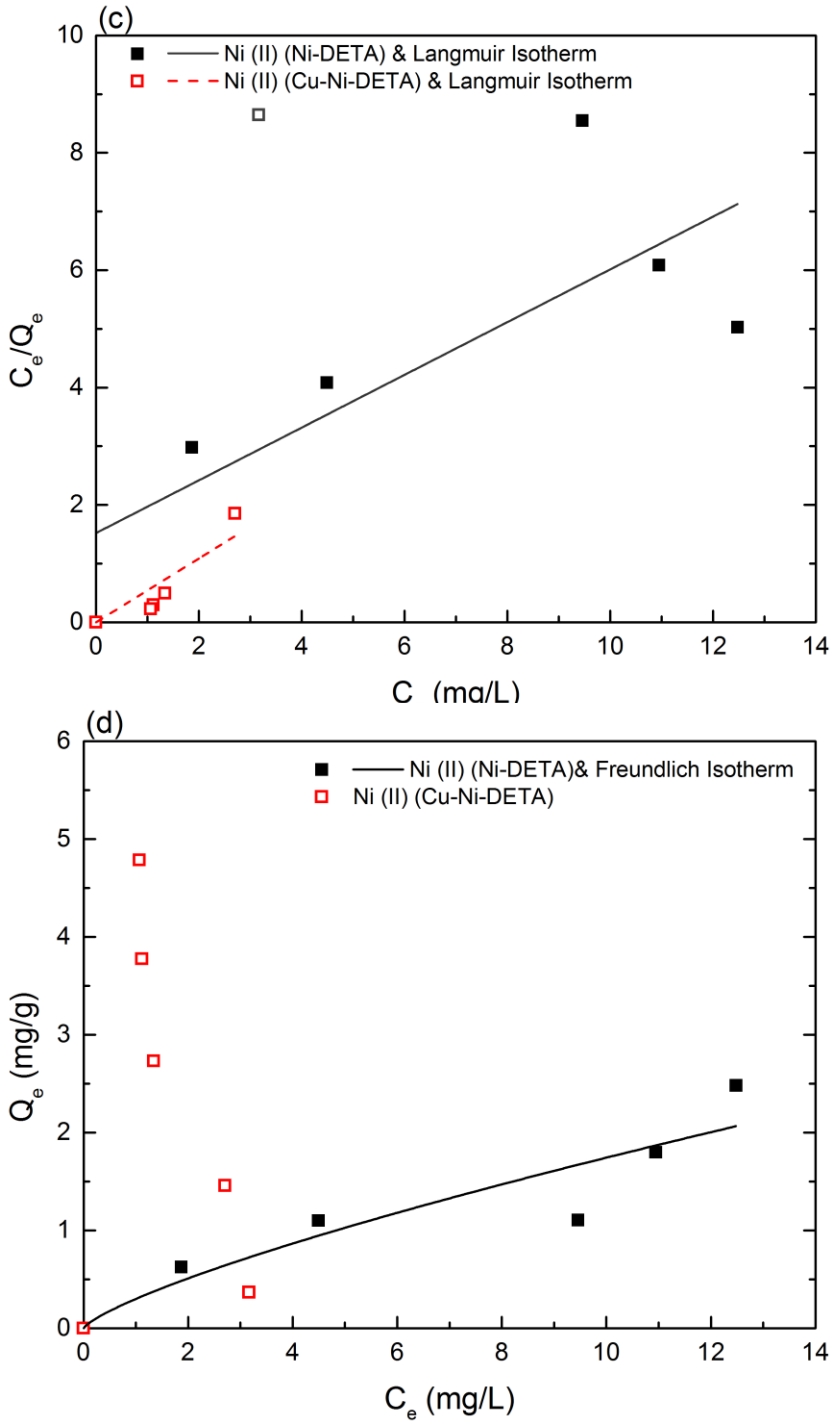

Figure 4.24 Adsorption isotherm plots for activated carbon in multi-component solution: (a) Langmuir isotherm plot for Cu (II) in Cu-DETA and Cu-Ni-DETA solutions, (b) Freundlich isotherm plot for Cu (II) in Cu-DETA and Cu-Ni-DETA solutions, (c) Langmuir isotherm plot for Ni (II) in Ni-DETA and Cu-Ni-DETA solutions, (d) Freundlich isotherm plot for Ni (II) in Ni-DETA and Cu-Ni-DETA solutions

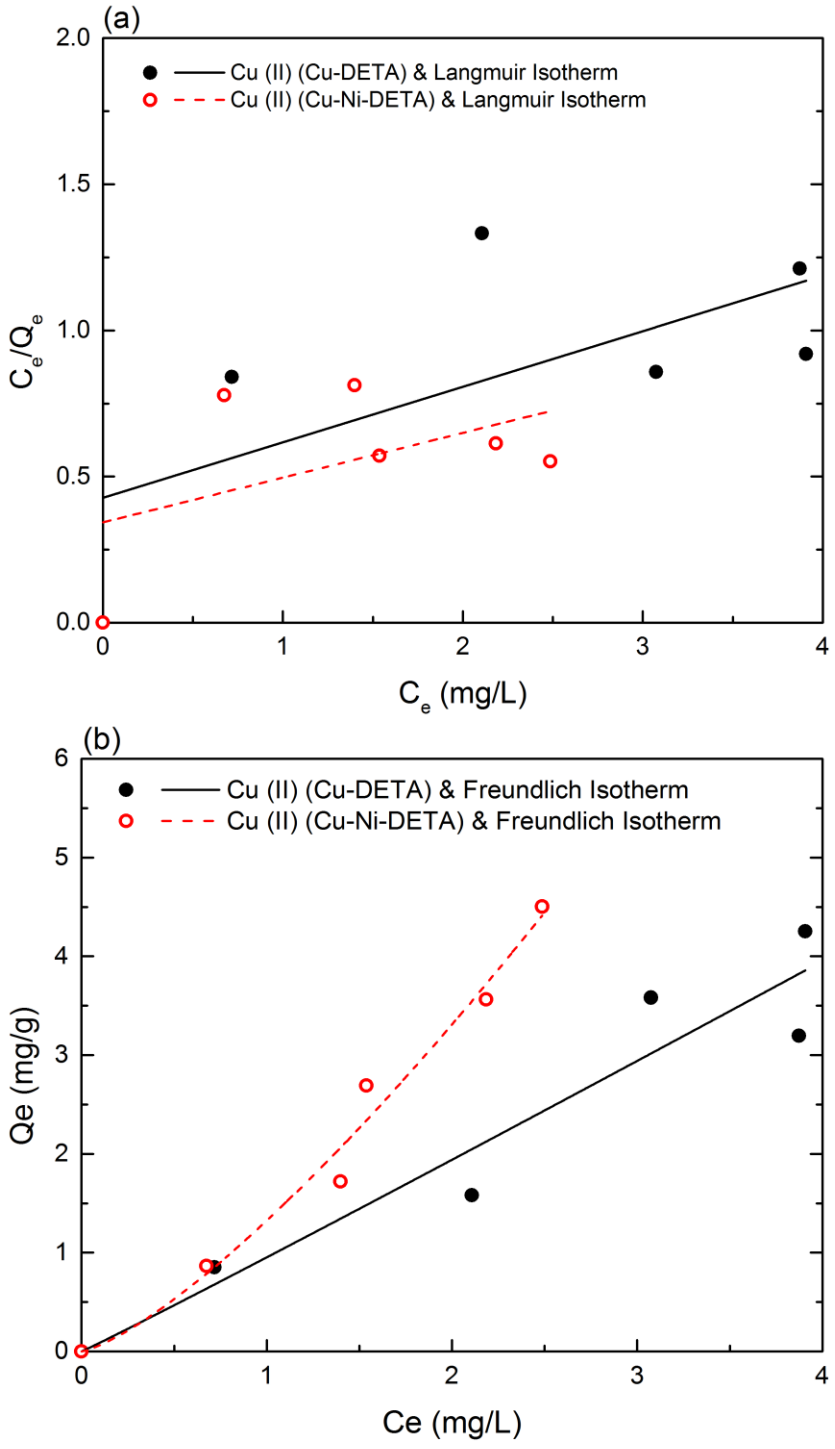

Figure 4.25 Adsorption isotherm plot for Fe_3O_4 in multi-component solution: (a) Langmuir isotherm plot for Cu (II) in Cu-DETA and Cu-Ni-DETA solution, (b) Freundlich isotherm plot for Cu (II) in Cu-DETA and Cu-Ni-DETA solution

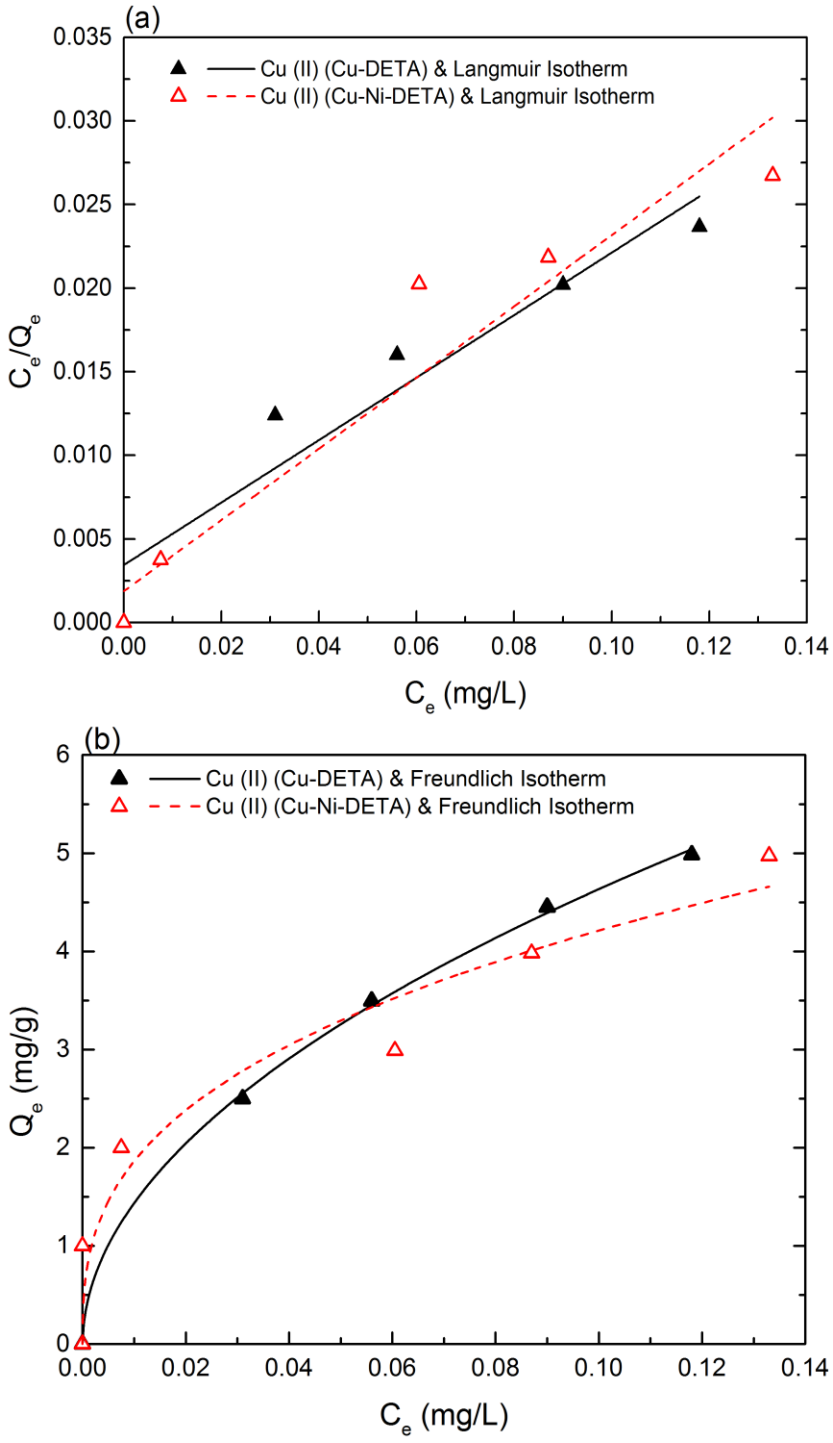

Figure 4.26 Adsorption isotherm plot for M-AC in multi-component solution: (a) Langmuir isotherm plot for Cu (II) in Cu-DETA and Cu-Ni-DETA solution, (b) Freundlich isotherm plot for Cu (II) in Cu-DETA and Cu-Ni-DETA solution

Table 4.6 Estimated Langmuir isotherm constants for multi-component adsoprtion on acitvated carbon, Fe_3O_4 and M-AC

Adsorbent	Parameters	Cu (II) (Cu-DETA)	Cu (II) (Cu-Ni-DETA)	Ni (II) (Ni-DETA)	Ni (II) (Cu-Ni-DETA)
Activated Carbon	R^2	0.4818	0.2929	0.6357	0.5386
	b	0.29	0.36	0.30	0.64
	q_m	2.49	2.27	2.23	0.64
Fe_3O_4	R^2	0.4469	0.2360	-	-
	b	0.44	0.45	-	-
	q_m	5.26	6.52	-	-
M-AC	R^2	0.9110	0.9306	-	-
	b	54.20	113.00	-	-
	q_m	5.35	4.70	-	-

Table 4.7 Estimated Freundlich isotherm constants for multi-component adsoprtion on acitvated carbon, Fe_3O_4, and M-AC

Adsorbent	Parameters	Cu (II) (Cu-DETA)	Cu (II) (Cu-Ni-DETA)	Ni (II) (Ni-DETA)	Ni (II) (Cu-Ni-DETA)
Activated Carbon	R^2	0.7506	0.9218	0.8570	-
	K	0.13	2.15E-6	0.30	-
	n	0.78	0.15	1.31	-
Fe_3O_4	R^2	0.9213	0.9802	-	-
	K	0.95	1.32	-	-
	n	0.97	0.76	-	-
M-AC	R^2	0.9992	0.9140	-	-
	K	14.95	9.52	-	-
	n	1.97	2.82	-	-

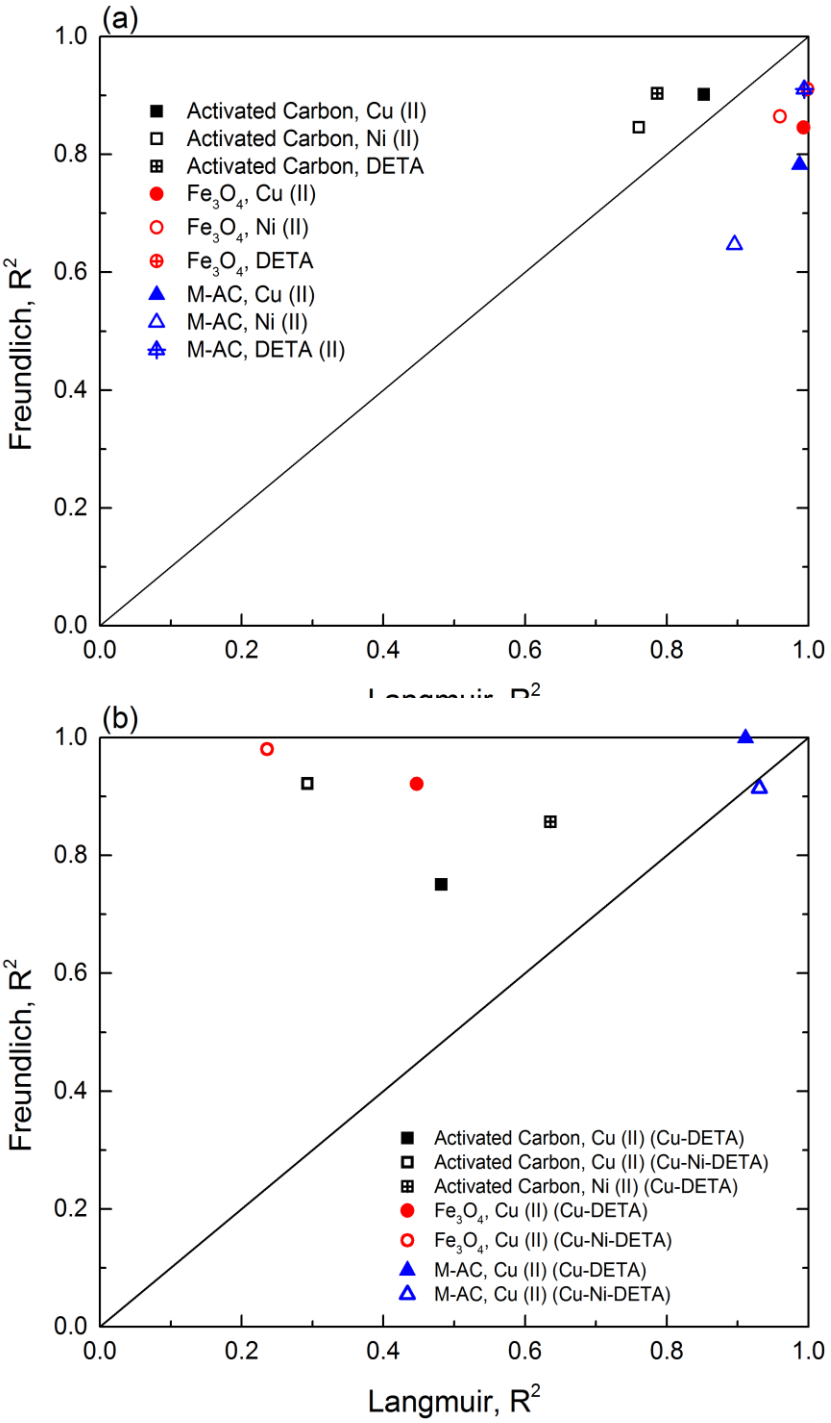

Figure 4.27 Comparative evaluation of Langmuir and Freundlich correlation coefficients (R^2) for (a) single and (b) multi component adsorption onto various types of adsorbents

4.5 Stripping Off Species from M-AC and Regeneration of M-AC

A key feature of the M-AC is its ability to be recycled and reused. Recovering metal ions from M-AC surface and reusing M-AC after recovery are significant objectives of this study.

Since magnetic iron oxides on M-AC surface might be washed off from M-AC at strong acidic condition, releasing iron ions into effluent and leading to the loss of magnetic property of M-AC, it is important to find an acidic condition which enables a high efficiency of metal stripping without dissolving magnetite from M-AC surface. The capability to strip adsorbed species was presented by stripping efficiency. The stripping of specie (Q_s) was calculated as following:

$$Q_s = \left[\left(C_s - C_f\right) * V_s\right]/m \qquad [4 - 6]$$

where C_s is the specie concentration after stripping in mg/L, V_d indicates the volume of acid in stripping in L and m, the weight of adsorbent in g.

The stripping efficiency was calculated according to mass balance calculations as following:

$$Stripping\ (\%) = {}^{Q_d}/_{Q_0} * 100\% \qquad [4 - 7]$$

where Q_s is the stripping species from per mass of adsorbents in the presence of acid and Q_0 (mg/g) is the original adsorption capacity of the virgin adsorbent.

Figure 4.28 presents the Cu/Ni recovery and iron leaching amount in effluents after M-AC was washed by hydrochloride acid (HCl) of different concentrations. The initial copper/nickel concentrations were 15 mg/L. M-AC dosage was used as 0.1 wt.%. Three acid washing cycles were employed.

For copper ions, the final Cu (II) concentration was less than 0.1 mg/L after the first adsorption, leading to nearly 100 % of Cu (II) removal efficiency. Figure 4.28 (a) shows that more copper ions could be stripped off from M-AC surface with more concentrated HCl acid, especially in the first washing. For the 10^{-2} M HCl (pH = 2) washing, for per gram of M-AC, 13.2 mg copper ions could be stripped off after three times acid washing. However, at this condition, the iron leaching was relatively high, leading to deposited iron oxides dissolving and causing the second contaminant. 10^{-4} M HCl (pH = 4) could not efficiently wash Cu (II) from M-AC surface after three washing cycles, indicating this acidic condition was too weak to strip off copper ions from M-AC particles. Unlike HCl at 10^{-2} M or 10^{-4} M, HCl with 10^{-3} M at pH = 3 could strip off more than 80 % of Cu from M-AC surface while only leached out about 0.1 mg iron ions from per gram of M-AC into solution. Therefore, HCl (pH = 3) is an appropriate condition for copper recovery and M-AC reuse. Moreover, Figure 4.28 (b) shows that HCl (10^{-3} M, pH = 3) is also a suitable acid condition for nickel recovery by considering both the high stripping efficiency and low iron leaching.

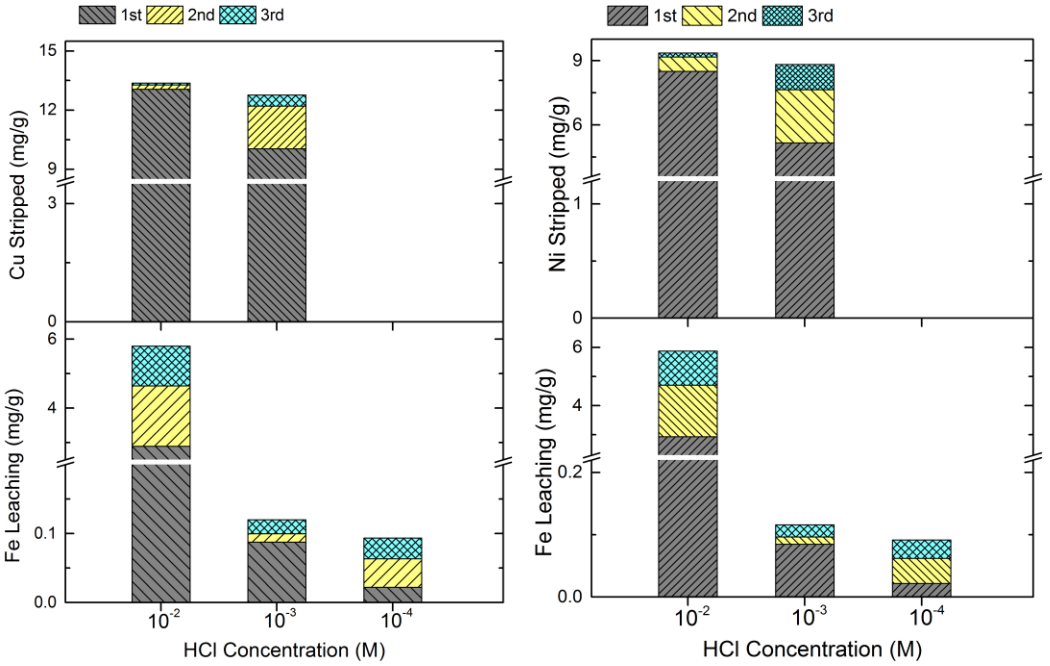

Figure 4.28 (a) Cu (II) (C_i = 15 mg/L, C_f < 0.1 mg/L, $Q_e \approx$ 15 mg/g) recovery and Fe leaching (b) Ni (II) (C_i = 15 mg/L, C_f = 5.7 mg/L, Q_e = 9.3 mg/g) recovery and Fe leaching, after stripping with hydrochloride acid of different concentrations

In this study, several methods were employed in regenerating M-AC particles after stripping off loaded copper ions. The regeneration efficiency was calculated using [93]:

$$Regeneration\ (\%) = {Q_r}/{Q_0} * 100\% \qquad [4 - 8]$$

where Q_r is the species adsorption capacity of the regenerated M-AC and Q_0 is the original adsorption capacity of the virgin adsorbent.

Figure 4.29 shows the M-AC regeneration efficiency through various different treating methods. If the M-AC (sample No. 1) was directly applied to next step adsorption after being washed for three times by HCl (10^{-3} M, pH =3) without further treatment, the regeneration efficiency of M-AC was as low as 1.9 %. This indicates that the M-AC particles need to be treated before reuse. Thus, we treated M-AC respectively with H_2SO_4 ($5*10^{-4}$ M, pH =3) (sample No. 2), pure water (sample No.3) and NaOH (10^{-3} M, 10^{-2} M, 10^{-1} M) (sample No. 4, 5, 6). It was found that regeneration efficiency was slightly improved to 8.2 % by pure water and greatly improved to more than 80 % after being treated with NaOH (10^{-1} M) solution. Thus, 10^{-1} M NaOH solution was employed to regenerate magnetic particles for recycling. This phenomenon indicates that H^+ ions occupy the binding sites of M-AC after acid washing and that OH^- ions neutralize the surface with H^+ to regenerate the surface binding sites. This observation also suggests the ion-exchange mechanism during metal ion adsorption onto M-AC surface.

Figure 4.30 (a) - (c) and Figure 4.31 summarize the recovery of adsorbed species with 10^{-3} M HCl and regeneration efficiency with 10^{-1} M NaOH for M-AC and Fe_3O_4 after Cu/Ni/DETA adsorption.

Figure 4.30 (a) presents the Cu (II) adsorption capacity onto M-AC and Fe_3O_4 respectively in the first adsorption, species recovery with acid washing and the species adsorption capacity in the second adsorption after magnetic particles regeneration. As shown in Figure 4.10 (b), with 160 mg/L copper ions initially, both M-AC and Fe_3O_4 surface were saturated and achieved maximum adsorption capacity. Therefore, the initial concentration of copper ions at 160 mg/L was employed for investigating the magnetic particle recycling and reuse for Cu (II). It was shown that Cu (II) adsorption capacity onto M-AC in 2nd adsorption test after stripping and regeneration was close to the 1st adsorption meanwhile most loaded copper ions could be recovered from M-AC surface after acid washing. In contrast, even though the Cu (II) adsorption capacity onto Fe_3O_4 was as high as 66 mg/g in the 1st adsorption, it dropped significantly to 22 mg/g after following the same stripping and regeneration procedure as M-AC particles. The regeneration efficiency of M-AC for copper ions was as high as 98 % while only 32 % of Fe_3O_4 from Figure 4.31.

For nickel ions, initial 140 mg/L concentration was used for regeneration study to get magnetic particle surface saturated. From Figure 4.30 (b) and Figure 4.31, the regeneration efficiency of M-AC for nickel adsorption was higher than 80 % while only 48 % for iron oxides. The regeneration efficiency of M-AC for DETA

was higher than 99 % and that of Fe_3O_4 was only 52 % for DEAT from Figure 4.30 (c) and Figure 4.31 with 200 mg/L DETA in solutions initially. The above investigation suggested the adsorption sites on M-AC surface were easier to be regenerated by sodium hydroxide solution after stripping off the loaded species with acid. Even though magnetic Fe_3O_4 presented higher affinity with copper ions and nickel ions, it was more difficult to be recycled compared with M-AC.

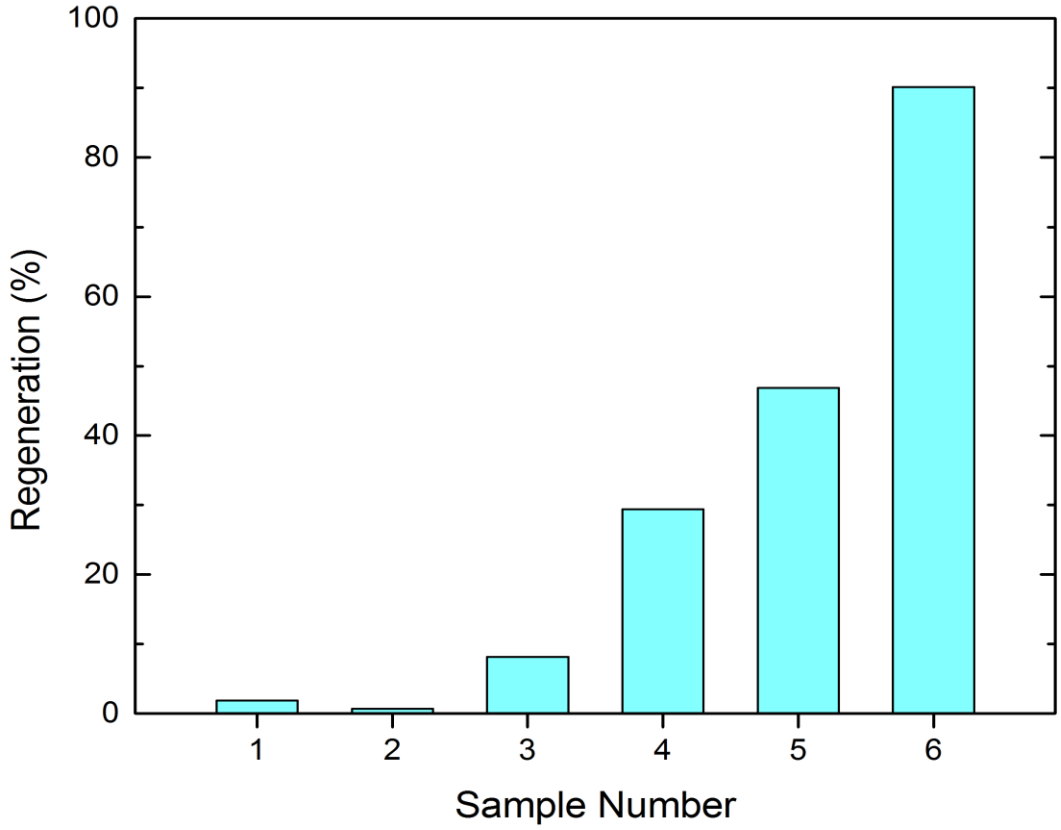

Figure 4.29 Regeneration efficiency of M-AC to adsorb Cu (II) through various regeneration methods (sample number listed as follows)

No. 1: 1st adsorption → Strip off copper ions with 10^{-3} M HCl (pH = 3) → 2nd adsorption

No.2: 1st adsorption → Strip off copper ions with 5 * 10^{-4} M H_2SO_4 (pH = 3) → 2nd adsorption

No. 3: 1st adsorption → Strip off copper ions with 10^{-3} M HCl → Wash M-AC two time with deionized water → 2nd adsorption

No. 4: 1st adsorption → Strip off copper ions with 10^{-3} M HCl → Wash M-AC two time with 10^{-3} M NaOH → 2nd adsorption

No. 5: 1st adsorption → Strip off copper ions with 10^{-2} M HCl → Wash M-AC two time with 10^{-2} M NaOH → 2nd adsorption

No. 6: 1st adsorption → Strip off copper ions with 10^{-1} M HCl → Wash M-AC two time with 10^{-1} M NaOH → 2nd adsorption

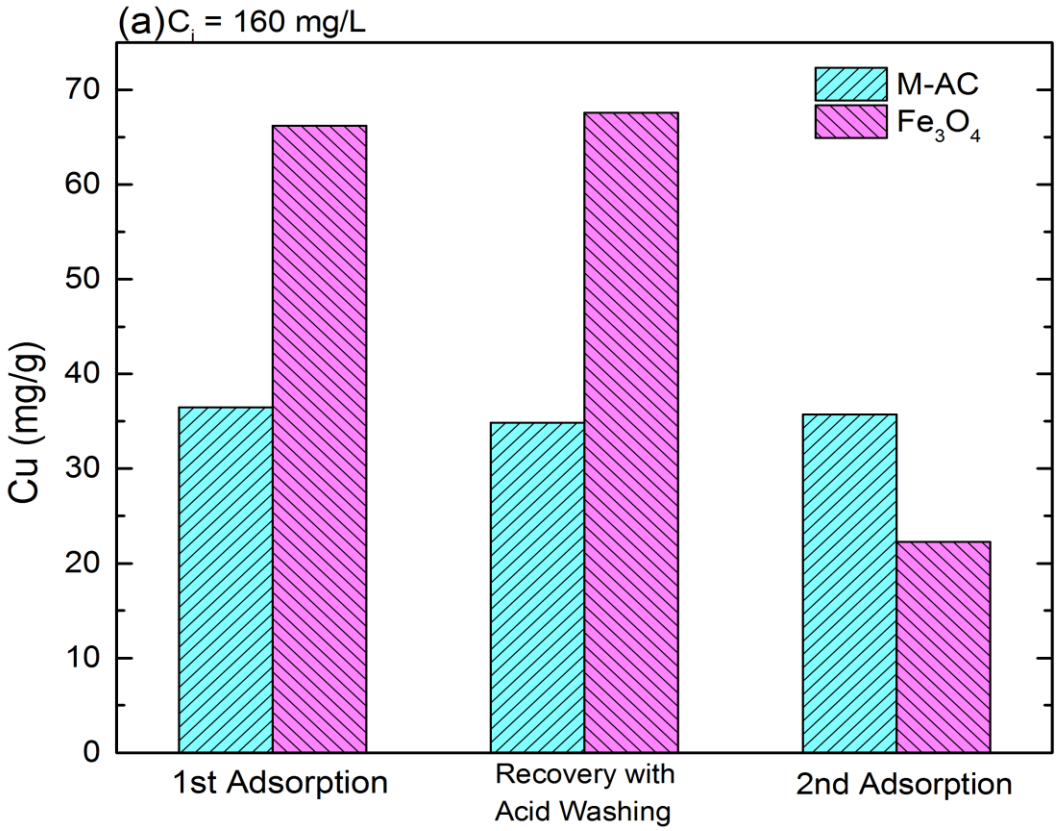
(a)C_i = 160 mg/L
Cu (mg/g)
0
10
20
30
40
50
60
70
M-AC
Fe_3O_4
1st Adsorption
Recovery with
Acid Washing
2nd Adsorption

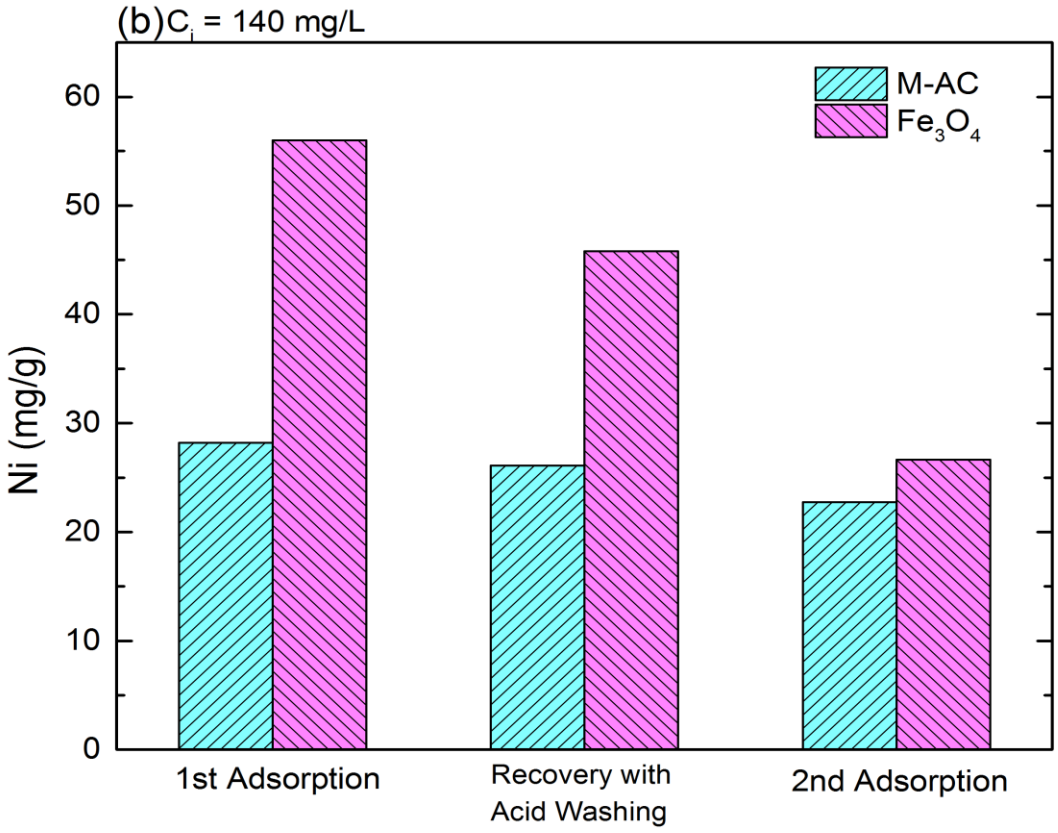
(b)C_i = 140 mg/L
Ni (mg/g)
0
10
20
30
40
50
60
M-AC
Fe_3O_4
1st Adsorption
Recovery with
Acid Washing
2nd Adsorption

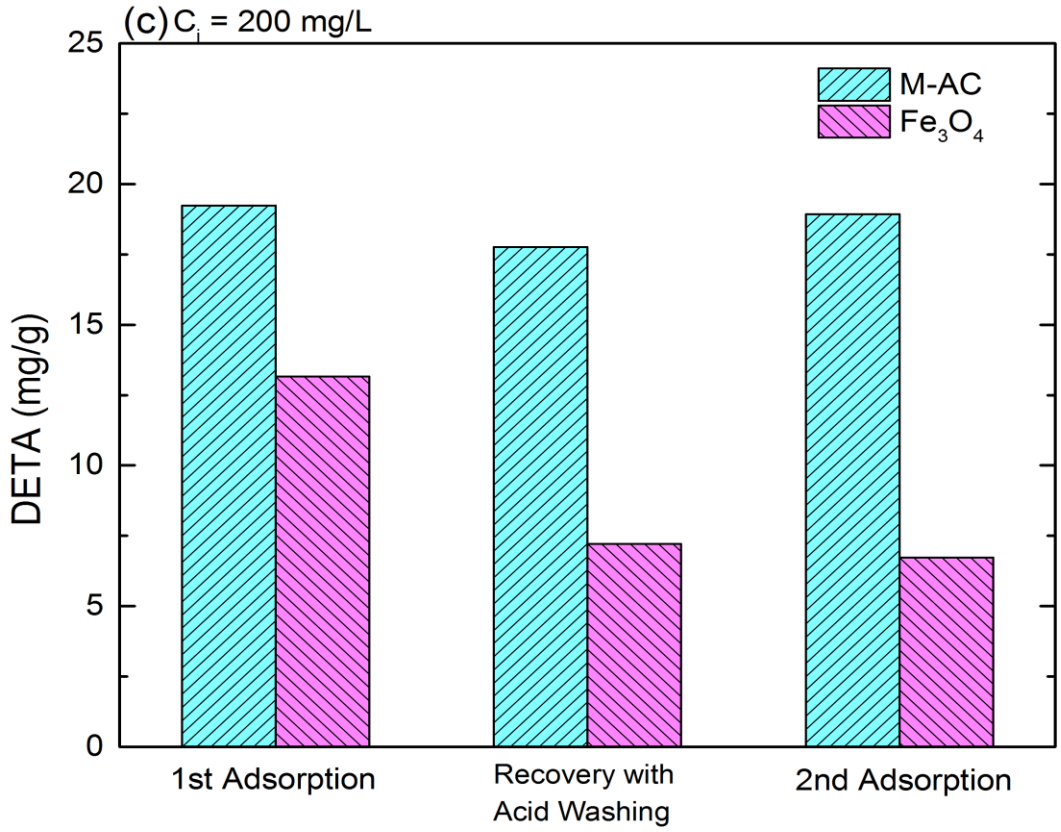

Figure 4.30 The (a) Cu (adsorbent dosage = 0.1 wt.%) (b) Ni (adsorbent dosage = 0.1 wt.%) and (c) DETA (adsorbent dosage = 0.5 wt.%) adsorption capacity onto M-AC and Fe_3O_4 in the 1st adsorption, the species recovery with acid washing, and the adsorption capacity in the 2nd adsorption

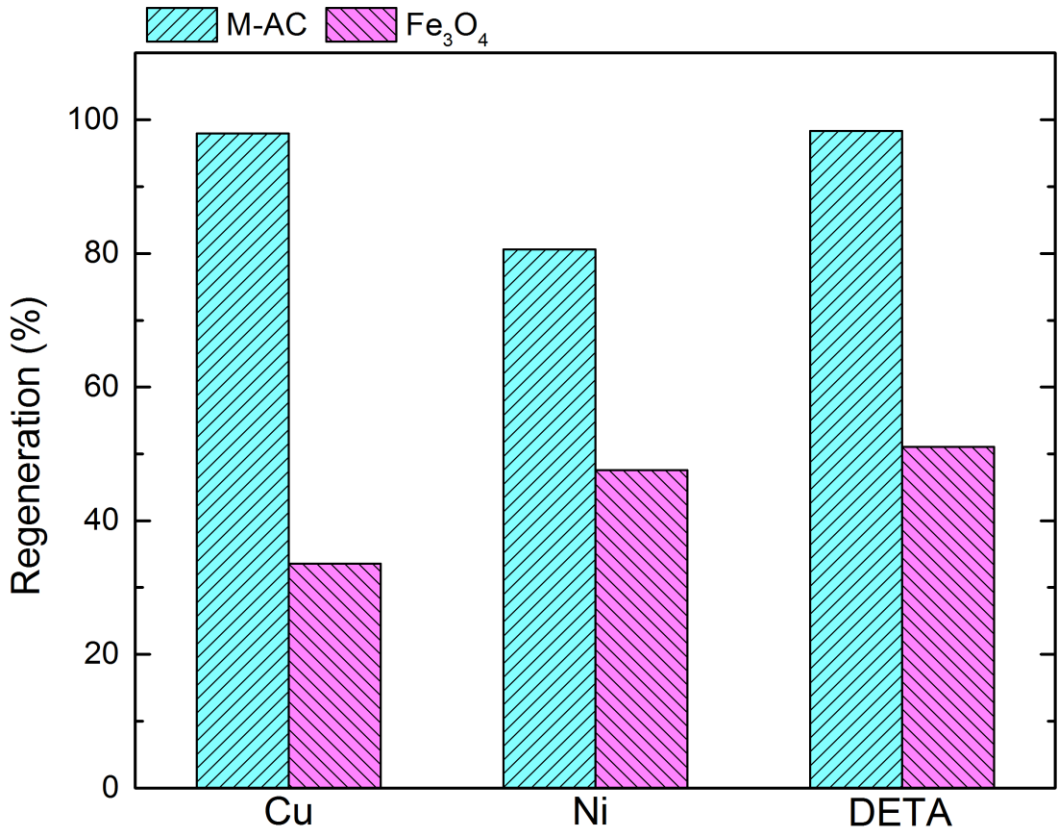

Figure 4.31 The regeneration effeciency of M-AC and Fe_3O_4 in Cu/Ni/DETA adsorption

4.6 Potential Applications in Gold Recovery

Activated carbon has been used in the commercial process of gold leaching and recovery. Carbon-in-pulp (CIP) process commonly uses activated carbon to adsorb the gold cyanide after the cyanidation procedure. The particle size of activated carbon has a significant effect on the rate of gold cyanide adsorption onto carbon [71]. However, the difficulty in the separation of fine activated carbon particles from the pulp limits the application of powder activated carbon in CIP process. Thus, M-AC was investigated as an alternative adsorbent for pure activated carbon to load gold cyanide in this study since M-AC particles could be separated from effluents easily by applied magnetic field.

Figure 4.32 (a) – (c) presented the gold recovery efficiency and adsorption onto per mass or per unit of surface area of pure activated carbon, Fe_3O_4 and M-AC respectively. Twenty four hours shaking time was employed in this study to reach the thermodynamic equilibrium condition. The pH of the solutions was adjusted to 11. The adsorbent dosage was set to 0.1 wt.%. In Figure 4.32 (a), the gold recovery efficiency of M-AC or activated carbon with 0.1 wt.% dosage decreased as increasing initial gold concentrations. Gold cyanide species showed higher affinity with activated carbon than M-AC. In other words, activated carbon has better gold recovery efficiency than M-AC. Activated carbon could recover more than 99 % of gold species from solution with 10 mg/L of gold solution initially while recovering around 14.7 % of gold from 1000 mg/L of gold solution. On the other hand, M-AC adsorbed 82.2 % of gold from 10 mg/L of gold solution and

adsorbed about 5.7 % of gold from solutions with 1000 mg/L gold concentrations. Moreover, the Fe_3O_4 particles showed no affinity with gold cyanide complexes.

Figure 4.32 (b) shows the gold adsorption capacity onto per mass of adsorbents. The gold adsorption capacity onto activated carbon and M-AC was enhanced with higher initial gold concentrations while the gold adsorption onto magnetic iron oxide particles was close to zero. The maximum gold adsorption capacity onto activated carbon is about 142 mg/g while only 55 mg/g gold adsorbed onto M-AC maximally. For certain mass of adsorbents, activated carbon has twice as much specific surface area as M-AC, the amount of gold loaded on unit weight (mg/g) of activated carbon was twice as much as the gold loaded on unit weight of M-AC (mg/g) (Figure 4.32 (b)). Figure 4.32 (c) presents the amount of gold adsorption onto the unit surface of activated carbon or M-AC.

Current results suggest that M-AC could be potentially employed in CIP for gold recovery after gold extraction by cyanidation, but activated carbon has better gold loading performance than M-AC. The reduction of gold adsorption onto M-AC compared with pure activated carbon could be attributed to the deposition of iron oxides on M-AC since magnetic iron oxides show no affinity with gold cyanide species.

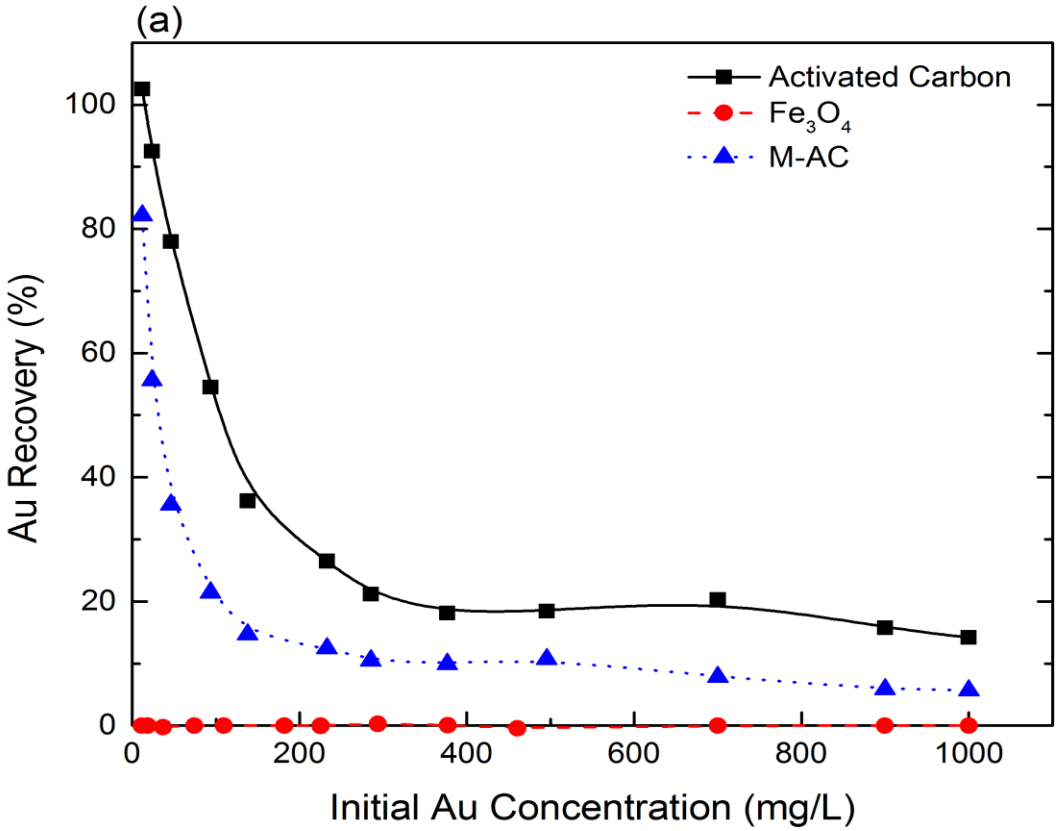
(a)
Activated Carbon
Fe3O4
M-AC
Au Recovery (%)
0
20
40
60
80
100
0
200
400
600
800
1000
Initial Au Concentration (mg/L)

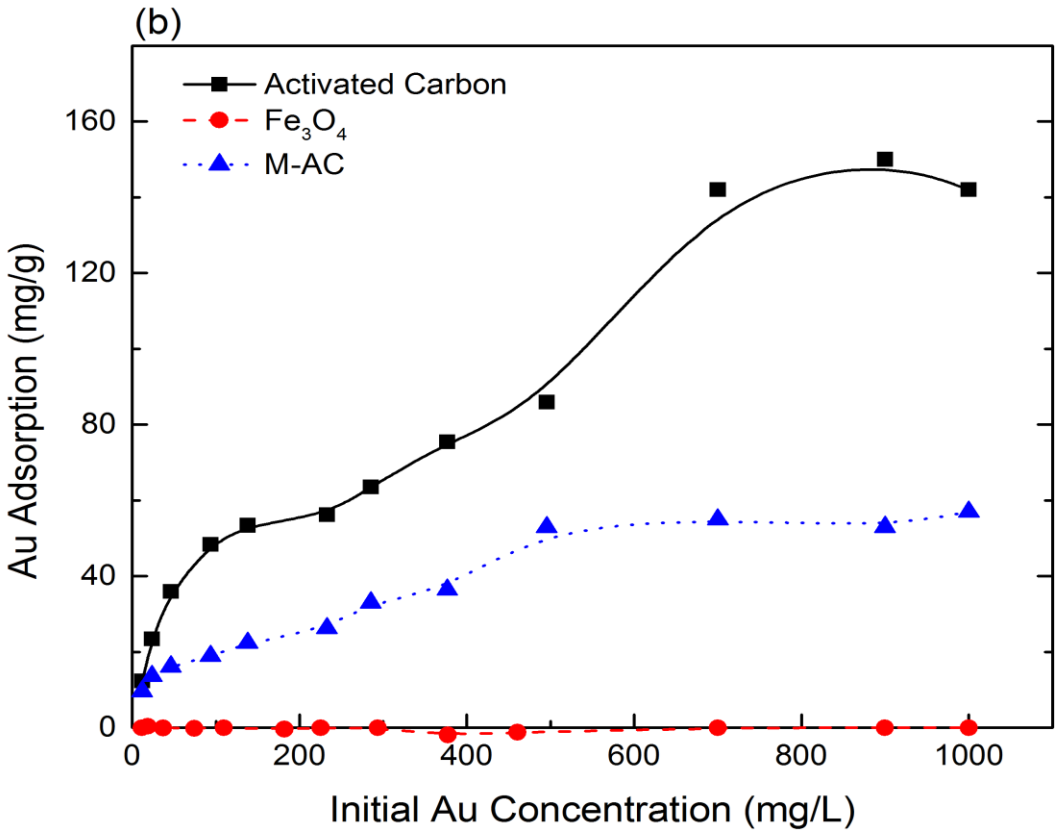
(b)
Activated Carbon
Fe3O4
M-AC
Au Adsorption (mg/g)
0
40
80
120
160
0
200
400
600
800
1000
Initial Au Concentration (mg/L)

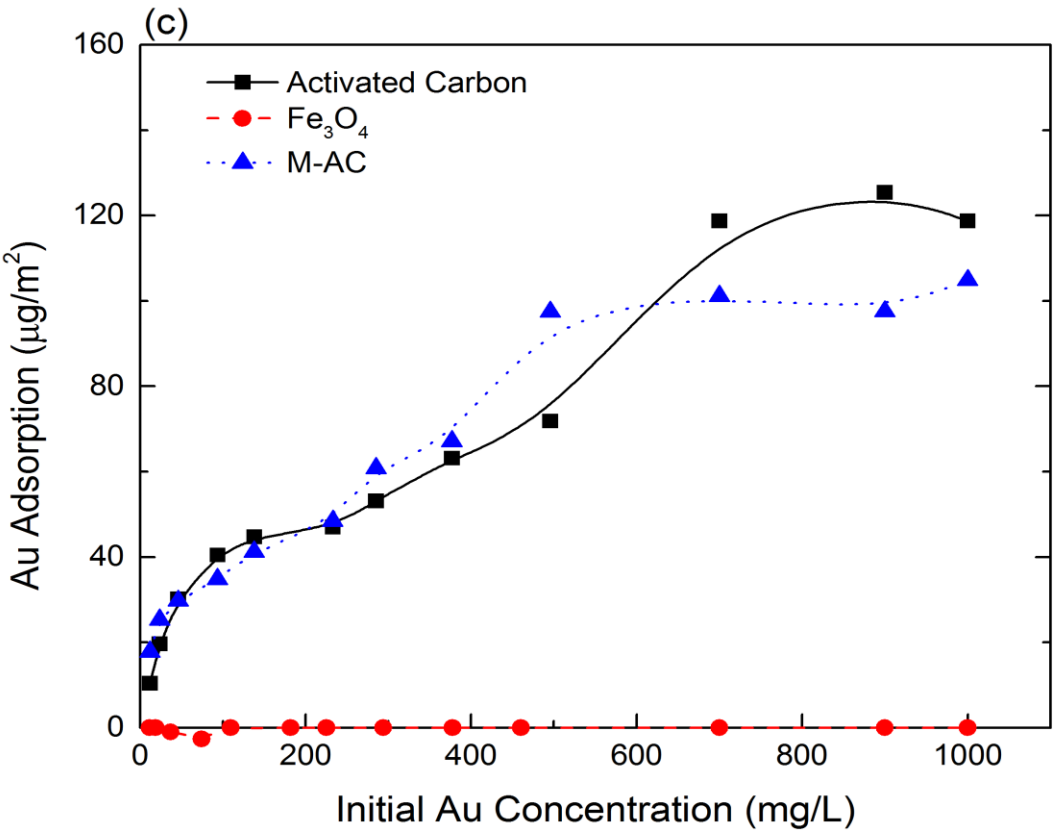

Figure 4.32 (a) Au (I) removal efficiency from solutions with various adsorbents, (b) Au (I) adsorption capacity onto per mass of various adsorbents, (c) Au (I) adsorption onto per unit surface area of various adsorbents, as a function of initial Au (I) concentrations (initial solution pH = 11, adsorbent dosages = 0.1 wt.%, contact time = 24 hours)

Figure 4.33 and Table 4.8 describes the isotherm modeling of gold adsorption behaviour on activated carbon and M-AC. It shows that the adsorptive behavior of gold species on both activated carbon and M-AC fits better with Freundlich isotherm model. That indicates the non-uniform activated carbon plays a significant role in the recovery of gold cyanide with M-AC.

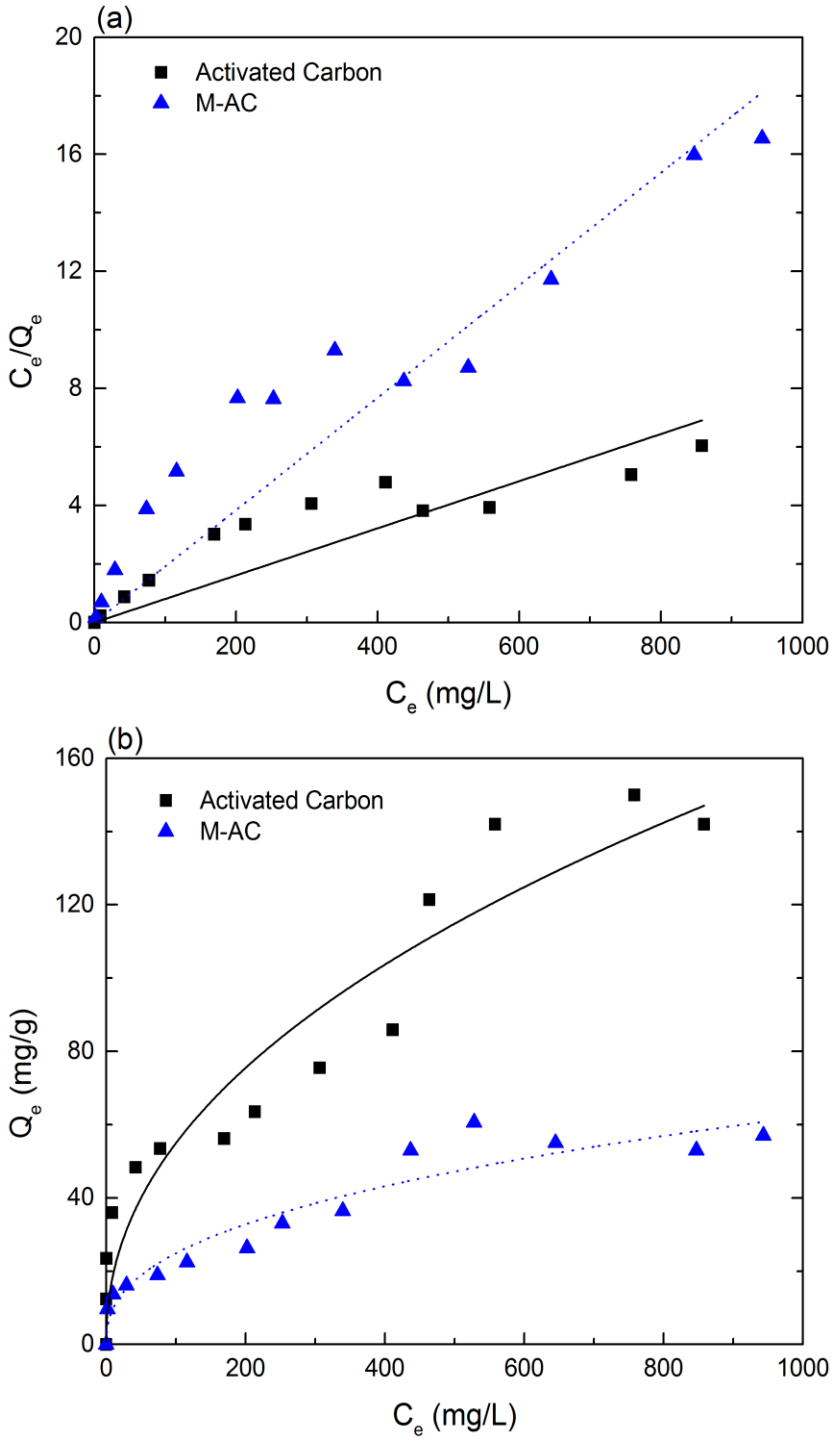

Figure 4.33 (a) Langmuir isotherm plot, and (b) Freundlich isotherm plot for adsorption of Au (I) onto various types of adsorbents

Table 4.8 Estimated isotherm models and their constant values for Au (I) adsorption onto various types of adsorbents

Adsorbent type	Langmuir equation $\frac{C_e}{Q_e} = \frac{1}{b * q_m} + \frac{C_e}{q_m}$			Freundlich equation $Q_e = K{C_e}^{1/n}$		
	R^2	b	q_m	R^2	K	n
Activated Carbon	0.7743	$-4.13*10^{25}$	124.21	0.9235	3.99	2.51
M-AC	0.8429	$-4.00*10^{17}$	52.05	0.9160	6.68	2.18

CHAPTER 5 SUMMARY AND CONCLUSIONS

5.1 Summary and Conclusions

The results of our research support the following conclusions:

- The co-precipitation method provides an easy and reliable technique to prepare magnetic activated carbon (M-AC).
- The predominant phase of iron oxides on activated carbon surface is magnetite (Fe_3O_4). M-AC shows an excellent magnetization property with a saturation magnetization of 38.3 emu/g.
- The specific surface area of M-AC is less than that of pure activated carbon due to the deposition of magnetite on the surface of activated carbon.
- In pure water, M-AC shows an excellent removal efficiency of Cu (II), Ni (II) and DETA in three single systems (Cu, Ni, DETA), two binary systems (Cu-DETA, Ni-DETA) and one ternary system (Cu-Ni-DETA). The deposition of magnetite on activated carbon improves the loading properties of pure activated carbon. M-AC shows less adsorption capacity than Fe_3O_4 for single Cu/Ni solution while achieves higher adsorption ability in multi component solutions with metal-DETA complexes due to the presence of larger DETA molecules in solutions.
- Adsorption behaviour of heavy metal ions and DETA species onto activated carbon could be described by Freundlich isotherm while Langmuir isotherm is a better fitting to the experimental data for

copper/nickel ions and DETA species adsorption onto magnetic iron oxides and M-AC.

- HCl (10^{-3} M) can strip off more than 80 % of loaded heavy metal ions (copper, nickel) from the surface of M-AC without dissolving magnetite of M-AC. After HCl washing M-AC could be regenerated by NaOH solutions. As the recycle and reuse of M-AC are feasible, M-AC can offset the high price of pure activated carbon in practical applications.
- M-AC shows a good affinity to gold cyanide, but activated carbon shows a better recovery efficiency for gold cyanide than M-AC. M-AC is a promising adsorbent in carbon-in-pulp process for gold recovery due to the recycle and reuse of M-AC.

5.2 Contributions to the Original Knowledge

Magnetic activated carbon (M-AC) was prepared through co-precipitation in this study. Different from previous reference [60], the phase of iron oxides deposited on activated carbon is magnetite rather than maghemite. Results showed that the magnetite on M-AC surface not only introduced a magnetic property to activated carbon but also improved the loading properties of activated carbon. In this study, DETA, a depressant which forms stable complexes with specific metal ions, was removed by M-AC at the first time. The results showed that M-AC particles worked effectively in loading DETA from effluents. Moreover, M-AC could be used effectively in loading gold cyanide, leading a potential application of M-AC in carbon-in-pulp process for gold recovery.

5.3 Future Work

In order to efficiently utilize the M-AC in real industrial applications, it will be important to modify and functionalize M-AC surface to achieve the selective adsorption of heavy metal ions and DETA from process water. As M-AC is a very promising material that could be used in carbon-in-pulp process, it will be interesting to conduct more research in this area.

BIBLIOGRAPHY

1. Hawley, J. E., The Sudbury ores, their mineralogy and origin: Part 1, The geological setting. *The Canadian Mineralogist* **1962**, 7, (1), 1-29.

2. Marticorena, M. A.; Hill, G.; Kerr, A. N.; Liechti, D.; Pelland, D. A., INCO develops new pyrrhotite depressant. *Innovations in Mineral Processing* **1994**, 3, 15-33.

3. Yoon, R. H.; Basilio, C.; Marticorena, M.; Kerr, A.; Stratton-Crawley, R., A study of the pyrrhotite depression mechanism by diethylenetriamine. *Minerals Engineering* **1995**, 8, (7), 807-816.

4. Xu, Z.; Rao, S.; Finch, J., Role of diethylenetriamine (DETA) in pentlandite-pyrrhotite separation. Pt. 1: complexation of metals with DETA. *Transactions of the Institution of Mining and Metallurgy. Section C. Mineral Processing and Extractive Metallurgy* **1997**, 106.

5. Xu, M.; Wilson, S., Investigation of seasonal metallurgical shift at INCO's clarabelle mill. *Minerals Engineering* **2000**, 13, (12), 1207-1218.

6. Agar, G. E., Floation of chalcopyrite, pentlandite, pyrrhotite ores. *International Journal of Mineral Processing* **1991**, 33, (1-4), 1-19.

7. Kim, D. S., Studies of the pyrrhotite depression mechanism with diethylenetriamine. *Bulletin-Korean Chemical Society* **1998**, 19, 840-840.

8. Basilio, C. I.; Marticorena, M. A.; Kerr, A. N.; StrattonCrawley, R.; Soc Min, M. E. T.; Explorat, I. N. C., Studies of the pyrrhotite depression mechanism with diethylenetriamine. *Proceedings of the XIX International Mineral Processing Congress, Vol 3: Flotation Operating Practices and Fundamentals* **1995**, p 275-279.

9. http://en.wikipedia.org/wiki/DETA

10. Rao, S.; Zu, X.; Finch, J., Selective solubilization of zinc (II), copper (II) and nickel (II) from iron (III) in metal hydroxide sludges by diethylenetriamine. *Waste Processing and Recycling in Mineral and Metallurgical Industries. II* **1995**, 69-77.

11. Dong, J.; Xu, M., Mitigation strategies to reduce diethylenetriamine (DETA) residual in tailings water at Vale's Sudbury operation. *Water in Mineral Processing* **2012**, 339.

12. Kelebek, S.; Fekete, S.; Wells, P., Selective depression of pyrrhotite using sulphur dioxide-diethylenetriamine reagent combination. *Proceeding of the XIX International Mineral Processing Congress* **1995**, pp 181-187.

13. Bozkurt, V.; Xu, Z.; Finch, J., Effect of depressants on xanthate adsorption on pentlandite and pyrrhotite: single vs mixed minerals. *Canadian Metallurgical Quarterly* **1999**, 38, (2), 105-112.

14. Mendiratta, N.; Yoon, R.; Wilson, S., Effects of diethylenetramine and sulfur dioxide on pyrrhotite depression. *Electrochemistry in Mineral and Metal Processing V* **2000**, 60.

15. Malysiak, V.; O'Connor, C.; Ralston, J.; Gerson, A. R.; Coetzer, L.; Bradshaw, D., Pentlandite-feldspar interaction and its effect on separation by flotation. *International Journal of Mineral Processing* **2002**, 66, (1-4), 89-106.

16. Shi, W.; Liu, Q.; Xu, Z. Reserach progress report II on "Fundamental study of diethylenetriamine (DETA) as pyrrhotite depressant for selective flotation of pentlandite". University of Alberta, **2011**.

17. Liu, Q. An innovative approach in magnetic carrier technology. McGill University, Montreal, **1999**.

18. Xu, Z.; Dong, J., Synthesis, characterization, and application of magnetic nanocomposites for the removal of heavy metals from industrial effluents. *Emerging Environmental Technologies* **2008**, 105-148.

19. Stumm, W., Morgan, JJ, Aquatic chemistry: chemical equilibria and rates in natural waters. *Wiley-Interscience*, New York, **1995**.

20. Feng, D.; Aldrich, C.; Tan, H., Treatment of acid mine water by use of heavy metal precipitation and ion exchange. *Minerals Engineering* **2000,** 13, (6), 623-642.

21. Cooney, D. O., Adsorption design for wastewater treatment. *CRC*: **1998**.

22. Carrott, P.; Carrott, M.; Roberts, R., Physical adsorption of gases by microporous carbons. *Colloids and Surfaces* **1991,** 58, (4), 385-400.

23. McKay, G.; Bino, M.; Altamemi, A., The adsorption of various pollutants from aqueous solutions on to activated carbon. *Water Research* **1985,** 19, (4), 491-495.

24. Paprowicz, J. T., Activated carbons for phenols removal from wastewaters. *Environmental Technology* **1990,** 11, (1), 71-82.

25. Pelekani, C.; Snoeyink, V. L., Competitive adsorption between atrazine and methylene blue on activated carbon: the importance of pore size distribution. *Carbon* **2000,** 38, (10), 1423-1436.

26. Carrott, P.; Carrott, M.; Nabais, J.; Ramalho, J., Influence of surface ionization on the adsorption of aqueous zinc species by activated carbons. *Carbon* **1997,** 35, (3), 403-410.

27. Macias-Garcia, A.; Valenzuela-Calahorro, C.; Gomez-Serrano, V.; Espinosa-Mansilla, A., Adsorption of Pb^{2+} by heat-treated and sulfurized activated carbon. *Carbon* **1993,** 31, (8), 1249-1255.

28. Carrott, P.; Carrott, M.; Nabais, J., Influence of surface ionization on the adsorption of aqueous mercury chlorocomplexes by activated carbons. *Carbon* **1998,** 36, (1-2), 11-17.

29. Koshima, H.; Onishi, H., Adsorption of metal ions on activated carbon from aqueous solutions at pH 1-13. *Talanta* **1986,** 33, (5), 391-395.

30. Marzal, P.; Seco, A.; Gabaldon, C.; Ferrer, J., Cadmium and zinc adsorption onto activated carbon: influence of temperature, pH and metal/carbon ratio. *Journal of Chemical Technology and Biotechnology* **1996,** 66, (3), 279-285.

31. Imamoglu, M.; Tekir, O., Removal of copper (II) and lead (II) ions from aqueous solutions by adsorption on activated carbon from a new precursor hazelnut husks. *Desalination* **2008,** 228, (1), 108-113.

32. Najm, I.; Snoeyink, V.; Lykins Jr, B.; Adams, J., Using powdered activated carbon: A critical review. *Influence and Removal of Organics in Drinking Water* **1992**, 35-66.

33. Gupta, V.; Carrott, P.; Carrott, M. M. L. R.; Suhas, Low-cost adsorbents: growing approach to wastewater treatment-a review. *Critical Reviews in Environmental Science and Technology* **2009,** 39, (10), 783-842.

34. Williams, R. A., Colloid and surface engineering: applications in the process industries. *Butterworth-Heinemann*: **1992**; Vol. 1.

35. Stemen, W. R., Process fob treating liquids. *US Patent* 2,232,294, **1941**.

36. Booker, N.; Keir, D.; Priestley, A.; Ritchie, C.; Sudarmana, D.; Woods, M., Sewage clarification with magnetite particles. *Water Science & Technology* **1991,** 23, (7-9), 1703-1712.

37. Šafařík, I.; Šafaříková, M.; Buřičová, V., Sorption of water soluble organic dyes on magnetic poly (oxy-2, 6-dimethyl-1, 4-phenylene). *Collection of Czechoslovak Chemical Communications* **1995**, 60, (9), 1448-1456.

38. Feng, D.; Aldrich, C.; Tan, H., Removal of heavy metal ions by carrier magnetic separation of adsorptive particulates. *Hydrometallurgy* **2000**, 56, (3), 359-368.

39. Denizli, A.; Özkan, G.; Arica, M. Y., Preparation and characterization of magnetic polymethylmethacrylate microbeads carrying ethylene diamine for removal of Cu (II), Cd (II), Pb (II), and Hg (II) from aqueous solutions. *Journal of Applied Polymer Science* **2000**, 78, (1), 81-89.

40. Petrova, T. M.; Fachikov, L.; Hristov, J., The magnetite as adsorbent for some hazardous species from aqueous solutions: A review. *International Review of Chemical Engineering* **2011**, 3, (2), 134-152.

41. Cornell, R. M.; Schwertmann, U., The iron oxides: structure, properties, reactions, occurrences, and uses. *John Wiley & Sons*: **2003**.

42. Schwertmann, U.; Cornell, R. M., Iron oxides in the laboratory. *Wiley Online Library*: **1991**, Vol. 2.

43. Olowe, A.; Génin, J., The mechanism of oxidation of ferrous hydroxide in sulphated aqueous media: Importance of the initial ratio of the reactants. *Corrosion Science* **1991**, 32, (9), 965-984.

44. Regazzoni, A.; Urrutia, G.; Blesa, M.; Maroto, A., Some observations on the composition and morphology of synthetic magnetites obtained by different routes. *Journal of Inorganic and Nuclear Chemistry* **1981**, 43, (7), 1489-1493.

45. Lee, J.; Isobe, T.; Senna, M., Magnetic properties of ultrafine magnetite particles and their slurries prepared via in-situ precipitation. *Colloids and Surfaces A: Physicochemical and Engineering Aspects* **1996,** 109, 121-127.

46. Yu, C.; Hao, X.; Jiang, H.; Wang, L., Fe_3O_4 nano-whiskers by ultrasonic-aided reduction in concentrated NaOH solution. *Particuology* **2011,** 9, (1), 86-90.

47. Perales Perez, O.; Umetsu, Y.; Sasaki, H., Precipitation and densification of magnetic iron compounds from aqueous solutions at room temperature. *Hydrometallurgy* **1998**, 50, (3), 223-242.

48. Faiyas, A.; Vinod, E.; Joseph, J.; Ganesan, R.; Pandey, R., Dependence of pH and surfactant effect in the synthesis of magnetite (Fe_3O_4) nanoparticles and its properties. *Journal of Magnetism and Magnetic Materials* **2010**, 322, (4), 400-404.

49. Erdemoğlu, M.; Sarıkaya, M., Effects of heavy metals and oxalate on the zeta potential of magnetite. *Journal of Colloid and Interface Science* **2006**, 300, (2), 795-804.

50. Parks, G., Equilibrium concepts in natural water systems. *Advances in Chemistry Series* **1967**, 67, 121.

51. Illés, E.; Tombácz, E., The role of variable surface charge and surface complexation in the adsorption of humic acid on magnetite. *Colloids and Surfaces A: Physicochemical and Engineering Aspects* **2003**, 230, (1-3), 99-109.

52. Kosmulski, M., Chemical properties of material surfaces. *CRC press*: **2001**; Vol. 102.

53. Turner, C. W.; Lister, D.; Smith, D., Deposition and removal of sub-micron particles of magnetite at the surface of alloy 800. *Atomic Energy of Canada Limited, AECL (Report)* **1994**.

54. Sun, Z. X.; Su, F. W.; Forsling, W.; Samskog, P. O., Surface characteristics of magnetite in aqueous suspension. *Journal of Colloid and Interface Science* **1998**, 197, (1), 151-159.

55. Tamura, H.; Matijevic, E.; Meites, L., Adsorption of Co^{2+} ions on spherical magnetite particles. *Journal of Colloid and Interface Science* **1983**, 92, (2), 303-314.

56. Wu, P.; Xu, Z., Silanation of nanostructured mesoporous magnetic particles for heavy metal recovery. *Industrial & Engineering Chemistry Research* **2005**, 44, (4), 816-824.

57. Gúdinas, S. Preparation of magnetic carriers through functionalization of nanosized maghemite particles. McGill University, **1999**.

58. Gudinas, S.; Finch, J.; Vreugdenhil, A., Complexation of copper ions by DETA-terminated magnetic carriers. *International Journal of Mineral Processing* **2000**, 59, (1), 1-7.

59. Gudinas, S.; Finch, J. A.; Vreugdenhil, A. J., Coupling of diethylenetriamine to carboxyl-terminated magnetic particles. *Colloids and Surfaces A: Physicochemical and Engineering Aspects* **2000**, 164, (2-3), 257-266.

60. Oliveira, L. C. A.; Rios, R. V. R. A.; Fabris, J. D.; Garg, V.; Sapag, K.; Lago, R. M., Activated carbon/iron oxide magnetic composites for the adsorption of contaminants in water. *Carbon* **2002**, 40, (12), 2177-2183.

61. Yang, N.; Zhu, S.; Zhang, D.; Xu, S., Synthesis and properties of magnetic Fe_3O_4-activated carbon nanocomposite particles for dye removal. *Materials Letters* **2008**, 62, (4-5), 645-647.

62. Pyrzyńska, K.; Bystrzejewski, M., Comparative study of heavy metal ions sorption onto activated carbon, carbon nanotubes, and carbon-encapsulated magnetic nanoparticles. *Colloids and Surfaces A: Physicochemical and Engineering Aspects* **2010**, 362, (1), 102-109.

63. Chen, J. P.; Lin, M., Surface charge and metal ion adsorption on an H-type activated carbon: experimental observation and modeling simulation by the surface complex formation approach. *Carbon* **2001**, 39, (10), 1491-1504.

64. Jeffrey, M.; Breuer, P.; Choo, W. L., A kinetic study that compares the leaching of gold in the cyanide, thiosulfate, and chloride systems. *Metallurgical and Materials Transactions B* **2001**, 32, (6), 979-986.

65. Ibrado, A.; Fuerstenau, D., Infrared and X-ray photoelectron spectroscopy studies on the adsorption of gold cyanide on activated carbon. *Minerals Engineering* **1995**, 8, (4), 441-458.

66. Adams, M.; Fleming, C., The mechanism of adsorption of aurocyanide onto activated carbon. *Metallurgical and Materials Transactions B* **1989**, 20, (3), 315-325.

67. Papirer, E.; Polania-Leon, A.; Donnet, J. B.; Montagnon, P., Fixation of potassium aurocyanide on active carbons. *Carbon* **1995**, 33, (9), 1331-1337.

68. Nicol, M.; Schalch, E.; Balestra, P.; Hegedus, H., A modern study of the kinetics and mechanism of the cementation of gold. *Journal of the South African Institute of Mining and Metallurgy* **1979**, 79, (7), 191-198.

69. McDougall, G.; Hancock, R.; Nicol, M.; Wellington, O.; Copperthwaite, R., The mechanism of the adsorption of gold cyanide on activated carbon. *Journal of the South African Institute of Mining and Metallurgy* **1980**, 80, (9), 344-356.

70. Chapman, T. G., Cynidation of ore pulps with limited agitation. *US Patent* 2,315,187, **1943**.

71. Davidson, R.; Veronese, V.; Nkosi, M., The use of activated carbon for the recovery of gold and silver from gold-plant solutions. *Journal of the South African Institute of Mining and Metallurgy* **1979**, 79, (10), 281-297.

72. Zadra, J., A process for the recovery of gold from activated carbon by leaching and electrolysis. US Department of the Interior, *Bureau of Mines*: **1950**; Vol. 4672.

73. Garten, V.; Weiss, D., The ion-and electron-exchange properties of activated carbon in relation to its behaviour as a catalyst and adsorbent. *Reviews of Pure and Applied Chemistry* **1957**, 7, S. 69-122

74. Dixon, S.; Cho, E.; Pitt, C. In The interaction between gold cyanide, silver cyanide, and high surface area charcoal, *Fundamental Aspects of Hydrometallurgical Processes* **1976**.

75. Cho, E.; Pitt, C., Kinetics and thermodynamics of silver cyanide adsorption on activated charcoal. *Metallurgical and Materials Transactions B* **1979,** 10, (2), 165-169.

76. Cullity, B. D.; Graham, C. D., Introduction to magnetic materials. *Wiley-IEEE Press:* **2011**.

77. Goldstein, J.; Newbury, D. E.; Joy, D. C.; Lyman, C. E.; Echlin, P.; Lifshin, E.; Sawyer, L.; Michael, J. R., Scanning electron microscopy and X-ray microanalysis (3 ed) *Springer:* **2003**.

78. Liu, Z.; Liu, Y.; Yao, K.; Ding, Z.; Tao, J.; Wang, X., Synthesis and magnetic properties of Fe_3O_4 nanoparticles. *Journal of Materials Synthesis and Processing* **2002,** 10, (2), 83-87.

79. El-Ashtoukhy, E. S. Z.; Amin, N.; Abdelwahab, O., Removal of lead (II) and copper (II) from aqueous solution using pomegranate peel as a new adsorbent. *Desalination* **2008,** 223, (1), 162-173.

80. Kadirvelu, K.; Faur-Brasquet, C.; Le Cloirec, P., Removal of Cu (II), Pb (II), and Ni (II) by adsorption onto activated carbon cloths. *Langmuir* **2000,** 16, (22), 8404-8409.

81. Chen, C.; Hu, J.; Shao, D.; Li, J.; Wang, X., Adsorption behavior of multiwall carbon nanotube/iron oxide magnetic composites for Ni (II) and Sr (II). *Journal of Hazardous Materials* **2009,** 164, (2-3), 923-928.

82. Hidmi, L.; Edwards, M., Role of temperature and pH in $Cu(OH)_2$ solubility. *Environmental Science & Technology* **1999,** 33, (15), 2607-2610.

83. Mohan, D.; Chander, S., Single component and multi-component adsorption of metal ions by activated carbons. *Colloids and Surfaces A: Physicochemical and Engineering Aspects* **2000,** 177, (2-3), 183-196.

84. De Celis, J.; Amadeo, N.; Cukierman, A., In situ modification of activated carbons developed from a native invasive wood on removal of trace toxic metals from wastewater. *Journal of Hazardous Materials* **2009,** 161, (1), 217-223.

85. Boehm, H., Surface oxides on carbon and their analysis: a critical assessment. *Carbon* **2002,** 40, (2), 145-149.

86. Kolarik, L.; Dixon, D.; Freeman, P.; Furlong, D.; Healy, T., Effects of pretreatment on the surface characteristics of a natural magnetite. *Proceedings of the American Institute of Mineral and Material Engineers* **1980**.

87. Prakash, S.; Das, B.; Mohanty, J.; Venugopal, R., The recovery of fine iron minerals from quartz and corundum mixtures using selective magnetic coating. *International Journal of Mineral Processing* **1999,** 57, (2), 87-103.

88. Anastassakis, G. N., A study on the separation of magnesite fines by magnetic carrier methods. *Colloids and Surfaces A: Physicochemical and Engineering Aspects* **1999,** 149, (1-3), 585-593.

89. Nguyen, A. V.; Schulze, H. J., Colloidal Science of Flotation. *CRC*: **2004**; Vol. 118.

90. Hu, J.; Chen, G.; Lo, I. M. C., Selective removal of heavy metals from industrial wastewater using maghemite nanoparticle: performance and mechanisms. *Journal of Environmental Engineering* **2006,** 132, (7), 709-715.

91. Rashchi, F.; Finch, J.; Sui, C., Action of DETA, dextrin and carbonate on lead-contaminated sphalerite. *Colloids and Surfaces A: Physicochemical and Engineering Aspects* **2004,** 245, (1), 21-27.

92. Dastgheib, S. A.; Rockstraw, D. A., A model for the adsorption of single metal ion solutes in aqueous solution onto activated carbon produced from pecan shells. *Carbon* **2002,** 40, (11), 1843-1851.

93. Gupta, V. K.; Sharma, S., Removal of cadmium and zinc from aqueous solutions using red mud. *Environmental Science & Technology* **2002,** 36, (16), 3612-3617.

APPENDIX

Equilibrium Constants of DETA and Other Related Species

I. DETA-H^+ species:

i. $DETA + H^+ \rightleftharpoons DETAH^+$

$$K_{a1} = \frac{[DETAH^+]}{[DETA][H^+]} = 10^{9.98} \quad \text{[Appendix - 1]}$$

ii. $DETAH^+ + H^+ \rightleftharpoons DETAH_2^{2+}$

$$K_{a2} = \frac{[DETAH_2^{2+}]}{[DETAH^+][H^+]} = 10^{9.17} \quad \text{[Appendix - 2]}$$

iii. $DETAH_2^{2+} + H^+ \rightleftharpoons DETAH_3^{3+}$

$$K_{a3} = \frac{[DETAH_3^{3+}]}{[DETAH_2^{2+}][H^+]} = 10^{4.32} \quad \text{[Appendix - 3]}$$

II. Cu-DETA species:

i. $Cu^{2+} + DETA \rightleftharpoons Cu(DETA)^{2+}$

$$K_{CuL} = \frac{[Cu(DETA)^{2+}]}{[Cu^{2+}]\,[DETA]} = 10^{15.9} \quad \text{[Appendix - 4]}$$

ii. $Cu^{2+} + 2DETA \rightleftharpoons Cu(DETA)_2^{2+}$

$$K_{CuL2} = \frac{[Cu(DETA)_2^{2+}]}{[Cu^{2+}]\,[DETA]^2} = 10^{20.9} \quad \text{[Appendix - 5]}$$

iii. $Cu(DETA)^{2+} + H^{+} \rightleftharpoons Cu(HDETA)^{3+}$

$$K_{CuHL} = \frac{[Cu(HDETA)^{3+}]}{[H^{+}]\,[Cu(DETA)^{2+}]} = 10^{3.2}$$ [Appendix - 6]

iv. $Cu(DETA)^{2+} + OH^{-} \rightleftharpoons Cu(OH)(DETA)^{+}$

$$K_{CuOHL} = \frac{[Cu(OH)(DETA)^{+}]}{[OH^{-}]\,[Cu(DETA)^{2+}]} = 10^{4.6}$$ [Appendix - 7]

v. $Cu(DETA)_2^{2+} + H^{+} \rightleftharpoons Cu(H)(DETA)_2^{3+}$

$$K_{CuHL2} = \frac{[Cu(H)(DETA)_2^{3+}]}{[H^{+}]\,[Cu(DETA)_2^{2+}]} = 10^{8.2}$$ [Appendix - 8]

III. Cu-OH^{-} species

i. $Cu^{2+} + OH^{-} \rightleftharpoons Cu(OH)^{+}$

$$K_{Cu(OH)^{-}} = \frac{[Cu(OH)^{+}]}{[Cu^{2+}][OH^{-}]} = 10^{6.3}$$ [Appendix - 9]

ii. $Cu^{2+} + 2OH^{-} \rightleftharpoons Cu(OH)_2$

$$K_{Cu(OH)_2} = \frac{[Cu(OH)_2]}{[Cu^{2+}]\,[OH^{-}]^2} = 10^{12.8}$$ [Appendix - 10]

iii. $Cu^{2+} + 3OH^{-} \rightleftharpoons Cu(OH)_3^{-}$

$$K_{Cu(OH)_3^{-}} = \frac{[Cu(OH)_3^{-}]}{[Cu^{2+}]\,[OH^{-}]^3} = 10^{14.5}$$ [Appendix - 11]

iv. $Cu^{2+} + 4OH^- \rightleftharpoons Cu(OH)_4^{2-}$

$$K_{Cu(OH)_4^{2-}} = \frac{[Cu(OH)_4^{2-}]}{[Cu^{2+}]\,[OH^-]^4} = 10^{15.6}$$ [Appendix - 12]

v. $2Cu^{2+} + 2OH^- \rightleftharpoons Cu_2(OH)_2^{2+}$

$$K_{Cu_2(OH)_2^{2+}} = \frac{[Cu_2(OH)_2^{2+}]}{[Cu^{2+}]^2[OH^-]^2} = 10^{17.8}$$ [Appendix - 13]

IV. Ni-DETA species:

i. $Ni^{2+} + DETA \rightleftharpoons Ni(DETA)^{2+}$

$$K_{NiL} = \frac{[Ni(DETA)^{2+}]}{[Ni^{2+}]\,[DETA]} = 10^{10.5}$$ [Appendix - 14]

ii. $Ni^{2+} + 2DETA \rightleftharpoons Ni(DETA)_2^{2+}$

$$K_{NiL2} = \frac{[Ni(DETA)_2^{2+}]}{[Ni^{2+}]\,[DETA]^2} = 10^{18.6}$$ [Appendix - 15]

V. Ni- OH^- species:

i. $Ni^{2+} + OH^- \rightleftharpoons Ni(OH)^+$

$$K_{Ni(OH)^-} = \frac{[Ni(OH)^+]}{[Ni^{2+}][OH^-]} = 10^{3.7}$$ [Appendix - 16]

ii. $Ni^{2+} + 2OH^- \rightleftharpoons Ni(OH)_2$

$$K_{Ni(OH)_2} = \frac{[Ni(OH)_2]}{[Ni^{2+}]\,[OH^-]^2} = 10^{8}$$ [Appendix - 17]

iii. $Ni^{2+} + 3OH^- \rightleftharpoons Ni(OH)_3^-$

$$K_{Ni(OH)_3^-} = \frac{[Ni(OH)_3^-]}{[Ni^{2+}]\,[OH^-]^3} = 10^{11}$$ [Appendix - 18]

iv. $2Ni^{2+} + OH^- \rightleftharpoons Ni_2(OH)^{3+}$

$$K_{Ni_2(OH)^{3+}} = \frac{[Ni_2(OH)^{3+}]}{[Ni^{2+}]^2[OH^-]} = 10^{13.31}$$ [Appendix - 19]

v. $4Ni^{2+} + 4OH^- \rightleftharpoons Ni_4(OH)_4^{4+}$

$$K_{Ni_4(OH)_4^{4+}} = \frac{[Ni_4(OH)_4^{4+}]}{[Ni^{2+}]^4\,[OH^-]^4} = 10^{28.3}$$ [Appendix - 20]

vi. $Ni(OH)_2(s) \rightleftharpoons Ni^{2+} + 2OH^-$

$$K_{sp,Ni(OH)_2} = [Ni^{2+}]\,[OH^-]^2 = 10^{-15.2}$$ [Appendix - 21]